

AD-A135 260

AN ASSESSMENT OF RECENT RESULTS ON PSEUDO-STATIONARY
OBLIQUE-SHOCK-WAVE R.: (U) TORONTO UNIV DOWNSVIEW
(ONTARIO) INST FOR AEROSPACE STUDIES M SHIROUZI ET AL.

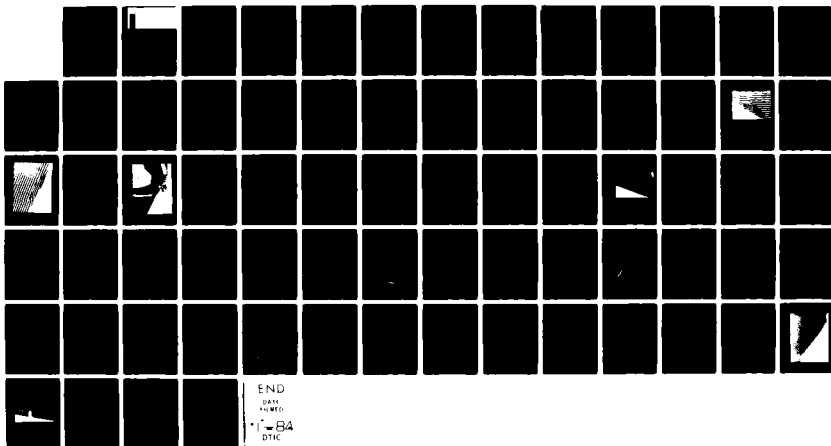
1/1

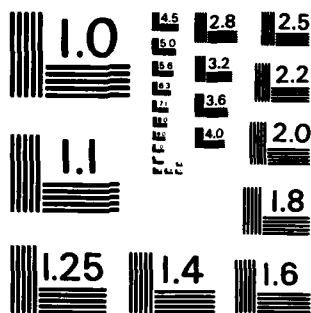
UNCLASSIFIED

NOV 82 UTIAS-264 AFOSR-TR-83-0924

F/G 20/4

NL





MICROCOPY RESOLUTION TEST CHART
NATIONAL BUREAU OF STANDARDS-1963-A

AD-A135260

DTIC FILE COPY



INSTITUTE
FOR
AEROSPACE STUDIES

UNIVERSITY OF TORONTO

AFOSR-TR- 33 - 0924

(14)

AN ASSESSMENT OF RECENT RESULTS
ON PSEUDO-STATIONARY OBLIQUE-SHOCK-WAVE REFLECTIONS

by

M. Shirouzu and I. I. Glass

DTIC

DEC 01 1983

Approved for public release
Distribution unlimited

November, 1982

UTIAS Report No. 264
CN ISSN 0082-5255

83 11 29 192

UNCLASSIFIED

SECURITY CLASSIFICATION OF THIS PAGE (When Data Entered)

REPORT DOCUMENTATION PAGE		READ INSTRUCTIONS BEFORE COMPLETING FORM
1. REPORT NUMBER AFOSR-TR- 83-0924	2. GOVT ACCESSION NO. AD-A135260	3. RECIPIENT'S CATALOG NUMBER
4. TITLE (and Subtitle) AN ASSESSMENT OF RECENT RESULTS ON PSEUDO-STATIONARY OBLIQUE-SHOCK-WAVE REFLECTIONS		5. TYPE OF REPORT & PERIOD COVERED INTERIM
		6. PERFORMING ORG. REPORT NUMBER
7. AUTHOR(s) M SHIROUZU I I GLASS		8. CONTRACT OR GRANT NUMBER(s) AFOSR-82-0096
9. PERFORMING ORGANIZATION NAME AND ADDRESS UNIVERSITY OF TORONTO INSTITUTE FOR AEROSPACE STUDIES 4925 DUFFERIN ST, DOWNSVIEW, ONTARIO, CANADA M3H 5T6		10. PROGRAM ELEMENT, PROJECT, TASK AREA & WORK UNIT NUMBERS 61102F 2307/A1
11. CONTROLLING OFFICE NAME AND ADDRESS AIR FORCE OFFICE OF SCIENTIFIC RESEARCH/NA BOLLING AFB, DC 20332		12. REPORT DATE November 1982
		13. NUMBER OF PAGES 67
14. MONITORING AGENCY NAME & ADDRESS (if different from Controlling Office)		15. SECURITY CLASS. (of this report) Unclassified
		15a. DECLASSIFICATION/DOWNGRADING SCHEDULE
16. DISTRIBUTION STATEMENT (of this Report) Approved for Public Release; Distribution Unlimited.		
17. DISTRIBUTION STATEMENT (of the abstract entered in Block 20, if different from Report)		
18. SUPPLEMENTARY NOTES		
19. KEY WORDS (Continue on reverse side if necessary and identify by block number) OBLIQUE-SHOCK-WAVE REFLECTIONS SHOCK-TUBE FLOWS OPTICAL METHODS NUMERICAL ANALYSIS		
20. ABSTRACT (Continue on reverse side if necessary and identify by block number) The assumptions and criteria used in existing analyses in determining the regions and transition lines of pseudo-stationary oblique-shock-wave reflections have been re-examined in order to improve the agreement between experiments and computed data for regular (RR), single-Mach (SMR), complex-Mach (CMR) and double-Mach reflection (DMR). It is shown that the relaxation lengths for vibration and dissociation determine whether frozen or equilibrium gas transition lines are applicable. For example, at an initial temperature of 300 K and a pressure of 15 torr		

DD FORM 1 JAN 73 1473

EDITION OF 1 NOV 65 IS OBSOLETE

UNCLASSIFIED

SECURITY CLASSIFICATION OF THIS PAGE (When Data Entered)

UNCLASSIFIED

SECURITY CLASSIFICATION OF THIS PAGE(When Data Entered)

(where much previous work was done) an equilibrium gas analysis would not be required for shock Mach numbers $M_s \leq 9$ in N_2 , $M_s \leq 6$ in O_2 , $M_s \leq 8$ in air and $M_s \leq 3$ in CO_2 . Yet, the available experimental data in N_2 , CO_2 and very recent results for air, which are based on the criterion (consistent with relaxation lengths) of angle δ , between the incident and reflected shock wave, do not conclusively support the frozen or equilibrium gas calculations for N_2 and air. It does support CO_2 as an equilibrium gas contrary to a previous conclusion of agreement with $\gamma = 1.29$. A new additional and necessary criterion for the transition from single to complex Mach reflection improves the agreement between analysis and experiment and is consistent with the requirements of the relaxation length and the angle δ . However, it now appears that a more accurate criterion is required for the boundary line between CMR and DMR. A more detailed examination of the boundary-layer-displacement slope at the point of regular reflection appears to eliminate the so-called von Neumann paradox, and explains the persistence of regular reflection below the transition line for the occurrence of Mach reflection. It is also shown that at the triple point the Mach stem can vary from being perpendicular to the wedge surface in actual experiments by as much as -3.10° to 7.5° . Consequently, calculations of the triple-point-trajectory angle χ on the basis that the stem is perpendicular is not always well founded. It is verified that at lower shock Mach numbers M_s and large wedge angles θ , the experimental evidence shows that the transition lines for SMR \rightarrow CMR and CMR \rightarrow DMR converge at a point on the RR \rightarrow MR line, contrary to a previous simplified analysis.

UNCLASSIFIED

SECURITY CLASSIFICATION OF THIS PAGE(When Data Entered)

AN ASSESSMENT OF RECENT RESULTS
ON PSEUDO-STATIONARY OBLIQUE-SHOCK-WAVE REFLECTIONS

by

M. Shirouzu and I. I. Glass

Submitted July, 1982

Accession For	
NTIS GRA&I	<input checked="" type="checkbox"/>
DTIC TAB	<input type="checkbox"/>
Unannounced	<input type="checkbox"/>
Justification	
By	
Distribution/	
Availability Codes	
Avail and/or	
Dist	Special
A-1	



November, 1982

UTIAS Report No. 264
CN ISSN 0082-5255

AIR FORCE OFFICE OF SCIENTIFIC RESEARCH (AFSC)
NOTICE OF TRANSMITTAL TO DTIC
This technical report has been reviewed and is
approved for public release IAW AFR 190-12.
Distribution is unlimited.
MATTHEW J. KERPER
Chief, Technical Information Division

Acknowledgements

We appreciate the assistance received from Bob Deschambault in making available recent extensive UTIAS experimental data for this assessment. His data will be reported on separately.

One of us (M. Shirouzu) is grateful to the National Aerospace Laboratory, Tokyo, Japan, for making possible my research leave.

The financial assistance received from the Canadian Natural Sciences and Engineering Research Council, the U.S. Air Force under grant AFOSR 82-0096, and the U.S. Army Research Office is acknowledged with thanks.

We are pleased to thank Mrs. W. Dillon for the careful and attractive typing of our report, and Mrs. L. Quintero and Mrs. I. Krauze for their fine drafting.

Summary

The assumptions and criteria used in existing analyses in determining the regions and transition lines of pseudo-stationary oblique-shock-wave reflections have been re-examined in order to improve the agreement between experiments and computed data for regular (RR), single-Mach (SMR), complex-Mach (CMR) and double-Mach reflection (DMR).

It is shown that the relaxation lengths for vibration and dissociation determine whether frozen or equilibrium gas transition lines are applicable. For example, at an initial temperature of 300 K and a pressure of 15 torr (where much previous work was done) an equilibrium-gas analysis would not be required for shock Mach numbers $M_s < 9$ in N_2 , $M_s < 6$ in O_2 , $M_s < 8$ in air and $M_s < 3$ in CO_2 .

Yet, the available experimental data in N_2 , CO_2 and very recent results for air, which are based on the criterion (consistent with relaxation lengths) of the angle θ between the incident and reflected shock wave, do not conclusively support the frozen or equilibrium gas calculations for N_2 and air. It does support CO_2 as an equilibrium gas contrary to a previous conclusion of agreement with $\gamma = 1.29$.

A new additional and necessary criterion for the transition from single to complex Mach reflection improves the agreement between analysis and experiment and is consistent with the requirements of the relaxation length and the angle θ . However, it now appears that a more accurate criterion is required for the boundary line between CMR and DMR.

A more detailed examination of the boundary-layer-displacement slope at the point of regular reflection appears to eliminate the so-called von Neumann paradox, and explains the persistence of regular reflection below the transition line for the occurrence of Mach reflection.

It is also shown that at the triple point the Mach stem can vary from being perpendicular to the wedge surface in actual experiments by as much as -3.0° to 7.5° . Consequently, calculations of the triple-point-trajectory angle χ on the basis that the stem is perpendicular is not always well founded.

It is verified that at lower shock Mach numbers M_s and large wedge angles θ_w , the experimental evidence shows that the transition lines for $SMR \neq CMR$ and $CMR \neq DMR$ converge at a point on the $RR \neq MR$ line, contrary to a previous simplified analysis.

Contents

	<u>Page</u>
Acknowledgements	ii
Summary	iii
Notation	v
1. INTRODUCTION	1
2. ANALYSES	2
2.1 Method of Calculations	2
2.2 Role of Relaxation Lengths	2
3. RESULTS AND DISCUSSIONS	3
3.1 Comparison of Experimental and Calculated Results for δ	4
3.2 Effect of Variation of Mach-Stem Angle at Triple Point from being Perpendicular to Wedge Surface	6
3.3 A New Additional Criterion for Transition from SMR to CMR	6
3.4 Persistence of Regular Reflection (RR) into the Region of Mach Reflection (MR) — <i>von Neumann's Paradox</i>	8
4. CONCLUSIONS	9
REFERENCES	9
TABLES	
FIGURES	
APPENDIX A: COMMENT ON <i>PERFECT</i> CO ₂	
APPENDIX B: THREE-SHOCK THEORY	
APPENDIX C: EFFECT OF SLIPSTREAM THICKNESS	
APPENDIX D: COMMENT ON TRANSITION CRITERION FOR CMR TO DMR	
APPENDIX E: SOME FUTURE STUDIES	

Notation

Ar	argon
CMR	complex Mach reflection
CO ₂	carbon dioxide
C _p	specific heat at constant pressure
C _v	specific heat at constant volume
DMR	double Mach reflection
E _{vib}	energy of vibrational modes
h	specific enthalpy
I	incident shock wave
K	kink
L	distance from wedge corner to incident shock wave along horizontal line
ℓ	distance from wedge corner to kink or second triple point along horizontal line
M	Mach number
M, M'	Mach stems
MR	Mach reflection
M _s	incident shock wave Mach number
M _{1T}	flow Mach number in region 1 relative to triple point
M _{2K}	flow Mach number in region 2 relative to kink
M _{2T}	flow Mach number in region 2 relative to triple point
NR	no reflection
N ₂	nitrogen
O ₂	oxygen
P	reflection point
P	pressure
R	gas constant
R, R'	reflected shock waves
RR	regular reflection
S, S'	slipstreams
SMR	single Mach reflection
T	temperature
T, T'	triple points
u	flow velocity
u _{sl}	velocity of incident shock wave relative to laboratory frame

1. INTRODUCTION

When a planar shock wave collides with a sharp compressive corner, four different types of reflection take place as a result of the shock-wave reflection and the deflection of the shock-induced flow (Refs. 1-4). The four types are called *regular reflection* (RR), *single-Mach reflection* (SMR), *complex-Mach reflection* (CMR) and *double-Mach reflection* (DMR). The latter three reflections as a group are called *Mach reflection* (MR). The two types, RR and SMR, which occur also in steady supersonic flows were first noticed by E. Mach in 1878 (Ref. 5). Much later, CMR and DMR were discovered by Smith (Ref. 6) in 1945 and White (Ref. 7) in 1951, respectively, while working in shock-tube flows. The four types are illustrated schematically in Fig. 1.

The simplest type of reflection, RR, is characterized by two shock waves, an incident shock wave, I, and a reflected shock wave, R, and their point of intersection, P, on the surface of the wedge. Depending on the wedge angle θ_w and the incident shock Mach number M_s , the intersection point of the two shock waves, P, detaches from the wedge surface and gives rise to MR. In MR a new shock-wave system appears including Mach stem M, triple point T, and slipstream (or contact surface) S. In SMR the curvature of the reflected shock wave is smooth. In CMR a kink K appears in the reflected shock wave with a narrow region of curvature reversal. In order for the kink to exist, a band of compression waves must converge in the region behind the reflected shock wave at the kink. This band is usually too weak to be seen in actual interferograms. In DMR the band of compression waves converges to a second Mach stem M', the kink becomes a second triple point T' and a second slipstream appears.

Several criteria have been proposed to define the transition between RR and MR. von Neumann (Ref. 8) proposed the *detachment criterion*, where transition takes place (see Fig. 2) when the wedge angle θ_w is decreased to a point where it forces θ_2 to exceed the maximum deflection angle θ_{2m} (Ref. 9). This criterion is sometimes called the *von Neumann criterion*. A *mechanical-equilibrium criterion* was proposed by Henderson and Lozzi (Ref. 10) on the basis that transition can only occur smoothly without discontinuous changes in pressure. This criterion can be formulated as $\theta_1 - \theta_2 = \theta_3 = 0^\circ$. These criteria can best be illustrated by using pressure-deflection (p, θ) shock polars as shown in Fig. 3. The reflected-shock polar R corresponds to transition according to the detachment criterion. The state behind the reflected shock wave jumps from point A, which corresponds to a RR state, to point B, which corresponds to a MR state. Consequently, there is a pressure jump during the transition. The polar R' corresponds to transition according to the mechanical-equilibrium criterion. The state behind the reflected shock wave comes along the p/p_0 axis from below as the wedge angle decreases in the RR region. At point C the transition takes place and RR turns smoothly into MR. After the transition, the state behind the reflected shock wave goes along the strong-shock portion of the incident shock wave I to the right. Further details are given in Ref. 1. These criteria can be expressed in another way as follows. The detachment criterion is the limit for the two-shock

theory to have solutions and the mechanical-equilibrium criterion is the limit for the three-shock theory to have solutions. In other words, the mechanical-equilibrium criterion corresponds to $\chi = 0^\circ$ in the three-shock theory and occurs in stationary supersonic flows. One more criterion was suggested by Hornung et al (Ref. 11). Their criterion is called the *sonic criterion* because the transition takes place when the sonic point D (where the flow behind the reflected shock wave is sonic) on the reflected shock wave R' coincides with the p/p_0 axis, as shown in Fig. 3. This criterion, however, gives a transition point which is so close to the point of detachment that it cannot be resolved experimentally.

The first precise transition-boundary map in a ($M_s - \theta_w$) or ($M_s - \theta_w$) plane based on the two-shock theory, the three-shock theory and the transition criteria described above was given by Ben-Dor and Glass for N_2 and Ar (Refs. 1, 2). Ando and Glass also gave a transition-boundary map for CO_2 (Ref. 13). Ben-Dor and Glass originally suggested, from a comparison between experiments and calculations in the transition-boundary maps, that in the range of their data N_2 should be treated as an equilibrium gas and Ar as a frozen gas ($\gamma = 1.667$). Ando and Glass, on the other hand, concluded that a fictitious perfect-gas model with $\gamma = 1.290$ for CO_2 is the most appropriate for that gas. Although their transition-boundary maps provide very useful information for practical applications, it must be concluded that any apparent agreement with experiment is accidental. In reality, only transition boundaries based on a frozen flow ($\gamma = 1.667$ for Ar and $\gamma = 1.40$ for N_2 , O_2 , air and CO_2) and equilibrium flow are consistent with relaxation length concepts. The actual experimental data does not agree with either model in transition-boundary maps. Consequently, it must be concluded that better criteria for the SMR \neq CMR and CMR \neq DMR transitions must be found, which would hold for all gases tested to date.

A much better and fundamental assessment can now be given, whether a flow is in equilibrium or not, through the appropriate relaxation length as represented by the angle δ between the incident and reflected waves rather than by the secondary standard of agreement with $M_s - \theta_w$ plots. A good case in point is the conclusion by Ando and Glass (Ref. 13) that the fictitious perfect-gas ($\gamma = 1.290$) model for the $M_s - \theta_w$ plot is the one that agrees best for CO_2 over the range $1 < M_s < 10$. However, a detailed examination of δ over this range shows that the flow is in vibrational equilibrium because the vibrational relaxation lengths for $M_s > 3$ are all too small (< 1 mm). On the other hand, for Ar, N_2 , O_2 and air, this shock-tube data, by and large, can be considered as consistent with perfect-gas (frozen) states. The above leaves little doubt that even more precise SMR \neq CMR and CMR \neq DMR criteria are still required. A new necessary (but not sufficient) condition for SMR \neq CMR transition is presented which improves the agreement with experiment and is consistent with relaxation lengths. It is also shown that the experimental data (Refs. 13-16) do not agree with the CMR \neq DMR transition line at lower M_s and large θ_w . In fact, the two lines merge where the SMR \neq CMR transition line cuts the RR \neq MR line. Basically, this arises from the fact that the distance between the two triple points T and T' does not remain constant but vanishes at the point of

intersection of the foregoing three transition lines.

For nonstationary shock reflections, experimental results show that transition occurs in accordance with the detachment criterion. Experiments also show that RR persists beyond the limit of the detachment criterion. This persistence has been called the *von Neumann paradox*. Hornung et al (Ref. 11) suggest that it may be explained in terms of the displacement thickness of the boundary layer on the wedge surface. Ben-Dor et al (Ref. 12) showed that a persistent hysteresis loop exists in the RR * MR transition in experiments which depend on whether θ_w is increased or decreased for a given M_s . The reason for this persistence is still unclear and will be discussed in Section 3.4. Once RR terminates, three different types of Mach reflection can occur in nonstationary flows. White (Ref. 7) noticed that CMR and DMR will occur when the flow behind the reflected shock wave becomes supersonic in a frame of reference attached to the triple point T (i.e., $M_{2T} > 1$, Fig. 2). Henderson and Lozzi (Ref. 10) suggest that a band of compression waves must exist in a CMR and these compression waves converge to a shock wave, the second Mach stem, to form a DMR when $M_{2K} > 1$. The criteria for transition from SMR to CMR and from CMR to DMR, respectively, are taken as $M_{2T} > 1$ and $M_{2K} > 1$.

It is now also quite certain that the *von Neumann paradox* can be explained on the basis of the viscous boundary-layer-displacement thickness at the reflection point P of RR.

Some useful discussions on the effect of Mach-stem curvature and its influence on calculating precise values of the triple-point-trajectory angle are given.

Comments are also presented in the appendices on the nature of the solutions of the three-shock theory, the effect of slipstream thickness and the transition CMR * DMR.

2. ANALYSES

2.1 Method of Calculations

The basic equations and assumptions used in the present calculations are the same as those used by Ben-Dor (Ref. 3) unless, in some cases, the assumptions and boundary conditions are changed to evaluate their effects on the solutions. The method employed for the calculations is briefly described below.

The phenomena are assumed to be pseudo-stationary and all the velocities in the equations below are those relative to a reference frame attached to a point which moves with a constant velocity. The reference point is the reflection point P, in RR, and the triple point T, in MR, respectively (see Fig. 2). Each region which is divided by shock waves and a slipstream is designated by 0 to 3, as shown in Fig. 2. The physical quantities on both sides of each shock wave in the vicinity of the reference point satisfy the following equations:

Conservation of tangential velocity:

$$\rho_i \tan \phi_i = \rho_j \tan(\phi_i - \theta_j) \quad (1)$$

Continuity:

$$\rho_i u_i \sin \phi_i = \rho_j u_j \sin(\phi_i - \theta_j) \quad (2)$$

Normal momentum:

$$p_i + \rho_i u_i^2 \sin^2 \phi_i = p_j + \rho_j u_j^2 \sin^2(\phi_i - \theta_j) \quad (3)$$

Energy:

$$h_i + \frac{1}{2} u_i^2 \sin^2 \phi_i = h_j + \frac{1}{2} u_j^2 \sin^2(\phi_i - \theta_j) \quad (4)$$

where i and j are the upstream and downstream values, respectively.

In the case of regular reflection, or the *two-shock theory*, two sets of equations for $i = 0$, $j = 1$ and $i = 1$, $j = 2$ are solved under the boundary condition $\theta_1 = \theta_2$. This means that the direction of the flow behind the reflected shock wave is along the wedge surface. The physical validity of the boundary condition will be discussed later in Section 3.4. In the case of Mach reflection, or the *three-shock theory*, three sets of equations $i = 0$, $j = 1$; $i = 1$, $j = 2$; and $i = 0$, $j = 3$ (ϕ_i is called ϕ_3 in this case) are solved under the boundary conditions $\theta_3 = \theta_1 - \theta_2$ and $p_2 = p_3$, which mean that the flows are parallel and the pressures are identical on both sides of the slipstream. In the case of MR, it is also assumed that the Mach stem is perpendicular to the wedge surface, which is reasonable but not precise experimentally. This assumption will be discussed in Section 3.2. The boundary conditions $\theta_3 = \theta_1 - \theta_2$ is also discussed in Appendix C. The computer program used to solve these sets of equations for obtaining the transition boundaries in the $(M_s - \theta_w')$ or $(M_s - \theta_w)$ planes is shown in Ref. 30.

2.2 Role of Relaxation Lengths

When a shock wave is propagated through a gas, the translational degrees and rotational degrees of freedom of the gas molecules are excited to the new state of equilibrium within the length of a few mean-free-paths, which is the thickness of a shock wave. The other internal degrees of freedom, however, take a longer time to reach equilibrium. In analyses of gasdynamic phenomena including shock waves, the role of relaxation lengths is very important. That is, if the relaxation length of an internal degree of freedom is much longer than a characteristic length of the phenomenon, the internal degree of freedom can be treated as frozen at the initial state. If an internal degree of freedom whose relaxation length is considerably shorter than a characteristic length of the phenomenon it can be assumed to be in equilibrium immediately behind the shock wave. The gas is in nonequilibrium when the relaxation length and the characteristic length lie between the two extreme cases of frozen and equilibrium flow.

In the problem of oblique-shock-wave reflections, the flow Mach number at the second triple point is used as a criterion for the transition from CMR to DMR. Therefore, the distance between the first triple point T and the second triple point T' (Fig. 1) can be considered as a characteristic length since the state at the second triple point depends on the relaxation process which begins at the incident shock wave. Consider the

angle δ (Fig. 10), which is the angle between the incident shock wave and the reflected shock wave. If the latter is curved then a tangential line is drawn at the triple point in order to measure δ . In this case, the length of the portion of the reflected shock wave required to draw a tangential line may be considered as another characteristic length. Define a *practical* resolved length on a photograph. (*Practical* means that it is different from the usual resolution determined from the ability to separate two close points.) The practical resolved length depends on whether the photograph is an interferogram, schlieren record or a shadowgram, and generally it is harder to see the exact position or direction of a shock wave on an interferogram than on a schlieren record or a shadowgram. It is reasonable to choose 1 mm as a practical resolved length on an interferogram under the conditions of the experiments in the present study.

Strictly, it is not possible to determine one single characteristic length for all phenomena of shock-wave reflections. The measurement of an angle has its characteristic length, which may be the shortest one, and the criterion for transition between CMR and DMR has another characteristic length, which may be the longest one in the present discussion. The two characteristic lengths differ by a factor of about 10 in a typical case. If the relaxation length has an intermediate value between these two characteristic lengths, the phenomena cannot be analysed by the simplified method used in the present report, which assumes the internal degrees of freedom as being either in equilibrium or frozen. It is reasonable to assume that the solution of this case lies between the two extreme cases.

The characteristic lengths have an uncertainty factor of about 10. It should be recalled that the relaxation process itself does not have a precise length for it takes a considerably longer distance than the relaxation length [defined as $(1 - 1/e)$ of the final value] to reach the final equilibrium state. This does not mean that an analysis based on relaxation length is uncertain. As discussed later in this section, the relaxation lengths vary easily by a factor of $10^5 \sim 10^7$ between $M_s = 2$ and $M_s = 10$ under the same initial conditions, which is much greater than the uncertainty of the characteristic length and the relaxation process. In the discussions which follow, a characteristic length of 1 mm is chosen. This is essential as the most quantitative discussion in the present report is based on the values of various angles. Since the relaxation process has a finite length, it is true that the angle must be that of the frozen-gas case in the infinitesimal vicinity of the intersection point of two shock waves. It is not possible, however, to measure the angle so close to the intersection point. In an actual measurement, at least 1 mm of a shock wave is required to measure an angle. Consequently, the δ and other angles measured are those between a tangential line in a 1 mm region when the shock wave is curved. Consequently, whether or not an actual transition of an internal degree of freedom from the frozen to the equilibrium state takes place in some finite region over the transition Mach number, is determined from the condition, whether or not its relaxation length is longer than this characteristic length.

In the present report, the frozen and equilibrium-gas assumptions are defined as follows. The frozen-gas assumption means that only the translational and rotational degrees of freedom are excited to their equilibrium values and that the internal degrees of freedom are all frozen at their initial states. That is, $\gamma = 1.667$ for Ar and $\gamma = 1.40$ for N_2 , O_2 and also for CO_2 (see Appendix A). As discussed later in this section, the internal degrees of freedom of the gases considered, other than the vibrational degrees, can be assumed as frozen at their initial states in the range of the experiments, except for high Mach numbers for CO_2 , since the relaxation lengths of the internal degrees are much longer than the defined characteristic length of the phenomena. Therefore, in this analysis only vibrational excitation is the additional internal degree of freedom required for the calculation of equilibrium-gas properties, as compared with those for a frozen gas. A fictitious perfect-gas case, which has a constant γ of 1.29 for CO_2 is also computed, even though it has no physical significance (see Appendix A). Nevertheless, the agreement of the CO_2 data (experimental and numerical) in the $(M_s - \theta_w)$ or $(M_s - \theta_w)$ planes is excellent by accident and indicates the need for better criteria for SMR \neq CMR and CMR \neq DMR transition lines.

Figure 4 shows the vibrational relaxation length of CO_2 (Ref. 17) in region 1 (the region behind the incident shock wave) at the initial conditions $p_0 = 15$ torr and $T_0 = 300$ K. The pressure, temperature and flow velocity in region 1 which are based on the frozen-gas assumption ($\gamma = 1.40$) are used in the calculation of the relaxation lengths. The relaxation length is 1 mm at $M_s = 3$. Therefore, CO_2 is considered to change its behaviour from a frozen gas to an equilibrium gas in a certain region at $M_s = 3$. Ando (Ref. 14) discussed the vibrational relaxation of CO_2 in his paper. He misinterpreted, however, the pressure behind a shock wave as an initial pressure when referring to the experimental results of Gaydon and Hurle, for example. Consequently, he obtained extremely long vibrational relaxation lengths and concluded that the vibrational degrees of freedom of CO_2 are frozen at their initial states under the conditions of his experiments.

Figure 5 shows an interferogram for CO_2 at $M_s = 2.04$, $p_0 = 50$ torr and $T_0 = 297.3$ K taken by Ando (Ref. 14). A relaxation process behind the incident shock wave can be seen clearly. The vibrational relaxation length at $M_s = 2.04$ is predicted to be about 4 mm according to Fig. 4. If the difference in the initial pressures between the case shown in the interferogram and in Fig. 4 (which are 50 torr and 15 torr, respectively) is taken into account, the relaxation length in the case of the interferogram is predicted to be about 1.3 mm. The relaxation length behind the incident shock wave in Fig. 5 is measured as 1.7 mm, which is in quite good agreement with the prediction.

The dissociational relaxation length of CO_2 for the same initial conditions as Fig. 4 is about 70 times longer than its vibrational relaxation length and is about 2 mm at $M_s = 10$ (Ref. 17). There might be some effect of dissociational excitation near $M_s = 10$ on the transition boundaries and these would have to be included for given initial conditions in calculating the boundaries.

Figure 6 shows the vibrational relaxation length of N_2 (Refs. 18, 19). The initial conditions are the same as Fig. 4 and the calculation of p_1 , T_1 and u_1 are based on a frozen-gas assumption ($\gamma = 1.4$). Although there are two experimental curves, it is probable that at Mach numbers $M_S \sim 10$ the vibrational excitation affects the flow phenomena.

Figure 7 shows an interferogram of N_2 taken by Ben-Dor (Ref. 4) at $M_S = 8.06$, which is the highest Mach number in his N_2 experiments. The initial pressure is 5.1 torr and temperature is 298.2 K. A relaxation process is seen behind the incident shock wave. (It is easier to see if a tangent line is drawn along a fringe.)

The dissociational relaxation length in the case of N_2 is much longer than its vibrational relaxation length like other gases. The dissociational relaxation length under the initial conditions of Fig. 6 is about 200 mm, even at $M_S = 15$ (Ref. 20). Therefore, the dissociation of N_2 can be neglected in the range of experiments referred to in the present report.

Figure 8 shows the vibrational relaxation length of O_2 (Refs. 18, 19). The initial conditions and the calculation of p_1 , T_1 , u_1 are the same as those in the case of N_2 . The vibrational relaxation length is 1 mm at about $M_S = 6 \sim 6.5$ from both references. The experiments referred to in the present report are not for pure O_2 but air. The vibrational relaxation length of O_2 in air may have different values from those shown in Fig. 8, as the collisions with N_2 molecules are more frequent than with O_2 . However, it is reasonable to use the value for pure O_2 since N_2 is considered to have similar collision properties to O_2 .

Figure 9 shows an interferogram of a double-Mach reflection in air at $M_S = 8.7$, $p_0 = 30.75$ torr and $T_0 = 299$ K taken by Deschambault (Ref. 21). It shows a clear relaxation process behind the incident shock wave. The relaxation length is not measured since it is difficult to determine the precise point in a finite interferogram at which the density has approached the equilibrium value by $1/e$ from the frozen value. The relaxation process seen in this interferogram is interpreted as that of N_2 because the relaxation length of N_2 at the conditions of this interferogram is predicted to be about 2 mm, from Fig. 6, which is in agreement with the relaxation length seen in the interferogram. No interferogram was available showing the relaxation process in O_2 , which occurs at a lower Mach number than that in N_2 . This is considered due to the fact that the concentration of O_2 in air is only 20%, so that the density change due to the relaxation of O_2 is probably too small to be seen in an interferogram.

The dissociational relaxation length of O_2 at $M_S = 10$, under conditions of Fig. 8, is about 30 mm (Ref. 20). Consequently, the dissociation of O_2 also can be neglected.

In the case of Ar, since Ar is a monatomic gas, there is neither vibrational excitation nor dissociation. Therefore, Ar can be treated as a frozen gas unless electronic excitation and ionization begin to take place. In the range of experiments referred to in the present report, electronic excitation and ionization can be neglected and Ar can be treated as a frozen gas.

A summary of the discussions in this section and Section 3.1 are given in Table 1.

3. RESULTS AND DISCUSSIONS

3.1 Comparison of Experimental and Calculated Results for δ

As expected, the calculated results based on the frozen-gas model differ from the equilibrium-gas model. By comparing an experimental result with the frozen or equilibrium-gas model for a given flow property, we can determine which model is valid. It is important to choose a basic quantity for comparison in order to avoid the effects of other assumptions used in the calculations. From a practical point, the chosen property should be measured easily and accurately. Needless to say, the conclusions from a comparison of models must be consistent with the discussion on relaxation lengths.

The angle δ was chosen for this purpose. As shown in Fig. 10, it is the angle between the incident and reflected shock waves. The comparison of δ is essentially equivalent to the comparison of ω' , which is the angle between the incident shock wave and the triple-point-trajectory path at angle χ (Fig. 10). The comparisons are identical if an experimental result is compared with a calculated result which has the same value of θ_W' (since $\delta = 90^\circ + \theta_W' - \omega'$). The use of δ or ω' obtained experimentally is not identical, if compared to a calculated result which has the same value of θ_W as that of the experiment, as done in the previous papers (since $\delta = 90^\circ + \theta_W + \chi - \omega'$). A knowledge of χ is then required and at present there is no precise way of calculating it. This will be discussed further. A comparison of δ has some advantages over ω' when comparing results, for δ is a monotonic function of θ_W at fixed M_S . However, ω' has a minimum point at a certain θ_W for some part of the Mach number range (Ref. 23). Also, since δ will be used as a new criterion for transition between SMR and CMR (Section 3.3), it is necessary to check the agreement between measured values of δ and the calculated results.

The important difference between the present and previous comparisons (Refs. 14, 23) is that, in the present comparison, the experimental values of δ are compared with calculated results for the same θ_W' , instead of θ_W . It is because the two incident wave angles of a Mach reflection, ϕ_0 and ϕ_3 , together with M_S show that the wave system can be derived from θ_W' and χ , respectively ($\phi_0 = 90^\circ - \theta_W'$, $\phi_3 = 90^\circ - \chi$). In the latter, the Mach stem is assumed perpendicular to the wedge surface at the triple point, which is not valid experimentally, as described in Section 3.2. However, θ_W' and χ (or ϕ_0 and ϕ_3) are not independent of each other. The three-shock theory allows us to choose only one parameter from θ_W' , χ and θ_W besides M_S . Therefore, θ_W' should be chosen as the parameter since it has a valid relation with ϕ_0 , while χ or θ_W have only an assumed Mach-stem perpendicularity relation with ϕ_3 or both ϕ_3 and ϕ_0 , respectively. Therefore, comparison with a calculation having the same θ_W as the experiment is not suitable until an accurate prediction of χ is found. Consequently, if we compare the results of an experiment with a

calculation having the same value of θ_w means, effectively, that we are comparing δ from two different trajectory directions. Comparisons using both ways are shown in Figs. 11 and 12, for the case of CO_2 .

It is important to note that the experiments which have different initial pressures have different relaxation lengths even at fixed M_S and T_0 . In addition, factors such as the magnification factor of the photograph, the direction and spacing fringes in finite-fringe interferograms and a residual initial fringe in infinite-fringe interferograms should be considered in the reduction of experimental data.

Figure 11 shows the experimental results for θ_w in CO_2 (Ref. 14) plotted in the $(\delta-M_S)$ plane. The number beside each experimental point shows the value of θ_w measured by Ando. The values of δ are determined from the given θ_w and γ . The solid lines and the broken lines are the calculated θ_w for frozen ($\gamma = 1.40$) and equilibrium CO_2 , respectively. Also a perfect-gas case ($\gamma = 1.29$) is shown by dotted lines. The experimental results show quite good agreement with the calculated results based on the equilibrium-gas assumption for the entire Mach number and θ_w ranges in which experimental data were obtained. At low Mach numbers, the difference between the calculated results of each gas model becomes so small that it is of the same order as the experimental error. This result is consistent with the conclusion in Section 2.2, that CO_2 begins to change its behaviour from a frozen gas ($\gamma = 1.40$) to an equilibrium gas at about $M_S = 3$ for $T_0 = 300$ K.

Gvozdeva et al (Ref. 16) compared their experimental results of CO_2 with their analysis in the $\theta_1^0-\theta_2^0$ plane (according to their notation, θ_1^0 and θ_2^0 are equal to our δ and θ_0 , respectively). They concluded that the imperfect gas, including vibrational excitation, showed good agreement. It is consistent with the present result although their experiments were done at only one Mach number (they quote a shock-wave velocity of 1600 m/s).

Figure 12 shows a plot using θ_w rather than θ_1^0 for the equilibrium and perfect-gas models. The frozen-gas case ($\gamma = 1.40$) was omitted as it gave results in poor agreement with experiments. The agreement is not as good as obtained in Fig. 11. This illustrates the additional errors caused by δ when using θ_w rather than θ_1^0 .

Ando (Ref. 14) compared his experimental data (replotted on Fig. 11) with several models ranging from a fictitious perfect gas ($\gamma = 1.29$) to complete equilibrium in vibration and dissociation for γ . Since he compared his experimental data with his calculated results for the same θ_w , rather than θ_1^0 , the agreement was not very good. Instead he chose to base his agreement in the $(M_S-\theta_w)$ or $(M_S-\theta_1^0)$ plane transition boundaries as indicators of agreement with analysis. In those planes the agreement is accidentally good and he concluded that the perfect-gas model ($\gamma = 1.29$) was the best. However, his comparison of θ_1^0 with imperfect-gas cases including excitation of three or four vibrational modes showed the best agreement. This contradiction was not resolved in his work. Consequently, we must conclude that the $\text{SMR} \neq \text{CMR}$ and $\text{CMR} \neq \text{DMR}$ transition lines must be replaced by new criteria such

that better agreement is obtained in the $(M_S-\theta_1^0)$ or $(M_S-\theta_w)$ planes for all tested gases.

Figure 13 shows a similar plot for N_2 of Ben-Dor's data (Ref. 4) in the $(M_S-\delta)$ plane. The number beside each experimental point shows the value of θ_w measured by Ben-Dor. In this case (and for Ar, Fig. 15) the values of δ had to be measured from the photographs in his report, since neither the values of δ nor θ_1^0 were listed. The calculated results are shown for a frozen gas ($\gamma = 1.4$) (solid lines) and a vibrationally equilibrium gas (broken lines) for each fixed θ_w . Here the agreement is not as clear-cut as in CO_2 . The experimental points lie closer to the equilibrium lines for $\theta_w = 30^\circ$ and closer to the frozen N_2 for $\theta_w = 30^\circ$.

Ando (Ref. 22) remeasured the values of θ_w for N_2 from Ben-Dor's original photographs and obtained values different from those shown in Ben-Dor's paper. All values but one obtained by Ando for θ_w have the same values, or greater, than those by Ben-Dor. The greatest difference was 1.5° . Ando's measurements are shown separately in Fig. 14. The experimental results in Fig. 14 exhibit the same general features as in Fig. 13. It is worth noting that the error in the measurements is of the same order as the difference between the frozen and equilibrium-gas cases. Consequently, a clear conclusion cannot be drawn from this comparison. However, the results do not contradict the previous discussions on relaxation lengths. Therefore, N_2 can be treated as a frozen gas ($\gamma = 1.40$) except at high Mach numbers, $M_S > 10$. However, in the case of CO_2 the error in the measurements does not play as important a role since the differences between the frozen and equilibrium-gas calculations are larger than the experimental error and points to the validity of CO_2 being in equilibrium for $M_S > 3$.

Figure 15 shows the $(M_S-\delta)$ plot for Ar derived from Ben-Dor's data (Ref. 4). As Ar is not excited over the given M_S range only the frozen-gas ($\gamma = 1.667$) results are shown as solid lines for each fixed θ_w . Good agreement is obtained with experimental results, although the experimental δ 's are slightly larger than the calculated results at higher θ_w .

Figure 16 shows the $(M_S-\delta)$ diagram based on the experiments of Deschambault (Ref. 21), in air. The solid and broken lines are the calculated results for fixed θ_w for air as a frozen ($\gamma = 1.4$) and equilibrium gas, respectively. The experimental results do not show any clear-cut picture. For example, at $\theta_w = 25^\circ$, the agreement favours the equilibrium solution up to $M_S \approx 9$. Whereas, at $\theta_w = 35^\circ$, agreement is best with the frozen line up to $M_S \approx 9$. The equilibrium lines are also favoured for $4 < M_S < 6$ at $\theta_w = 35^\circ$ and 45° . Consequently, the experimental results for air again do not show as a clear-cut experimental decision between the frozen and equilibrium-gas cases in N_2 and air. Quantitatively accurate measurements are required since the differences between the two models are not as large as in CO_2 .

It should be noted that the angle δ was calculated on the basis of conditions in state 1. However, state 2 is also involved. Conditions in state 2 depend on the wedge angle θ_w and it is

possible, for example, for state 1 to be frozen and for states 2 and 3 to be in equilibrium. Consequently, the present computer program will have to be modified and the $(M_5-\delta)$ plots will have to be corrected at a future date. Better agreement may result.

3.2 Effect of Variation of Mach-Stem Angle at Triple Point from being Perpendicular to Wedge Surface

The available analytical results for the triple-point-trajectory angle χ as a function of θ_w and M_5 are not sufficiently accurate. For example, Ando (Ref. 14) compared his predictions of χ with the experimental results [see Appendix B, Fig. B1(a)~(e) in Ref. 14]. The experimental data did not agree with his predictions based on various models of CO_2 excitation. The fictitious perfect-gas model ($\gamma = 1.29$) accidentally agreed best with the experimental data, and is inconsistent with the concepts of relaxation lengths. This inconsistency and fortuitous agreement can be partly attributed to the assumption that the Mach stem is perpendicular to the wedge surface as described below.

In the three-shock theory, the effective wedge angle θ_w^* plays an important role. That is, once a value of θ_w^* is given at a fixed M_5 , the directions of the reflected shock wave and the Mach stem are determined along with the flow variables from the solution of the three-shock theory. In this sequence, a value of the actual wedge angle θ_w is obtained if the Mach stem at the triple point is assumed perpendicular to the wedge surface. In other words, assumptions other than the perpendicular condition would give other values for θ_w^* . This means that θ_w^* is a function of θ_w including the assumption concerning the orientation of the Mach stem to the wedge surface. Therefore, the value of χ is also affected by the orientation of the Mach stem. In all previous calculations of the three-shock theory (Refs. 1, 2, 13, 23), the Mach stem was assumed perpendicular to the wedge surface although discrepancies were observed experimentally owing to the lack of a better one. This assumption is satisfied exactly at the foot of the Mach stem to meet the boundary condition that flows on both sides of the Mach stem must be along the wedge surface (neglecting the effects of the viscous boundary layer). It would also be valid at the triple point if the Mach stem were perfectly straight.

Experimentally, however, the Mach stem generally is curved and the angle ϵ between the Mach stem at the triple point and the line perpendicular to the wedge (see Fig. 10) has been found from present experiments to have a concave and convex distribution between -3° and 7.5° , respectively. Figure 17 shows an example of a Mach stem in CO_2 which is not perpendicular to the wedge surface. The angle ϵ in this case is 7.5° . Calculations using these values instead of $\epsilon = 0^\circ$ give different results for χ . The results, taking into account the effects of ϵ , were obtained graphically in order to save computer time. Therefore, the results were not obtained for all experimental cases and are given in round numbers in most cases. Table 2 shows the measured values of ϵ from existing photographs (Refs. 14, 4) and the calculated values of ϵ which are consistent with values of both θ_w^* and χ (and consequently with θ_w). The calculated values are given for the frozen, perfect

equilibrium-gas cases. The experimental results for θ_w less than 20° are not compared with calculations since for small wedge angles an error of 0.5° in χ corresponds to more than an error of 3° in ϵ . Therefore, the accuracy of the comparison is poor.

In the case of CO_2 , the equilibrium-gas case showed better agreement with experiments, contrary to the comparison based on the assumption of $\epsilon = 0^\circ$. [Calculations based on the $\epsilon = 0^\circ$ assumption agrees best with the perfect ($\gamma = 1.29$) case.] However, there are still non-negligible discrepancies between the calculated and experimental values of ϵ . In the case of N_2 , the equilibrium-gas case showed rather good agreement with experiments, which seems inconsistent with the discussion on relaxation lengths. In the case of Ar, the discrepancies between the calculated and experimental ϵ are smaller than those of N_2 or CO_2 . This is due to the fact that ϵ is close to 0° for Ar. The discrepancies which remain even if the effect of ϵ is taken into account are considered to arise from other factors. For example, the displacement thickness of the slipstream between regions 2 and 3 violates one of the boundary conditions of the three-shock theory, and is discussed in Appendix C. Unfortunately, it does not minimize the discrepancies.

It should be noted that the value of ϵ has a significant effect on the solutions, especially on χ , when they are described as functions of θ_w . It means that discussions arising from a comparison of experimental results with solutions of the three-shock theory (which includes the assumption that $\epsilon = 0^\circ$) are no longer accurate if they are made by comparing the results which have the same value of θ_w . However, the assumption that $\epsilon = 0^\circ$ does not affect the comparisons if the experimental results are compared with analysis based on the same value of θ_w^* . As noted previously, ϵ affects the values of θ_w^* , whereas solutions based on θ_w^* are independent of ϵ . Therefore, the transition boundaries, except for $\text{RR} \neq \text{MR}$, are more accurate in the $(M_5-\theta_w^*)$ plane than in the $(M_5-\theta_w)$ plane as long as the available predictions of χ remain imprecise. However, the $(M_5-\theta_w^*)$ plane suffers from the limitations that the transition boundary lines are too close together, especially at higher M_5 , and it is more difficult to differentiate between frozen and equilibrium-gas boundaries as well as to determine if experiment and analysis of the various regions are in agreement. In addition, the $(M_5-\theta_w^*)$ plane has a multi-valued portion near the $\text{RR} \neq \text{MR}$ boundary as described in Section 3.4. A precise analytical determination of χ is therefore a much needed future requirement.

3.3 A New Additional Criterion for Transition From SMR to CMR

In the previous sections, it was concluded that CO_2 behaves as a gas in equilibrium except at low Mach numbers. As shown in Fig. 18 there are significant discrepancies between the experimental data of the three types of MR and the calculated transition boundaries based on an equilibrium-gas assumption. These discrepancies are considered as arising from inappropriate transition criteria. The criteria $M_{2T} > 1$ and $M_{2K} > 1$ are only necessary conditions for the transitions. The existence of other necessary conditions for the transition from SMR to CMR may push the boundary line into the CMR

region and the CMR to DMR line into the DMR region. This would improve the agreement significantly.

Complex-Mach reflection has been characterized by the existence of a band of compression waves at the kink behind the reflected shock wave whether it can be seen in an interferogram or not (Refs. 10, 16). The condition for the existence of a band of compression waves may be related to the angle δ between the incident shock wave I and the reflected shock wave R at the triple point T (Fig. 10), as follows.

Experimental results (Ref. 24) have shown that the ratio between the distance from the wedge corner to the kink along the horizontal line ℓ and the distance from the wedge corner to the incident shock wave along the horizontal line L is equal to the ratio between the flow velocity behind the incident shock wave (in the laboratory frame) u_1 and the incident shock-wave velocity u_{s1} , except for wedge angles near the RR boundary. That is, $\ell/L = u_1/u_{s1}$ (see Fig. 19a). In other words, the kink is moving with the flow velocity in region 1 as far as the horizontal component is concerned. Therefore, it is seen that the flow velocity in region 1 relative to the kink has only a vertical component. This means that the flow moves downward (or parallel to the incident shock wave) as seen from a frame of reference attached to the kink (Fig. 19b).

If we call the incident angles and the densities behind the reflected shock wave on either side of the kink as ϕ_{1K} , ϕ_{2K} , ρ_1 , ρ_2 , as illustrated in Fig. 19c, then the existence of a band of compression waves is equivalent to the relation of $\phi_{1K} > \phi_{2K}$ and is also equivalent to $\phi_{1K} - 90^\circ > \phi_{2K} - 90^\circ$ because the flow variables upstream on either side of the kink are the same. This means that the closer to 90° to the shock front that the incident streamlines are, the stronger the shock wave, and consequently the greater the density change across the wave. There are four possible geometrical inclinations for the reflected shock wave on either side of the kink as illustrated in Fig. 19d. (It must be remembered that a configuration which has a convex angle to the upstream flow direction cannot maintain a sharp corner like a kink. Only configurations A and B of the four satisfy the condition $|\phi_{1K} - 90^\circ| > |\phi_{2K} - 90^\circ|$, and in both A and B the angle δ is greater than 90° . Therefore, $\delta > 90^\circ$ is considered a necessary condition for the existence of a band of compression waves, which is required for the transition to CMR. (It is only a necessary condition because configuration C, which does not satisfy the condition $|\phi_{1K} - 90^\circ| > |\phi_{2K} - 90^\circ|$, also has $\delta > 90^\circ$.)

Figure 20 shows a plot of the experimental values of δ with shock Mach number M_s for the various types of reflections for N_2 , Ar, CO_2 and air. All experimental CMR but one in CO_2 lie below the $\delta = 90^\circ$ line, which means that they satisfy the condition $\delta > 90^\circ$. This provides good evidence that $\delta > 90^\circ$ is a necessary condition. It must be pointed out that results in Fig. 20 do not include any calculation or assumptions. They show only the experimental relation between the SMR \neq CMR boundary line and δ . It means that this is a direct comparison between the new necessary condition and the experimental data.

As mentioned, the new condition for transition $\delta > 90^\circ$ is only a necessary condition. Therefore,

the condition $M_{2T} > 1$ remains along with the new condition. The transition takes place when both of these two conditions are satisfied. Consequently, the term *new criterion* quoted below includes both necessary conditions, and the criterion $M_{2T} > 1$ is the *former criterion*.

Figure 21 shows a transition boundary plot for equilibrium CO_2 in the $(M_s - \theta_w)$ plane with emphasis on the SMR \neq CMR transition. The solid line shows the *new criterion* and the broken line shows the *former criterion* $M_{2T} = 1$. One of the two SMR points which was calculated in the CMR region of the former criterion now lies in the SMR region of the new criterion.

Figure 22 shows a similar transition boundary plot in the $(M_s - \theta_w)$ plane of frozen N_2 and air emphasizing the SMR \neq CMR transition. The solid line and the broken line show the transition boundaries between SMR and CMR based on the *new criterion* and the *former criterion*, respectively. Most of the SMR points which were previously in the CMR region now fall into the SMR region of the new criterion. The experimental distribution of SMR and CMR show very good agreement with the new criterion line except for two points in air at $M_s \approx 8$. This tendency is consistent with the discussion on vibrational relaxation lengths for O_2 and N_2 . Figure 23 shows the calculated transition boundary lines of the new criterion for frozen (solid line) and equilibrium air (broken line). It can be seen clearly in this figure that the experimental boundary of air between SMR and CMR approaches the equilibrium-air line at high Mach numbers.

Figure 24 shows the calculated lines for $M_{2T} = 1$ and $\delta = 90^\circ$ for Ar. In this case, the $\delta = 90^\circ$ line lies below the $M_{2T} = 1$ line for $M_s \approx 6$ and slightly above for $M_s \approx 6$. The addition of the condition $\delta > 90^\circ$ makes little difference since the region above both lines satisfies both necessary conditions and therefore the line which lies above is the new transition line, which is close to the $M_{2T} = 1$ line in this case.

It can be concluded that the new criterion, composed of conditions $M_{2T} > 1$ and $\delta > 90^\circ$, gives a transition boundary line between SMR and CMR which agrees well with the distribution of experimental points for all gases tested using calculations consistent with δ and relaxation lengths.

There are also discrepancies in the transition boundaries between CMR and DMR. In the case of CO_2 , for example, as shown in Fig. 18, the equilibrium-gas assumption gives a CMR \neq DMR transition boundary line which is not in good agreement with the experimental result if the boundary line is based on the criterion $M_{2K} < 1$. Results for other gases also have discrepancies. Perhaps an additional necessary criterion is required in the case of the transition from CMR to DMR. However, no additional criterion ($M_{2K} < 1$ is one of the necessary conditions) has been found so far. Some comments on this problem are given in Appendix D.

It should also be noted that the CMR \neq DMR transition line is based on the assumption that the distance $(L - \ell)$ between the two triple points T and T' (see Fig. 19a) remains finite. As noted above, this is a reasonable assumption for the gases investigated as long as $\theta_w \leq 40^\circ$ and $M_s \geq 2$.

That is, beyond this region it is found experimentally that the second triple point T' approaches and merges with the first triple point T (Refs. 13, 15). Consequently, the $CMR \neq DMR$ line approaches and becomes coincident with the $SMR \neq CMR$ line at the $RR \neq MR$ boundary at point P , as illustrated in Fig. 25. No analytical solution has been found for this behaviour. It can be seen that an experimentally drawn line in this region results in much better agreement with the remaining data in the CMR and DMR region.

3.4 Persistence of Regular Reflection (RR) into the Region of Mach Reflection (MR) - von Neumann's Paradox

Experimental results show that RR persists beyond the $RR \neq MR$ boundary of the detachment criterion. Figure 26 shows the persistence of RR in the case of CO_2 . In this figure, the experimental points are plotted in the $(M_S - \theta_W)$ plane instead of the $(M_S - \theta'_W)$ plane since it has a multi-valued portion near the $RR \neq MR$ boundary. [At the RR boundary of the MR region, χ has a finite value. Therefore, $\theta'_W = \theta_W + \chi$ has a larger value than θ_W at the boundary. On the other hand, θ'_W is equal to θ_W in the RR region. Consequently, the $RR \neq MR$ boundary corresponds to two separate lines (θ_W and $\theta_W + \chi$) in the $(M_S - \theta_W)$ plane. A point between these two lines in the $(M_S - \theta_W)$ plane corresponds to two physical points, one in RR and the other in MR .] Therefore, a discussion on the persistence of RR is best made in the $(M_S - \theta_W)$ plane, unlike the boundaries in the MR region which are best described in the $(M_S - \theta'_W)$ plane (see Section 3.2). This inconsistency can be removed in the future if an accurate prediction of χ can be found, then the $(M_S - \theta_W)$ plane could be used throughout. As can be seen in Fig. 26, RR persists down to $\theta_W = 42^\circ$ at $M_S = 7.2$. The persistence depends on M_S and the data points are well below the boundary of the detachment criterion. However, the experimental boundary is not unique. In $2 < M_S < 3$, DMR points were obtained at $\theta_W = 48^\circ$ in Ref. 26. In Ref. 22, RR points were again obtained at a lower wedge angle of $\theta_W = 47^\circ$. This fact suggests that the extent of the persistence depends on factors other than M_S and θ_W . Figure 27 shows the persistence of RR in the case of air. No unique experimental boundary exists in this case also, despite the fact that the persistence is very apparent.

Hornung et al (Ref. 11) suggest that the persistence of RR could be explained in terms of the viscous boundary layer which develops behind the reflection point P (Fig. 28) on the wedge surface. In the viscous boundary layer produced after the passage of the reflection point, the flow has progressively lower velocities (and is zero at the wall) than the flow in the free stream in a laboratory frame. However, the flow in the boundary layer has higher velocities than the flow outside in a reference frame attached to the reflection point. This corresponds to the fact that the wedge surface is moving with a velocity equal and opposite to the incident shock speed from the reflection point P . As a result, the displacement thickness of the boundary layer has a negative value (see Fig. 28). Therefore, the deflection angle through the reflected shock wave is less than required without the boundary layer. The displacement angle θ_d , or the angle between the flow affected by the boundary layer and the actual wedge surface, enables RR to persist to lower wedge angles because

the point at which the deflected angle through the reflected shock wave increases to the maximum deflection angle and θ_{2m} is now lower than that without the displacement angle. It should be pointed out that the displacement angle is not equal to the difference in the transition wedge angle caused by the boundary-layer effect. In fact, the displaced wedge has a larger inclination despite the fact that the displacement effect lowers the transition wedge angle and also the wedge angle in front of the incident shock wave is still equal to the actual wedge angle θ_W . Since the reflected shock wave is of the weak family of the two possible solutions, the angle ω' is smaller than the one without a boundary layer. Hornung et al (Ref. 11) mentioned that the opposite was observed experimentally. However, the present analysis of previous experiments gives a smaller ω' than obtained from a calculation without the boundary-layer displacement effect, as expected.

The angle ω' is a very good indicator of the boundary-layer displacement. Figure 29 shows a $(M_S - \omega')$ plot for CO_2 experiments (Refs. 14, 22) compared with calculations using several displacement angles. There are no analytical solutions of ω' above the lines corresponding to the $RR \neq MR$ transition boundaries (for each θ_d). The experimental ω' are smaller than those for $\theta_d = 0^\circ$. The differences from the calculated line $\theta_d = 0^\circ$ are larger when the wedge angle is lower, in other words, closer to the MR region. This agrees qualitatively with the analytical fact that the effect of the boundary-layer-displacement angle on ω' becomes smaller at higher wedge angles. The experimental results agree with a displacement angle of $\theta_d = -1^\circ \sim -2^\circ$. A quantitative discussion of this value is given subsequently. Figure 30 shows similar experimental results for air and N_2 . For simplicity, only experimental points of $\theta_W = 50^\circ$ are plotted and compared with calculations. In the case of air, the comparison is complicated because air and N_2 changes from a frozen to an equilibrium gas at an intermediate Mach number. (The reason why the frozen line $\theta_d = 0^\circ$ does not exist at high Mach number is that $\theta_W = 50^\circ$ with $\theta_d = 0^\circ$ (frozen) is in the MR region.) At lower Mach numbers, the experimental results agree approximately with the calculation for a frozen gas with $\theta_d = -1^\circ$. At higher M_S , the tendency is for the points to approach the equilibrium lines. Experimental points for other θ_W are compared with the $\theta_d = -1^\circ$ case for frozen and equilibrium air in Fig. 31. Other θ_W show a behaviour similar to the case of $\theta_W = 50^\circ$. Figure 32 shows the results for Ar. The two available experimental points agree with the calculation of $\theta_d = -2^\circ$.

For a complete analysis, the displacement angles must be based on boundary-layer theory (Ref. 29). It is not possible to obtain a unique displacement angle even if the initial pressure is given. The displacement thickness itself can be calculated and is shown in Table 3 for the case of air. The displacement thickness is proportional to \sqrt{x} , which means that the slope of the displacement thickness, which is proportional to $1/\sqrt{x}$, becomes infinite in the limit as $x \rightarrow 0$. In other words, arbitrary angles can be obtained by choosing a distance from the reflection point in which the mean slope is calculated. Here we face a problem similar to the choice of a characteristic length in Section 2.2. An appropriate distance should be chosen as the distance for calculating a mean slope. It is

reasonable to choose 1 mm as the distance, similar to the case of the relaxation length. The mean slopes for 1 mm are given in Table 3 for the RR \neq MR boundary in air. The angles lie between -1° and -2° and are in good agreement with the present comparison.

The RR \neq MR transition boundary lines with several boundary-layer-displacement angles θ_d are compared with the experimental persistence of RR in Figs. 26 and 27 for CO_2 and air, respectively. In the case of CO_2 , a displacement angle of -1° changes the transition boundary by about 0.5° . All experimental RR are above the equilibrium-gas case of $\theta_d = -2^\circ$. At about $M_5 = 2$, which is in the region where CO_2 could be a frozen gas, RR persist below $\theta_d = -4^\circ$ of the frozen-gas case and they seem to correspond to about $\theta_d = -5^\circ$. The transition from RR to MR is dominated by the flow at the reflection point. Although it is meaningless to assume that the flow properties in the infinitesimal vicinity of the reflection point determines the reflection phenomena, the region which dominates the phenomena is considered to be much less than 1 mm, which is the characteristic length chosen in the discussion on relaxation lengths. Consequently, the Mach number at which vibrational-excitation effects begin to take place in the transition is higher than $M_5 = 3$. For the same reason, the displacement angle which dominates the transition must have a different value, which is larger than that for a change in the angle ω' . Since the size of the region which dominates the reflection phenomena is not known, no further quantitative comparison is possible. The variation of pressures must be taken into account in this discussion, even in the frozen-gas case, since the thickness of the boundary layer depends on the pressure or Reynolds number. Figure 27 shows the same comparison for air. Since air behaves as a frozen gas in the region shown in Fig. 27, only the frozen-gas cases are shown. Regular reflection (RR) persists down to the transition line of $\theta_d = -2^\circ$ at lower Mach numbers and $\theta_d = -4^\circ$ at higher Mach numbers. A further quantitative analysis is not possible for the reasons already given for CO_2 .

Detailed calculations of the flow quantities in the various states generated by pseudo-stationary oblique-shock-wave reflections in tabular form, for the convenience of the researcher, can be found in Ref. 30.

4. CONCLUSIONS

The recent results on pseudo-stationary oblique-shock-wave reflections were assessed based on criteria associated with molecular relaxation lengths, the basic angle δ between the incident shock wave and the reflected shock wave and transition boundaries in the $(M_5 - \theta_w')$ plane.

The following conclusions apply in the range $1 < M_5 < 10$; at Mach numbers lower than 3, CO_2 behaves as a frozen gas ($\gamma = 1.40$) and as an equilibrium gas with vibrational excitation for $M_5 > 3$; nitrogen and air are frozen ($\gamma = 1.40$) below $M_5 = 6 \sim 9$, depending on the initial pressure; argon is frozen in the present Mach number range. Dissociation and ionization can be neglected (except for CO_2 at lower pressures) up to $M_5 = 10$.

The curvature of the Mach stem affects the triple-point-trajectory angle χ significantly. This discrepancy accounts for most of the inaccuracies of predicting χ . There are, however, still non-negligible discrepancies between the experimentally-measured χ and the calculated χ even if the effect of Mach-stem curvature is taken into account.

The condition that the angle between the incident shock wave and the reflected shock wave is greater than 90° is an additional necessary condition for the transition from SMR to CMR. The addition of the new criterion improves the agreement between analysis and experiments.

The persistence of RR is explained in terms of the induced viscous boundary layer on the wedge surface. The measured reflected-wave angles ω' agree with the calculated values which take into account the boundary-layer-displacement effect. The value of the boundary-layer-displacement angle θ_d necessary to explain the persistence of RR is reasonable compared with the calculation of ω' . Rigorous quantitative predictions are difficult owing to the uncertainty in calculating the boundary-layer-displacement angle.

Large discrepancies at the CMR \neq DMR boundary between calculated and experimental results remain. In addition, the experimental results show that the CMR \neq DMR line and the SMR \neq CMR line merge at the RR line due to the merging of the two triple points in DMR. An analytical prediction for this effect is not available. Analytical predictions for Mach-stem curvature and its relation to the triple-point-trajectory angle χ at low shock Mach numbers are also required.

REFERENCES

1. Ben-Dor, G., Glass, I. I., "Domains and Boundaries of Non-Stationary Oblique Shock-Wave Reflexions. 1. Diatomic Gas", J. Fluid Mech. 92, 1979, p. 459.
2. Ben-Dor, G., Glass, I. I., "Domains and Boundaries of Non-Stationary Oblique Shock-Wave Reflexion. 2. Monatomic Gas", J. Fluid Mech. 96, 1980, p. 735.
3. Ben-Dor, G., "Regions and Transitions of Non-Stationary Oblique Shock-Wave Diffractions in Perfect and Imperfect Gases", UTIAS Report No. 232, 1978.
4. Ben-Dor, G., "Nonstationary Oblique-Shock-Wave Reflections in Nitrogen and Argon: Experimental Results", UTIAS Report No. 237, 1978.
5. Mach, E., Akad. Wiss. Wien 77, II, 1878, p. 1228.
6. Smith, L. G., "Photographic Investigation of the Reflection of Plane Shocks in Air", OSRO Report No. 6271, 1945.
7. White, D. R., "An Experimental Survey of the Mach Reflection of Shock Waves", Tech. Rep. II-10, Dept. of Physics, Princeton University, 1951.

8. von Neumann, J., "Oblique Reflection of Shocks", Explosives Research Report No. 12, Department of the Navy, Bureau of Ordnance, 1943.
9. Liepmann, H. W., Roshko, A., "Elements of Gas-dynamics", John Wiley, New York, 1957.
10. Henderson, L. F., Lozzi, A., "Experiments on Transition of Mach Reflexion", J. Fluid Mech. 68, 1975, p. 139.
11. Hornung, H. G., Oertel, H., Sandeman, R. J., "Transition of Mach Reflection of Shock Waves in Steady and Pseudosteady Flow With and Without Relaxation", J. Fluid Mech. 90, 1979, p. 541.
12. Ben-Dor, G., Takayama, K., Kawauchi, T., "The Transition from Regular to Mach Reflexion and from Mach to Regular Reflexion in Truly Non-Stationary Flows", J. Fluid Mech. 100, 1980, p. 147.
13. Ando, S., Glass, I. I., "Domains and Boundaries of Pseudostationary Oblique-Shock-Wave Reflections in Carbon Dioxide", 7th Int. Symp. of Military Applications of Blast Simulation, 1981.
14. Ando, S., "Pseudo-Stationary Oblique Shock-Wave Reflection in Carbon Dioxide - Domains and Boundaries", UTIAS Tech. Note No. 231, 1981.
15. Bazhenova, T. V., Fokeev, V. P., Gvozdeva, L. G., "Regions of Various Forms of Mach Reflection and Its Transition to Regular Reflection", Acta Astronautica 3, 1976, p. 131.
16. Gvozdeva, L. G., Bazhenova, T. V., Predvoditeleva, O. A., Fokeev, V. P., "Mach Reflection of Shock Waves in Real Gases", Astronautica Acta 14, 1969, p. 503.
17. Camac, M., "CO₂ Relaxation Processes in Shock Waves", AVCO Research Report 194, 1965.
18. Lifshitz, A., "Shock Waves in Chemistry", Marcel Dekker, New York, 1981.
19. Vincenti, W. G., Kruger, C. H., Jr., "Introduction to Physical Gas Dynamics", Wiley, New York, 1965.
20. Logan, J. G., Jr., "Relaxation Phenomena in Hypersonic Aerodynamics", IAS Preprint No. 728, presented at the 25th Annual Meeting, 1957.
21. Deschambault, R. L., University of Toronto, M.A.Sc. Thesis (to be published).
22. Ando, S., Private Communication.
23. Lee, J.-H., Glass, I. I., "Domains and Boundaries of Pseudo-Stationary Oblique Shock-Wave Reflections in Air", UTIAS Report No. 262, 1982.
24. Law, C. K., Glass, I. I., "Diffraction of Strong Shock Waves by a Sharp Compressive Corner", CASI Transactions 4, 1971, p. 2.
25. Deschambault, R. L., Private Communication.
26. Matsuo, K., Aoki, T., Kondo, N., Harada, T., "An Experimental Study on Shock-Wave Reflections on an Inclined Wall", Preprint of the Symp. on Shock Waves, 1981, p. 96 (in Japanese).
27. Bleakney, W., Taub, A. H., "Interaction of Shock Waves", Rev. of Modern Phys., 21, 1949, p. 584.
28. Henderson, L. F., "On the Whitham Theory of Shock-Wave Diffraction at Concave Corners", J. Fluid Mech. 99, 1980, p. 801.
29. Mirels, H., "Laminar Boundary Layer Behind Shock Advancing into Stationary Fluid", NACA Tech. Note NO. 3401, 1955.
30. Shirouzu, M., "Flow Properties of Pseudo-Stationary Oblique-Shock-Wave Reflections: Numerical Results", UTIAS Tech. Note No. 239, 1982.
31. Glass, I. I., Hall, J. G., Handbook of Supersonic Aerodynamics, NAVORD Report No. 1488, Vol. 6, Section 18, Shock Tubes, U.S. Government Printing Office, Washington, D.C., 1959 (out of print).

Table 1

Range of experimental pressure and shock Mach number
where gases can be treated as frozen or equilibrium
for oblique-shock-wave reflections

Gas	Frozen	Equilibrium
CO ₂	M _s < 3*	M _s > 3*
N ₂	M _s < 9*	M _s > 9*
Air	M _s < 6**	M _s > 6**
Ar	Whole range	—

*at p₀ = 15 torr

**at p₀ = 50 torr

Table 2

Comparison of calculated and experimental values of ε
(experimental values are measured from Ref. 14, 4)

Gas	θ _w (deg)	M _s	ε (exp) (deg)	Frozen (deg)	ε (cal) Perfect (deg)	Equilibrium (deg)
CO ₂	20.3	4.72	7.5	-0.5	1.5	3.5
	20.3	6.0	6.5	-1.0	1.0	3.5
	20.3	10.18	4.5	-0.5	1.5	4.5
	27.1	1.78	-1.0	-5.5	-3.0	-2.0
	27.1	2.50	4.0	-2.0	0.0	1.0
	27.1	3.47	5.5	0.0	1.5	3.0
	27.1	4.05	4.0	-0.5	1.0	2.5
	27.1	8.16	6.5	-1.0	1.0	3.5
	30.1	2.04	2.0	-3.0	-1.0	0.0
	30.1	3.44	4.5	0.0	1.5	2.5
	30.1	6.32	6.0	-0.5	1.0	3.0
	30.1	8.30	7.0	0.0	1.5	3.5
	30.1	9.77	6.5	-2.0	0.0	2.5
N ₂	20	1.93	0.0	-5.0	—	-4.5
	20	3.74	2.0	1.0	—	2.0
	20	4.81	5.0	2.5	—	4.0
	20	6.87	4.0	2.0	—	4.0
	30	1.97	0.0	-1.0	—	1.0
	30	3.68	2.0	1.5	—	2.0
	30	5.93	3.0	1.5	—	3.0
	30	7.97	4.0	0.5	—	2.0
Ar	20	2.00	-2.0	-2.5	—	—
	20	4.40	0.5	0.0	—	—
	20	5.20	0.0	-0.5	—	—
	20	7.76	0.5	0.0	—	—
	30	2.03	-2.5	-2.0	—	—
	30	4.51	0.5	0.0	—	—
	30	6.36	0.0	0.5	—	—
	30	8.01	1.0	0.0	—	—
	40	2.05	0.0	1.0	—	—
	40	5.28	0.5	-1.0	—	—
	40	6.02	1.0	-1.0	—	—

Table 3

Boundary-layer-displacement thickness δ^* and boundary-layer-displacement angle θ_d
on wedge surface

(frozen air at RR \neq MR boundary, $p_0 = 15$ torr, $T_0 = 300$ K, based on Ref. 29)

M_s	δ^*/\sqrt{x} $\text{cm}^{-1/2}$	θ_d° (mean value over 1 mm)
1.2	-5.83×10^{-3}	-1.06
1.4	-6.74×10^{-3}	-1.22
1.6	-6.82×10^{-3}	-1.24
1.8	-6.94×10^{-3}	-1.26
2.0	-6.90×10^{-3}	-1.25
2.5	-6.79×10^{-3}	-1.23
3.0	-6.85×10^{-3}	-1.24
4.0	-7.10×10^{-3}	-0.29
5.0	-7.55×10^{-3}	-1.37
7.0	-8.41×10^{-3}	-1.52
10.0	-9.84×10^{-3}	-1.78

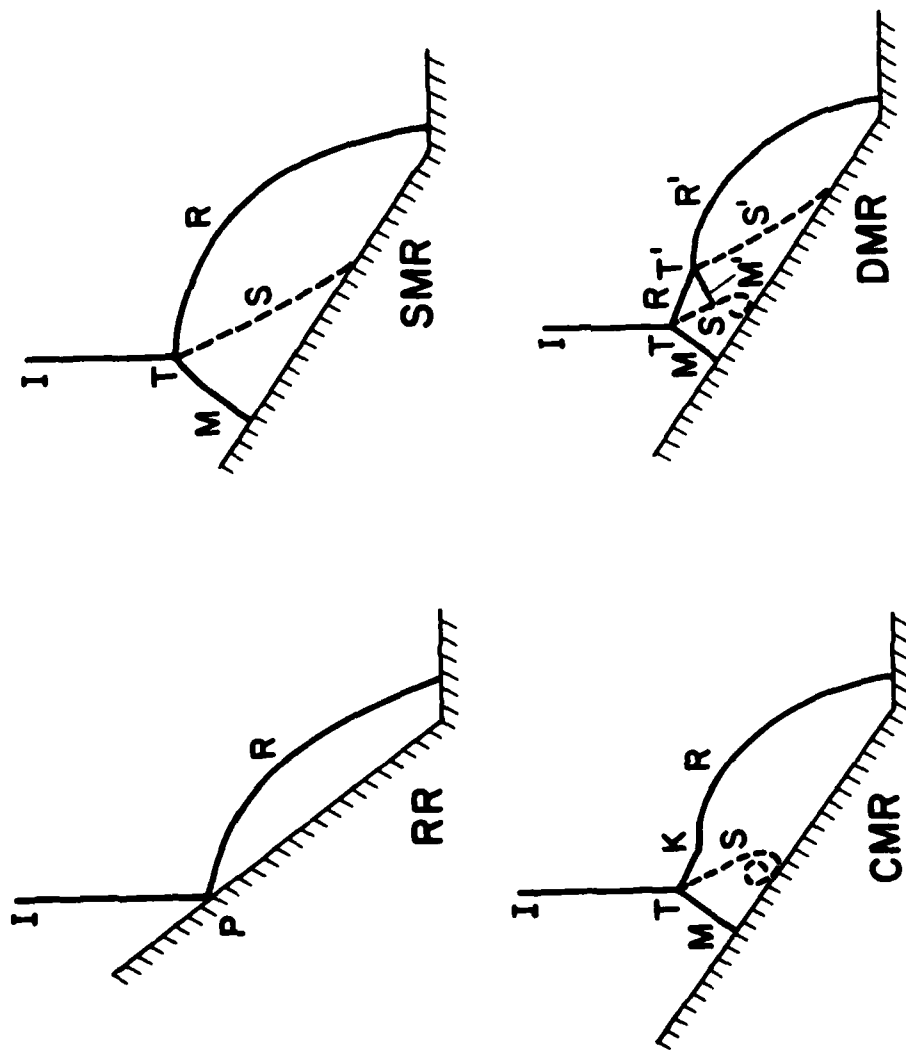



FIG. 1 FOUR TYPES OF OBLIQUE-SHOCK-WAVE REFLECTION IN PSEUDO-STATIONARY FLOWS (SCHEMATIC).

— SHOCK WAVE; - - - - SLIPSTREAM;  WALL OR WEDGE;
 I - INCIDENT SHOCK WAVE; R, R' - REFLECTED SHOCK WAVE;
 S, S' - SLIPSTREAM; M, M' - MACH STEM; P - REFLECTION POINT;
 T - TRIPLE POINT; K - KINK; T' - SECOND TRIPLE POINT.

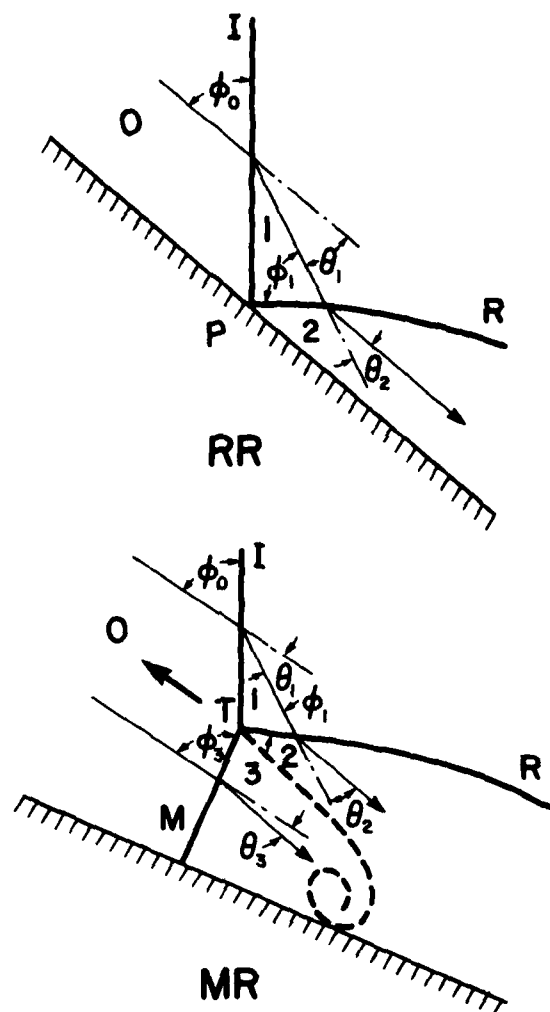


FIG. 2 REGULAR AND MACH REFLECTIONS IN STATIONARY COORDINATES WITH RESPECT TO POINTS P AND T, RESPECTIVELY.

0, 1, 2, 3 - REGIONS; I - INCIDENT SHOCK WAVE; R - REFLECTED SHOCK WAVE; M - MACH STEM; P - REFLECTION POINT; T - TRIPLE POINT; θ - DEFLECTION ANGLE; ϕ - WAVE ANGLE; WEDGE; \rightarrow - FLOW DIRECTION; ----- SLIPSTREAM; \leftarrow - DIRECTION OF TRIPLE-POINT PATH.

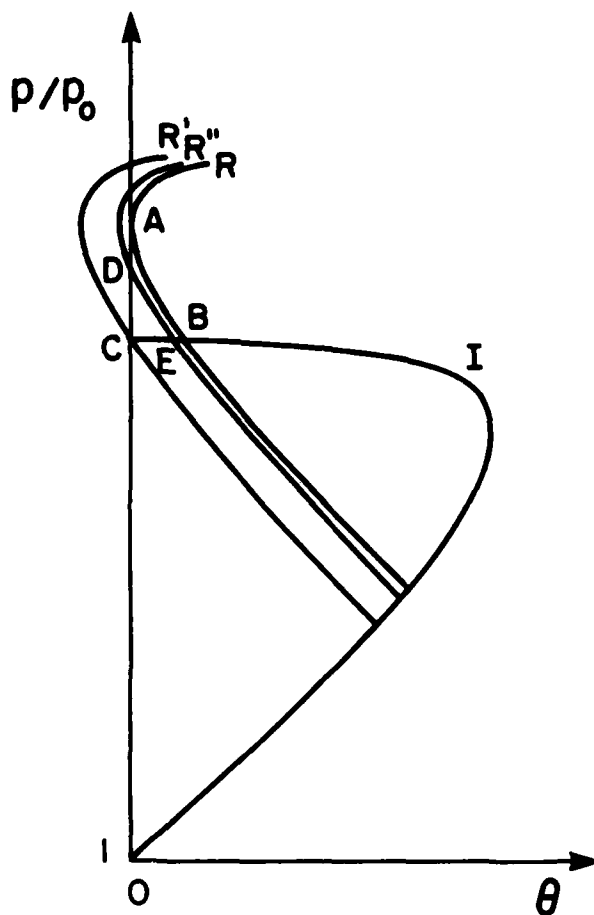


FIG. 3 SHOCK-POLAR ILLUSTRATING $RR \rightleftharpoons MR$ TRANSITION BASED ON THREE DIFFERENT CRITERIA.

I - INCIDENT SHOCK WAVE; R, R', R'' - REFLECTED SHOCK WAVE AT $RR \rightleftharpoons MR$ TRANSITION (R - DETACHMENT CRITERION AT A \rightarrow B; R' - MECHANICAL-EQUILIBRIUM CRITERION AT C; R'' - SONIC CRITERION AT D \rightarrow E); A, B, C, D, E - STATES BEHIND REFLECTED SHOCK WAVE AT $RR \rightleftharpoons MR$ TRANSITION (A - RR STATE OF DETACHMENT CRITERION; B - MR STATE OF DETACHMENT CRITERION; C - RR AND MR STATE OF MECHANICAL-EQUILIBRIUM CRITERION; D - RR STATE OF SONIC CRITERION; E - MR STATE OF SONIC CRITERION).

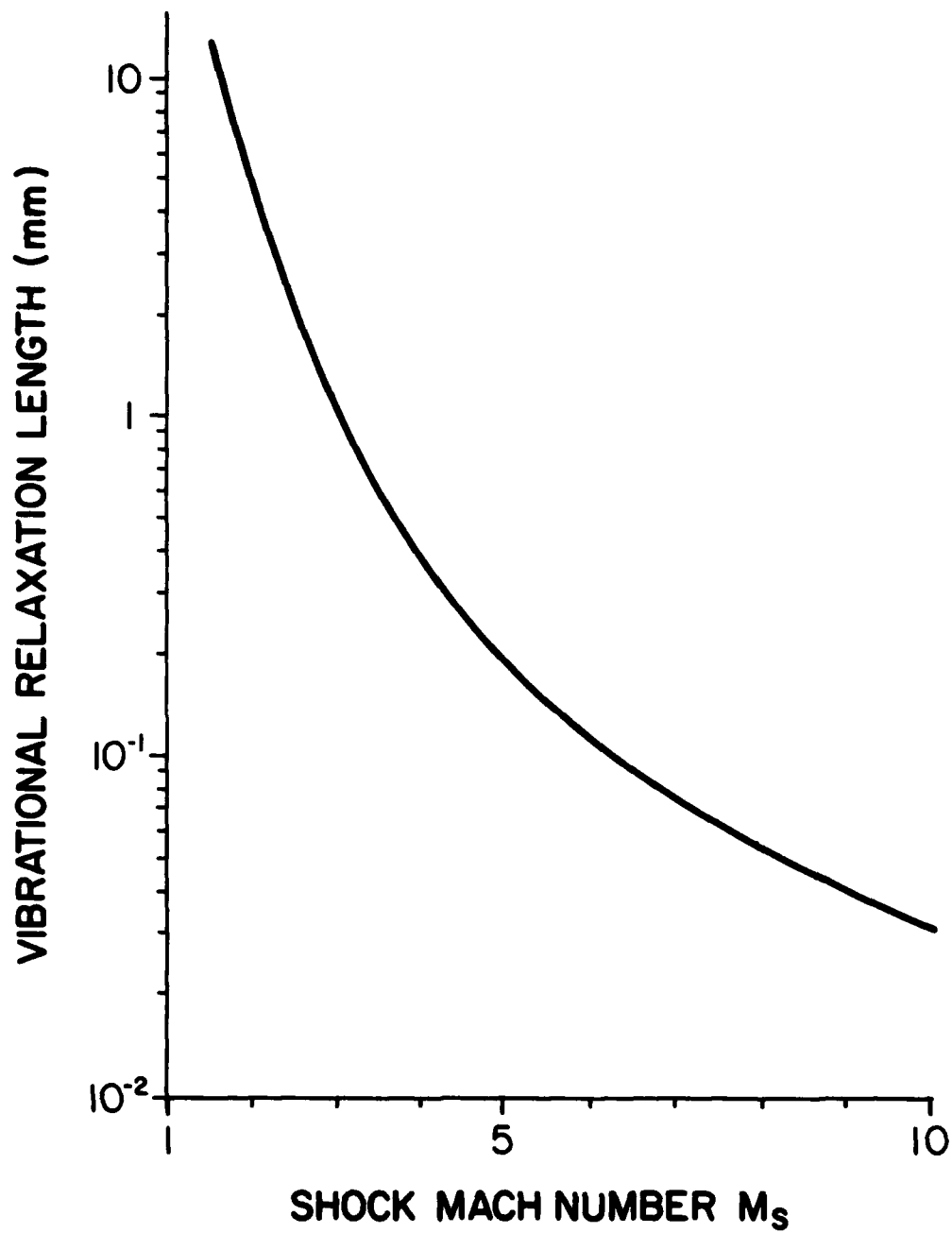


FIG. 4 VIBRATIONAL RELAXATION LENGTHS BEHIND SHOCK WAVES IN CO_2 .
INITIAL CONDITIONS: $p_0 = 15$ TORR, $T_0 = 300$ K (REF. 17).
FOR HIGHER OR LOWER INITIAL PRESSURES AT 300 K THE RELAXATION
LENGTHS ARE PROPORTIONATELY DECREASED OR INCREASED, RESPECTIVELY.

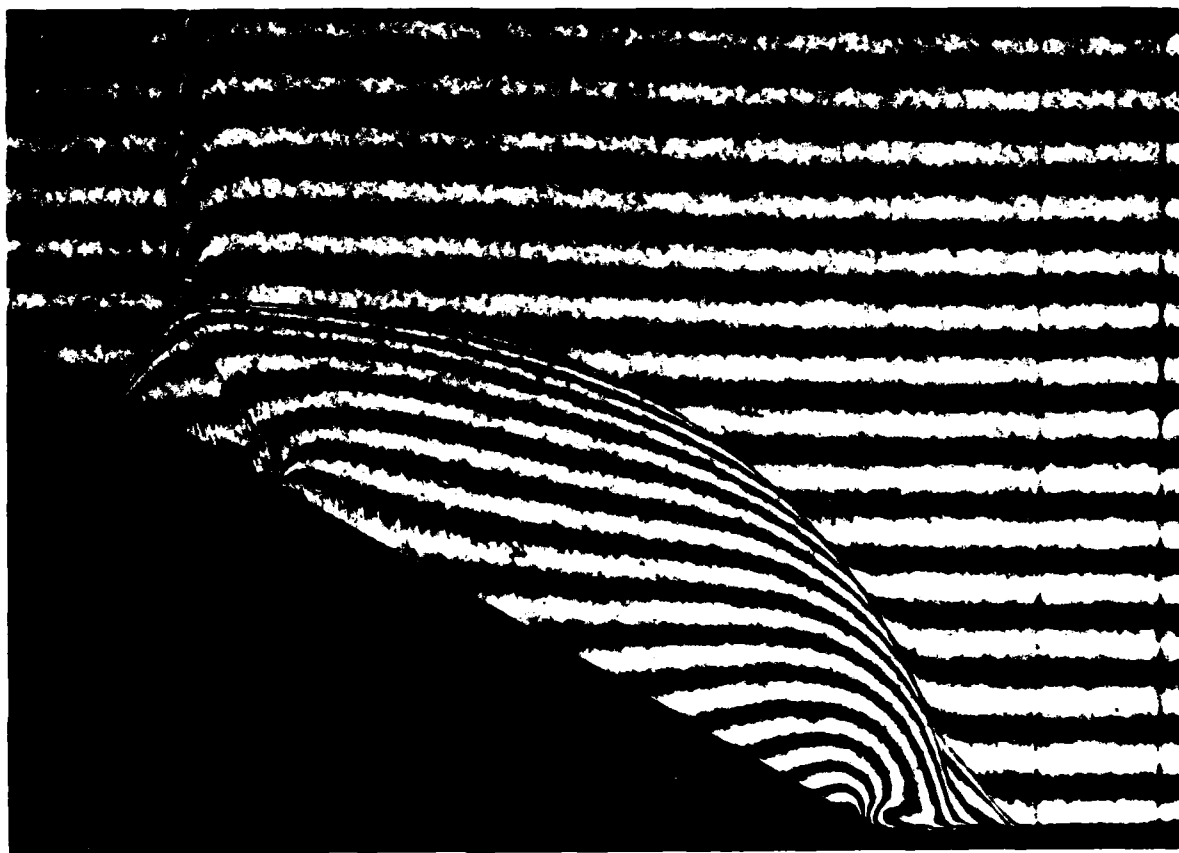


FIG. 5 SINGLE-MACH REFLECTION IN CO_2 SHOWING VIBRATIONAL RELAXATION
PROCESS BEHIND INCIDENT SHOCK WAVE (FINITE-FRINGE INTERFEROGRAM).
 $\theta_w = 30^\circ$, $M_s = 2.04$, $p_0 = 50$ TORR, $T_0 = 297.3$ K (REF. 14).

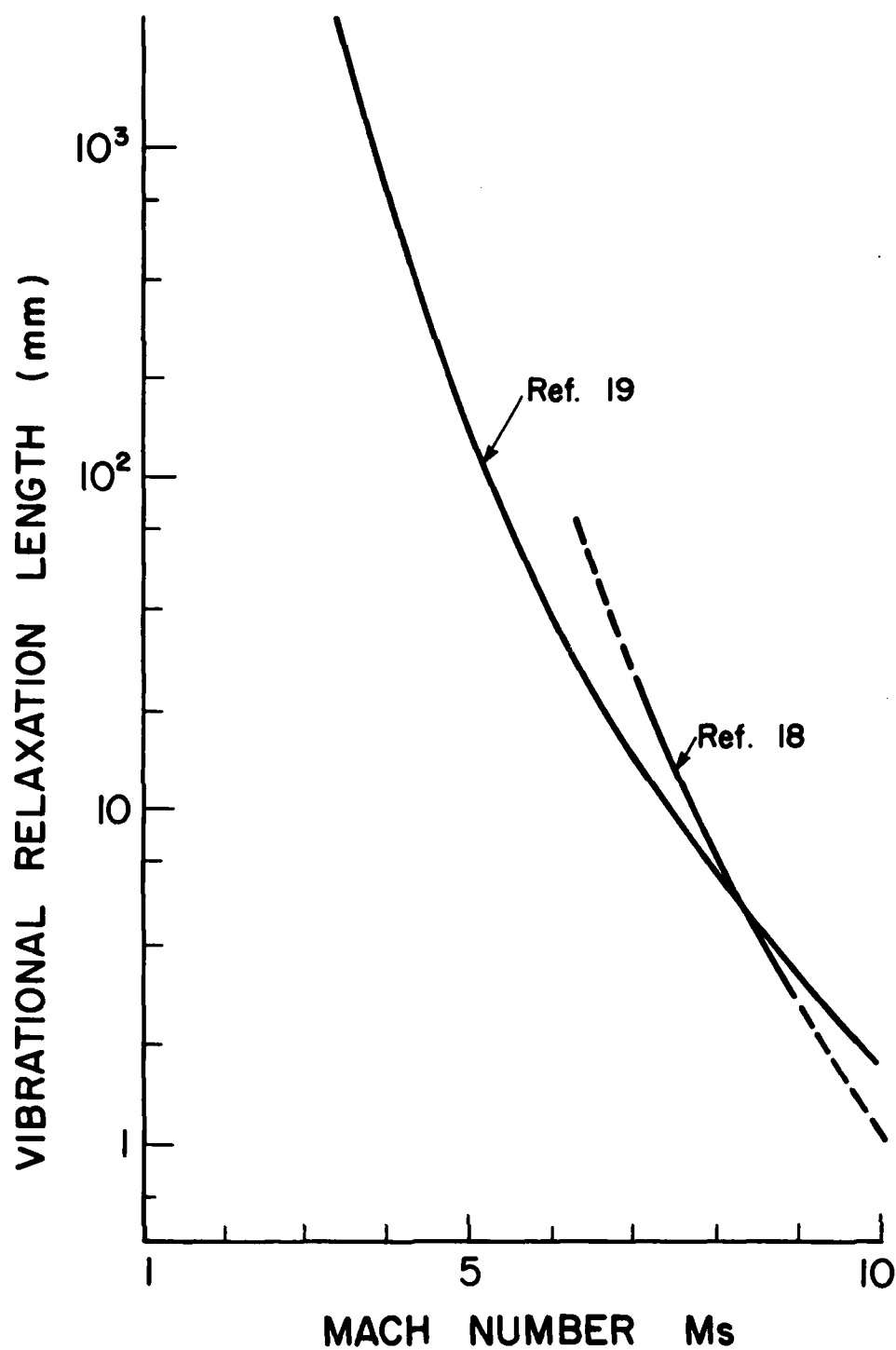


FIG. 6 VIBRATIONAL RELAXATION LENGTHS BEHIND SHOCK WAVES IN N_2 .
INITIAL CONDITIONS: $p_0 = 15$ TORR, $T_0 = 300$ K (REFS. 18, 19).



FIG. 7 DOUBLE-MACH REFLECTION IN N_2 SHOWING VIBRATIONAL RELAXATION
 PROGRESS BEHIND INCIDENT SHOCK WAVE (ORIENTATION OF FRINGES
 NOT AS EFFECTIVE AS IN FIG. 5)
 $Q_w = 26.33$; $M_s = 8.06$, $p_0 = 5.10$ TORR, $T_0 = 298.2$ K (REF. 4).

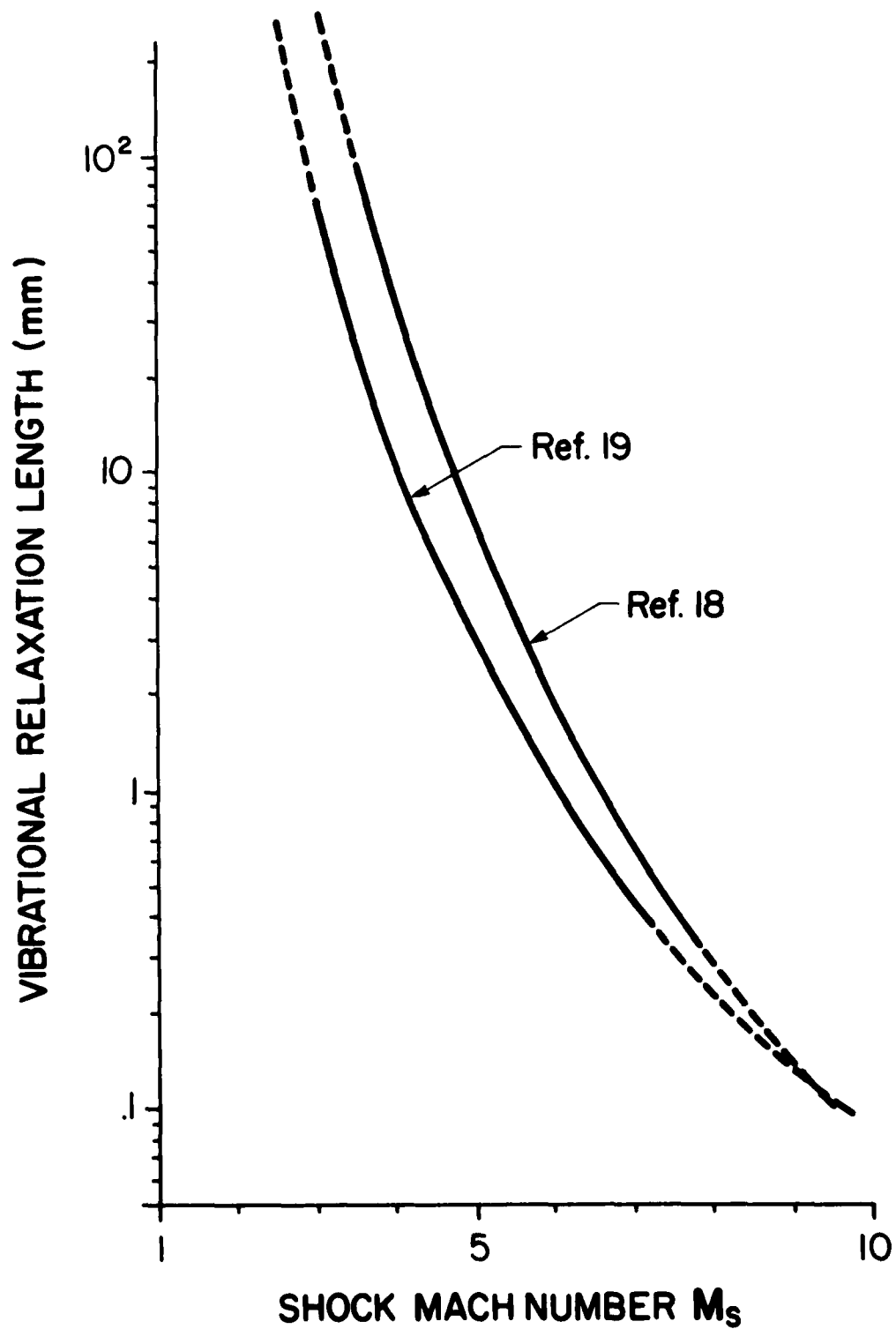


FIG. 8 VIBRATIONAL RELAXATION LENGTHS BEHIND SHOCK WAVES IN O_2 .
INITIAL CONDITIONS: $p_0 = 15$ TORR, $T_0 = 300$ K (REFS. 18, 19).



FIG. 9 DOUBLE-MACH REFLECTION IN AIR SHOWING VIBRATIONAL RELAXATION
PROCESS BEHIND INCIDENT SHOCK WAVE (INFINITE-FRINGE INTERFEROGRAM).
 $\tau_w = 27^\circ$, $M_s = 8.7$, $P_0 = 30.75$ TORR, $T_0 = 299$ K (REF. 2).

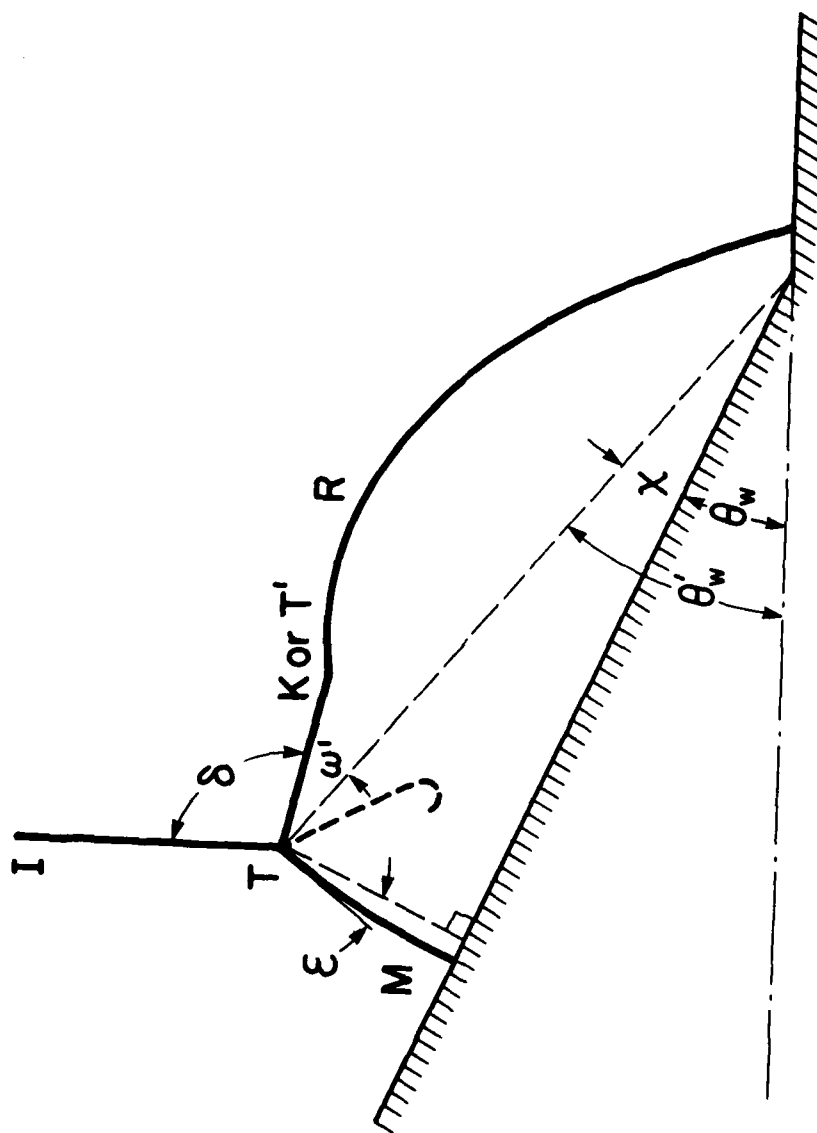


FIG. 10 DEFINITION OF SOME ANGLES IN MACH REFLECTION.

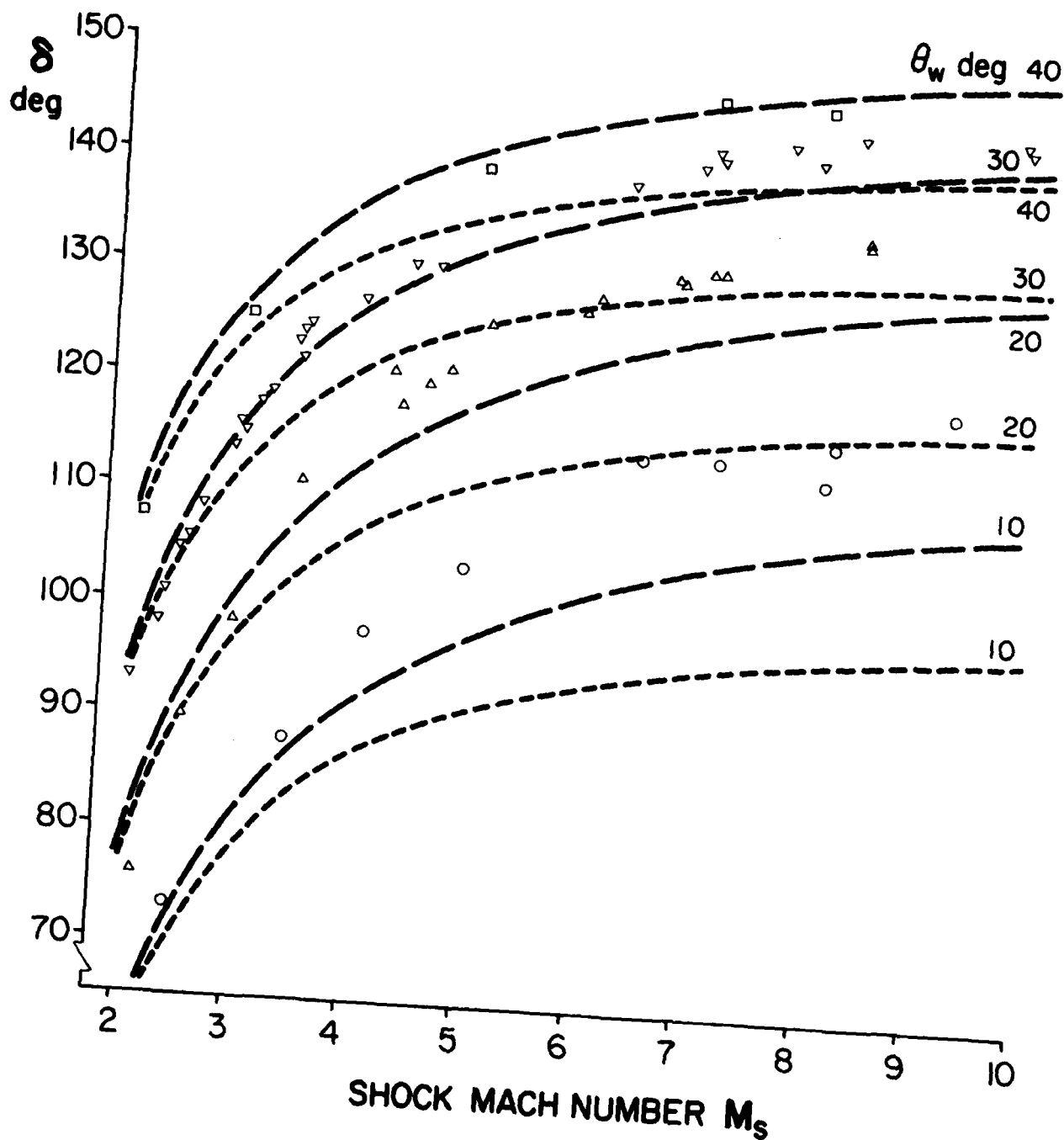


FIG. 12 VARIATION OF ANGLE δ VS SHOCK-MACH NUMBER AT FIXED θ_w (INSTEAD OF θ_w') FOR CO_2 .
 $T_0 = 300 \text{ K}$, $p_0 = 15 \text{ TORR}$, — — — EQUILIBRIUM CO_2 , - - - - - PERFECT CO_2 ($\gamma = 1.29$). EXPERIMENTS: o - $\theta_w = 10^\circ$, Δ - $\theta_w = 20^\circ$, ∇ - $\theta_w = 30^\circ$, \square - $\theta_w = 40^\circ$ (REF. 14).

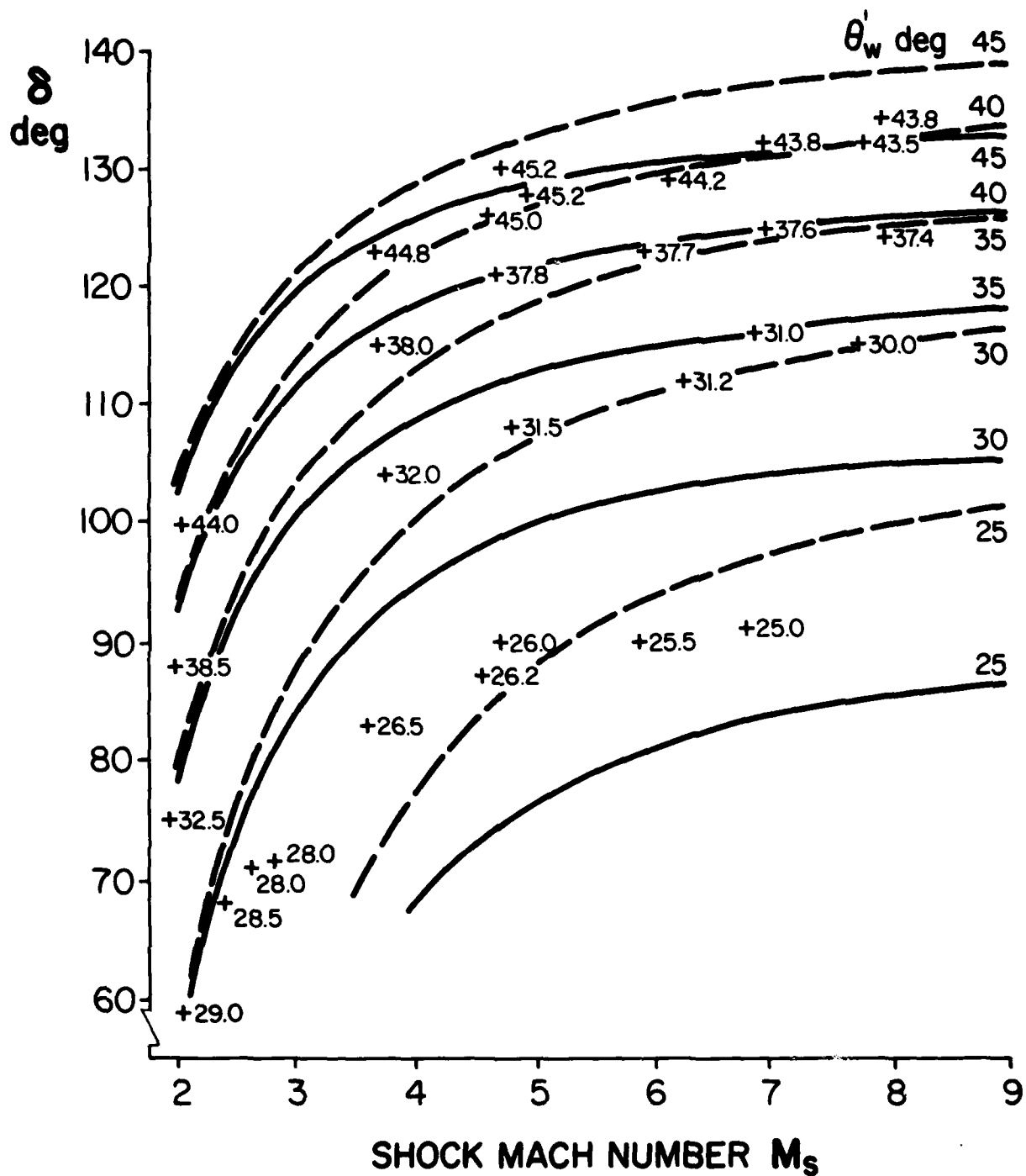


FIG. 13 VARIATION OF ANGLE δ VS SHOCK-MACH NUMBER AT FIXED θ'_w FOR N_2 .
 $T_0 = 300$ K, $p_0 = 15$ TORR, — FROZEN N_2 ($\gamma = 1.4$),
 --- EQUILIBRIUM N_2 , + EXPERIMENTAL DATA FOR θ'_w (θ'_w MEASURED
 BY BEN-DOR, REF. 4).

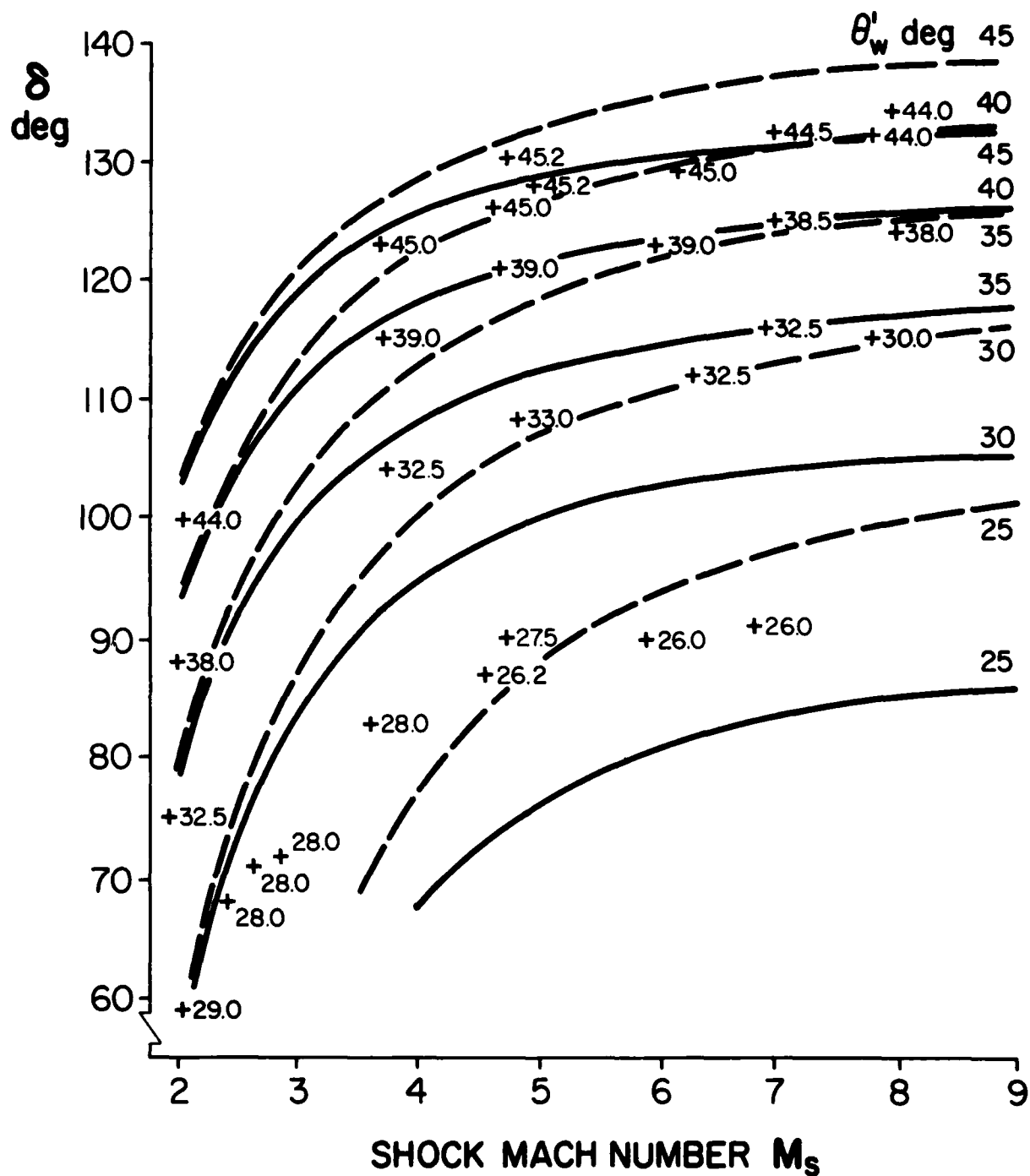


FIG. 14 VARIATION OF ANGLE δ VS SHOCK-MACH NUMBER AT FIXED θ'_w FOR N_2 .
 $T_0 = 300$ K, $p_0 = 15$ TORR, — FROZEN N_2 ($\gamma = 1.4$),
 - - - EQUILIBRIUM N_2 , + EXPERIMENTAL DATA FOR θ'_w (θ'_w MEASURED
 BY ANDO, REF. 22).

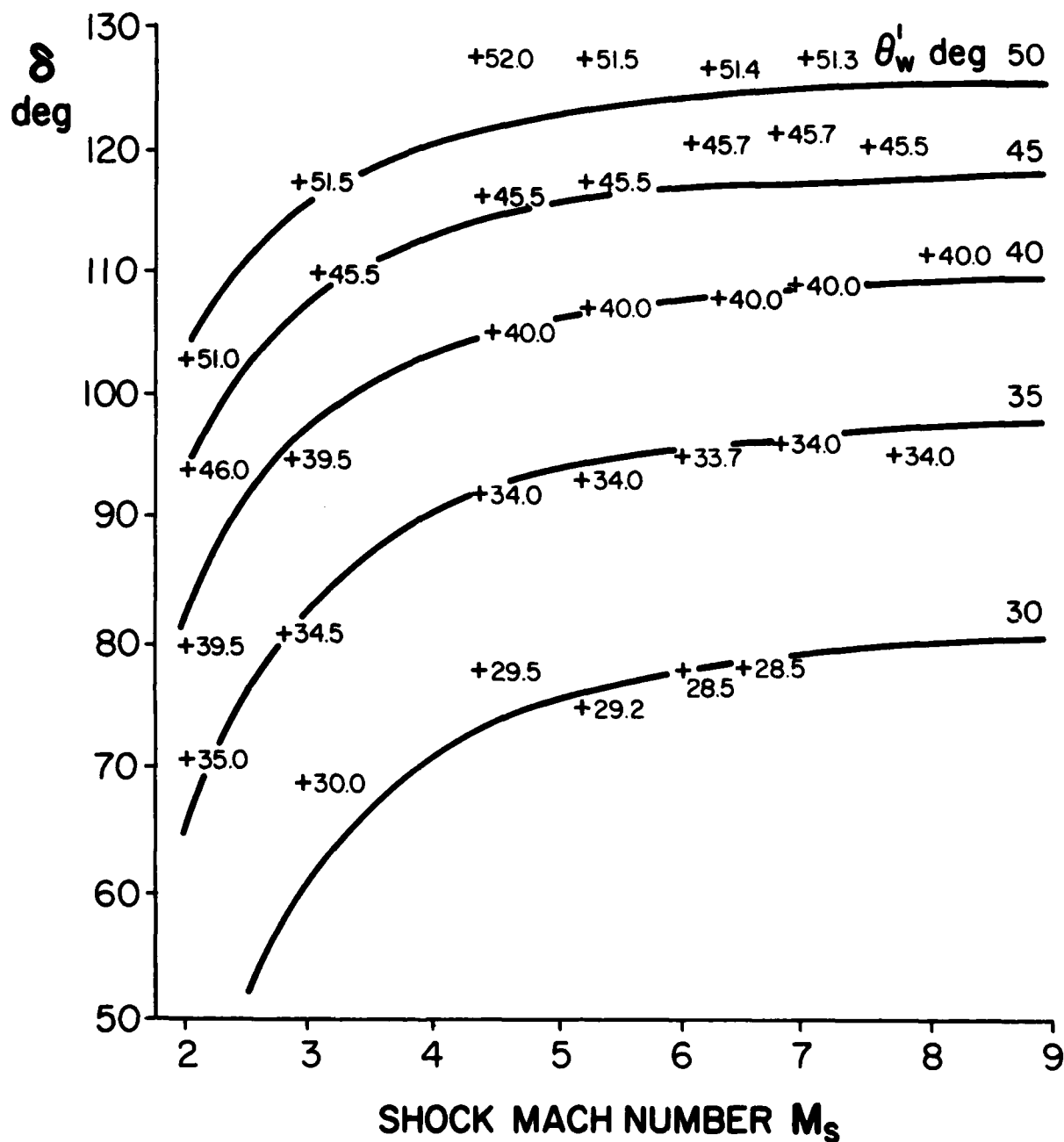


FIG. 15 VARIATION OF ANGLE δ VS SHOCK-MACH NUMBER AT FIXED θ'_w FOR Ar.
 — FROZEN Ar ($\gamma = 1.667$), + EXPERIMENTAL DATA FOR θ'_w
 (REF. 4).

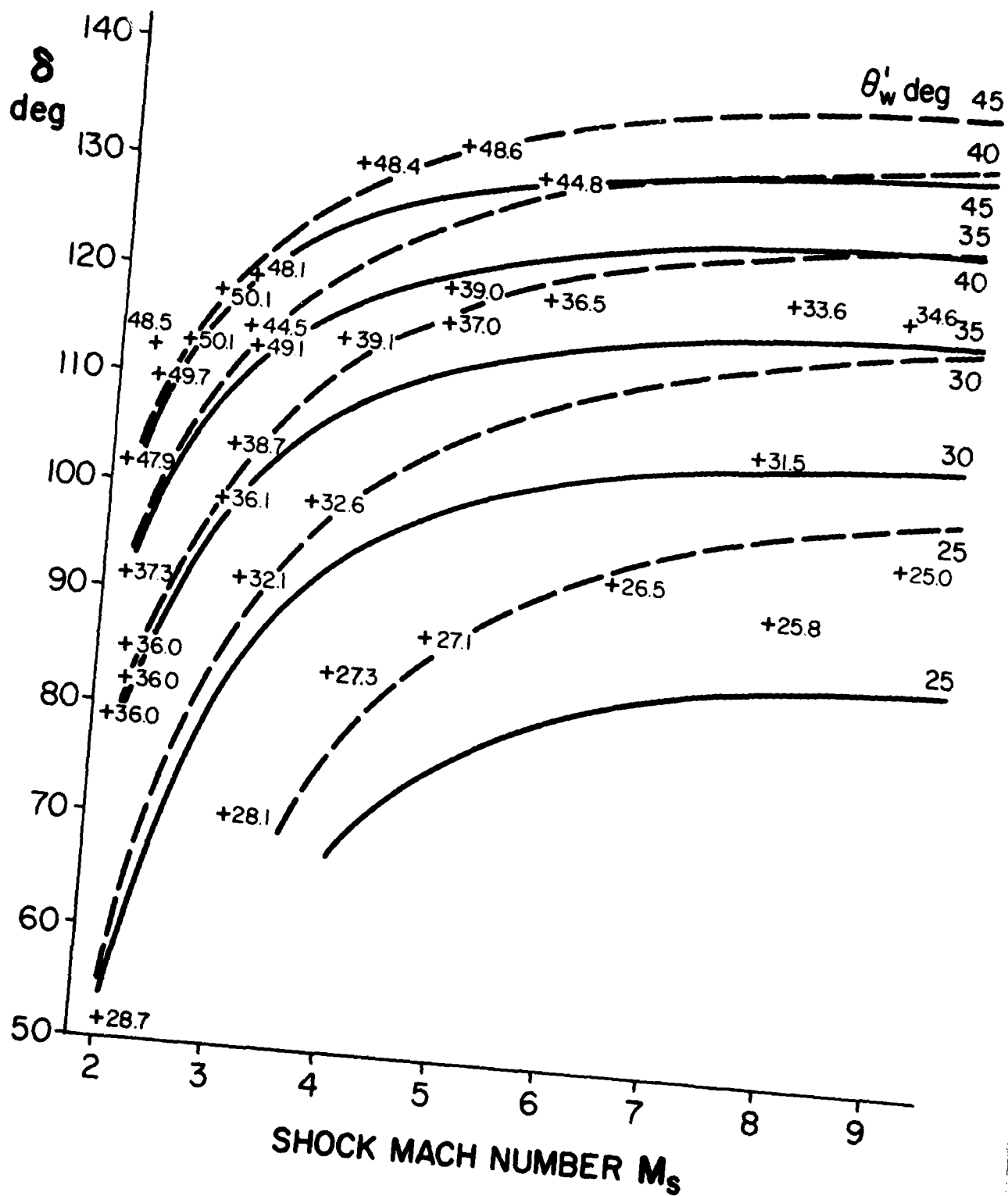


FIG. 16 VARIATION OF ANGLE δ VS SHOCK-MACH NUMBER AT FIXED θ'_w FOR AIR.
 $T_0 = 300$ K, $p_0 = 15$ TORR, — FROZEN AIR ($\gamma = 1.40$),
 --- EQUILIBRIUM AIR, + EXPERIMENTAL DATA FOR θ'_w (REF. 21).

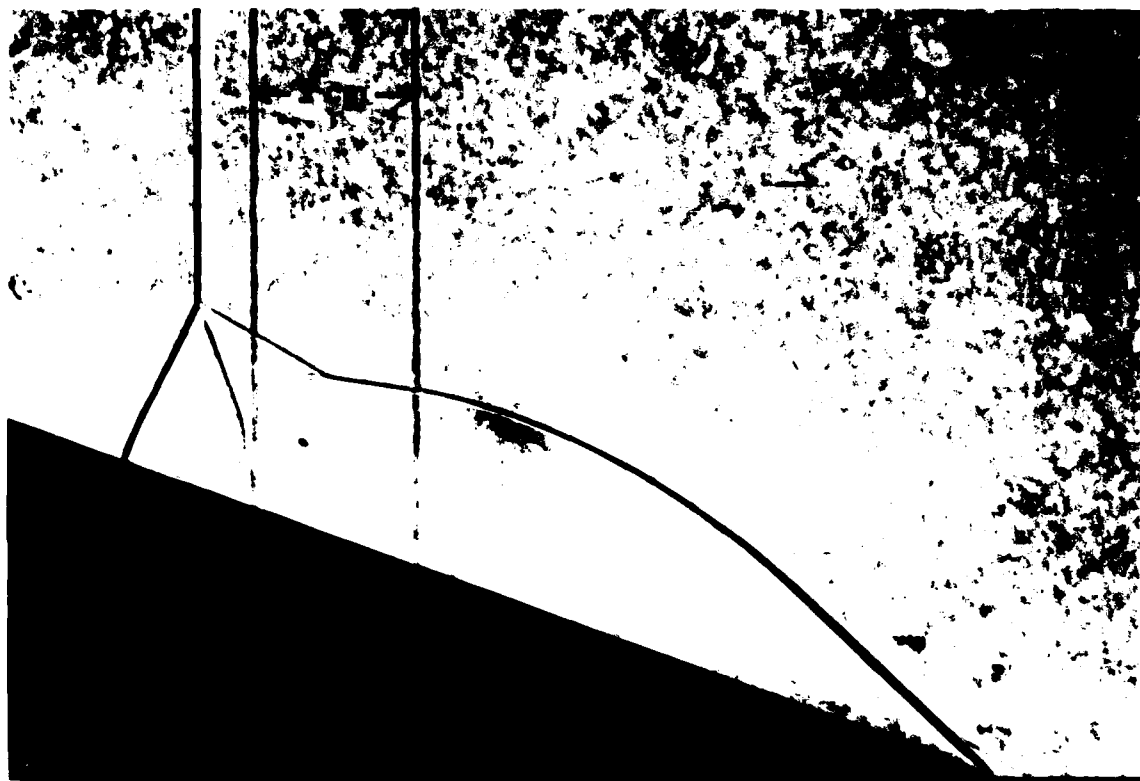


FIG. 17 EXAMPLE WHERE ENTIRE MACH STEM IS NOT PERPENDICULAR TO WEDGE SURFACE. $\theta_w = 20^\circ$, $M_s = 4.72$, $p_o = 14.5$ TORR, $T_o = .297.7$ K, CO_2 (REF. 14)

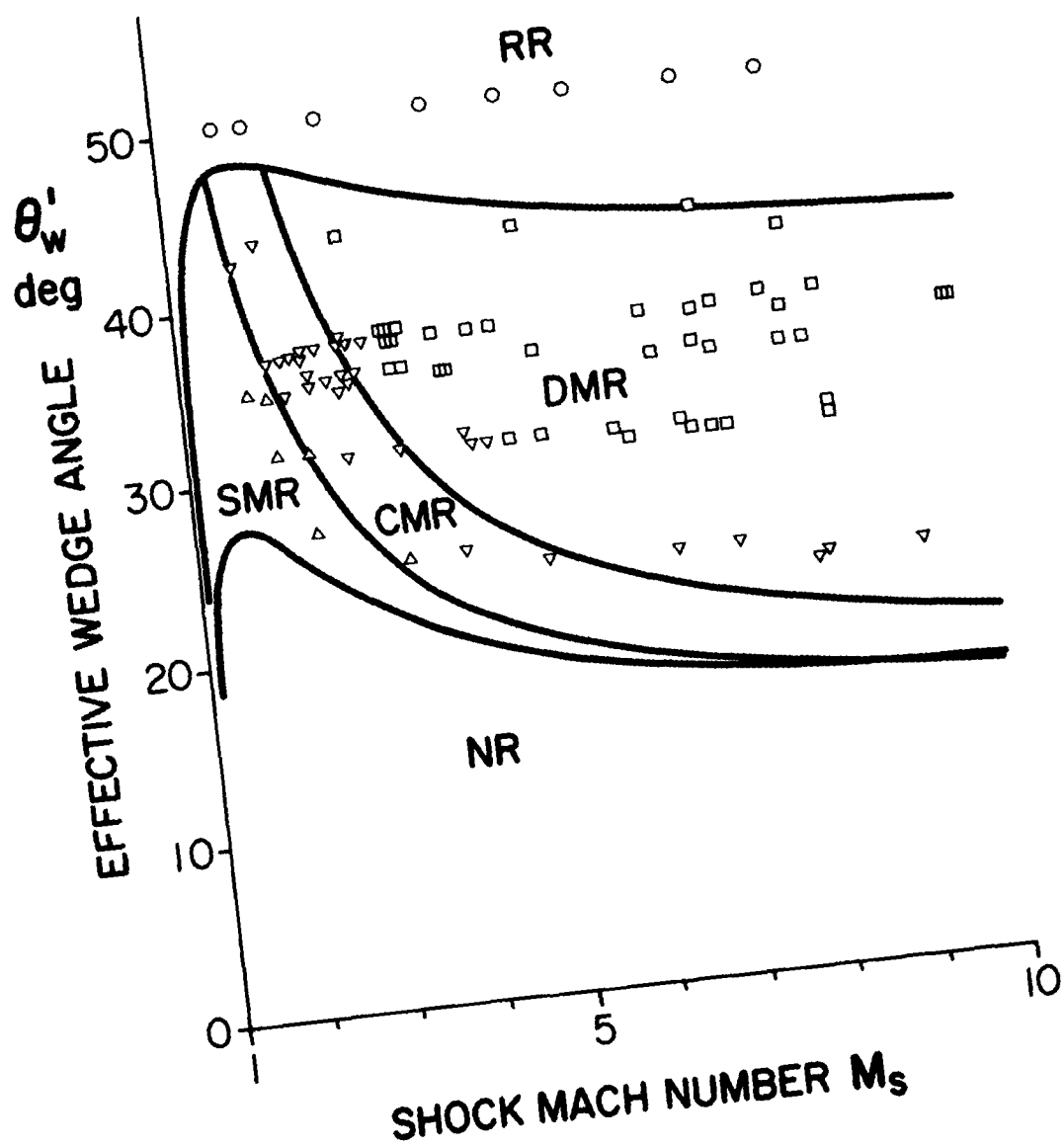


FIG. 18 COMPARISON OF EQUILIBRIUM-GAS TRANSITION BOUNDARIES WITH EXPERIMENTAL RESULTS FOR CO_2 .
EXPERIMENTS: \circ - RR, Δ - SMR, ∇ - CMR, \square - DMR (REF. 14).

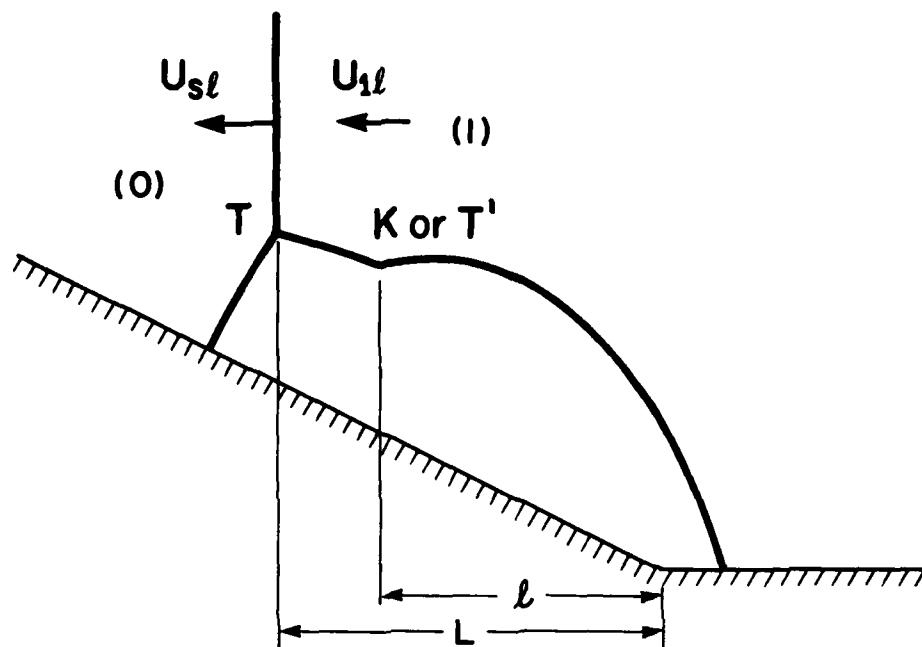


FIG. 19(a) SCHEMATIC DIAGRAM ILLUSTRATING ASSUMPTION OF POSITION OF KINK OR SECOND TRIPLE POINT AND FIRST TRIPLE POINT.

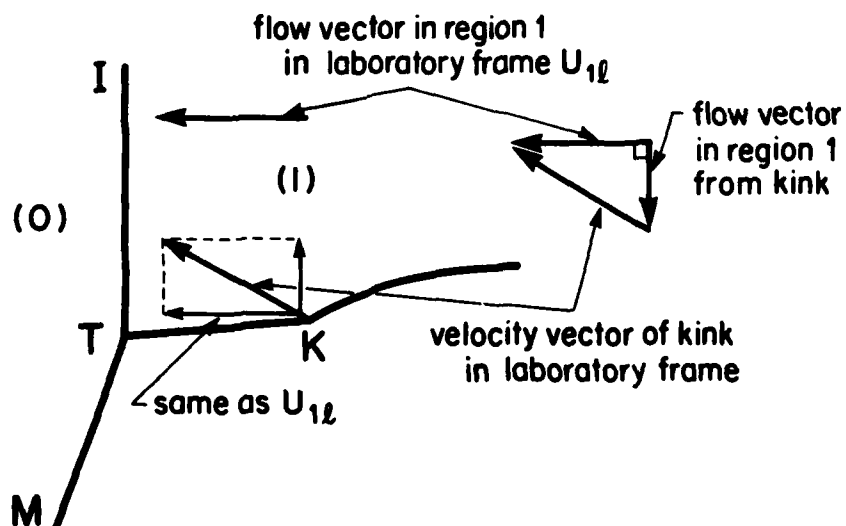


FIG. 19(b) SCHEMATIC DIAGRAM ILLUSTRATING FLOW DIRECTION IN REGION 1 RELATIVE TO KINK.

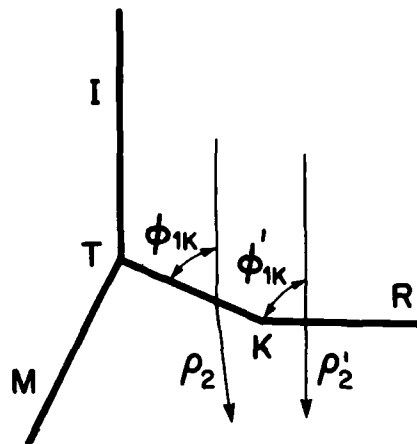


FIG. 19(c) DEFINITIONS OF ϕ_{1K} , ϕ'_{1K} , ρ_2 AND ρ'_2 .

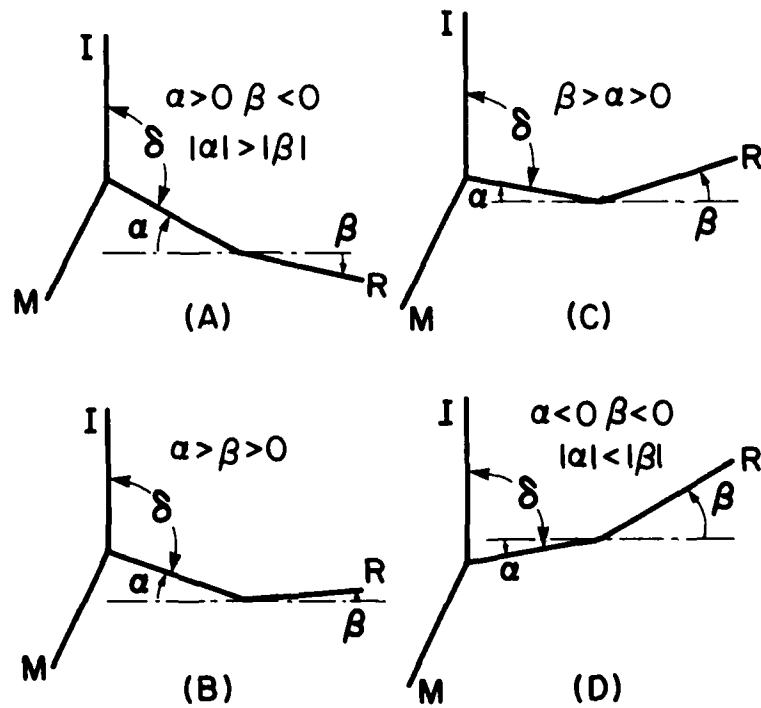


FIG. 19(d) FOUR POSSIBLE GEOMETRIC CONFIGURATIONS OF REFLECTED SHOCK WAVE.

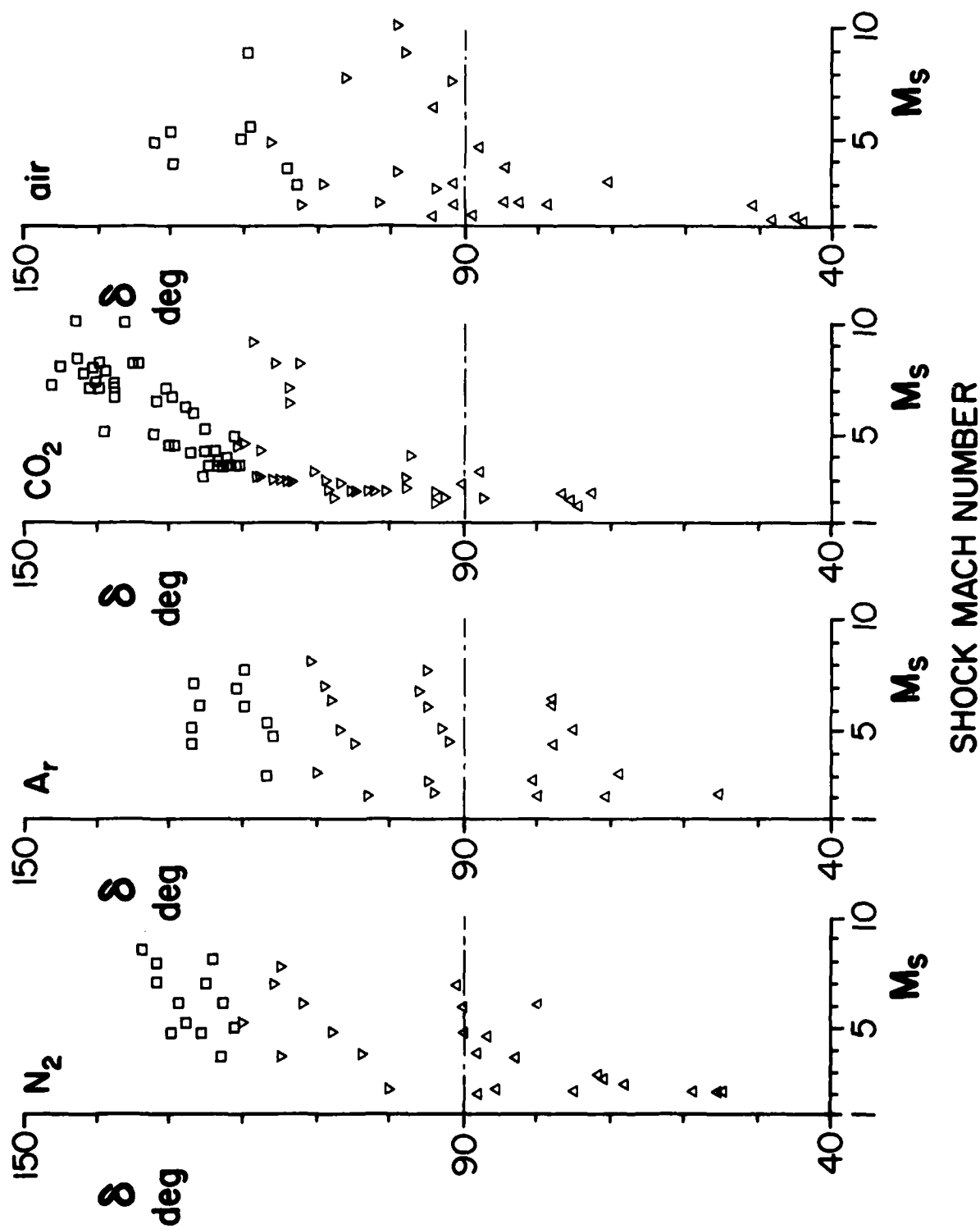


FIG. 20 EXPERIMENTAL RELATIONS BETWEEN δ AND TYPE OF REFLECTION.
 N_2 (REF. 4), Ar (REF. 4), CO_2 (REF. 14), AIR (REF. 21),
 Δ - SMR, ∇ - CMR, \square - DMR.

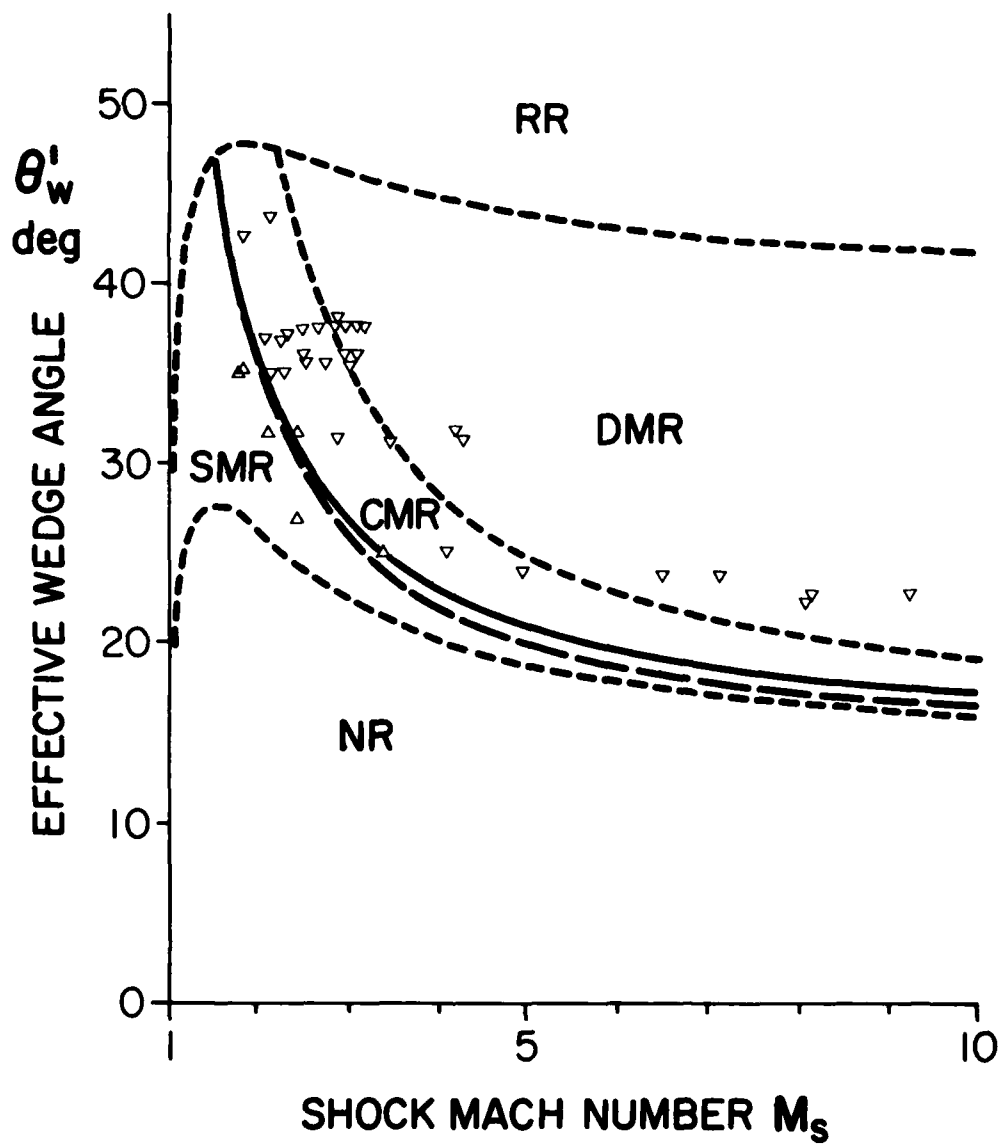


FIG. 21 SMR ∇ CMR TRANSITION BOUNDARIES OF "NEW" AND "FORMER" CRITERIA FOR EQUILIBRIUM CO_2 .
 ——— NEW CRITERION, - - - FORMER CRITERION. EXPERIMENTS:
 Δ - SMR, ∇ - CMR (REF. 14).

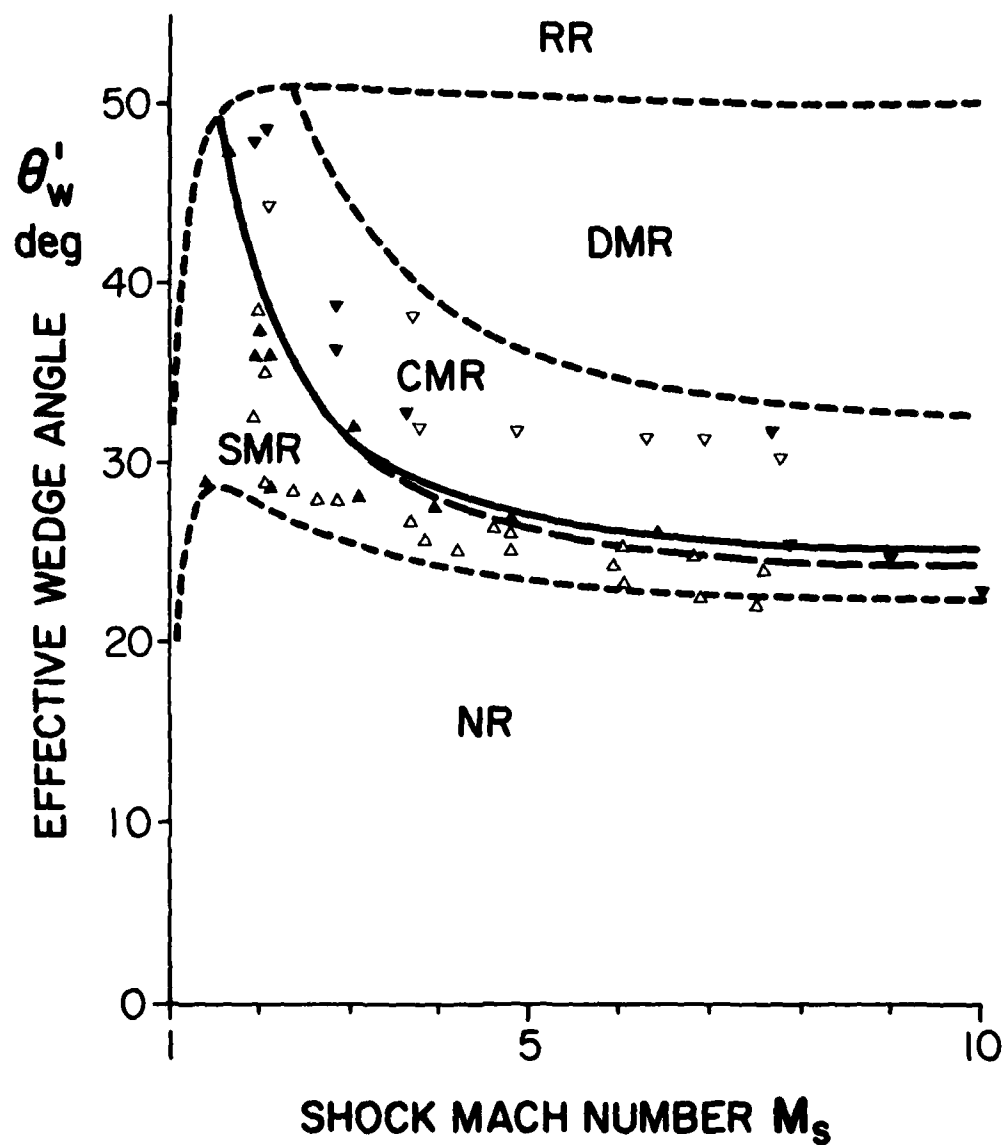


FIG. 22 SMR \nleftrightarrow CMR TRANSITION BOUNDARIES OF "NEW" AND "FORMER" CRITERIA FOR FROZEN N_2 AND AIR ($\gamma = 1.40$).
 — NEW CRITERION, --- FORMER CRITERION. EXPERIMENTS:
 N_2 : Δ - SMR, ∇ - CMR (REF. 4); AIR: \blacktriangle - SMR, \blacktriangledown - CMR (REF. 21).

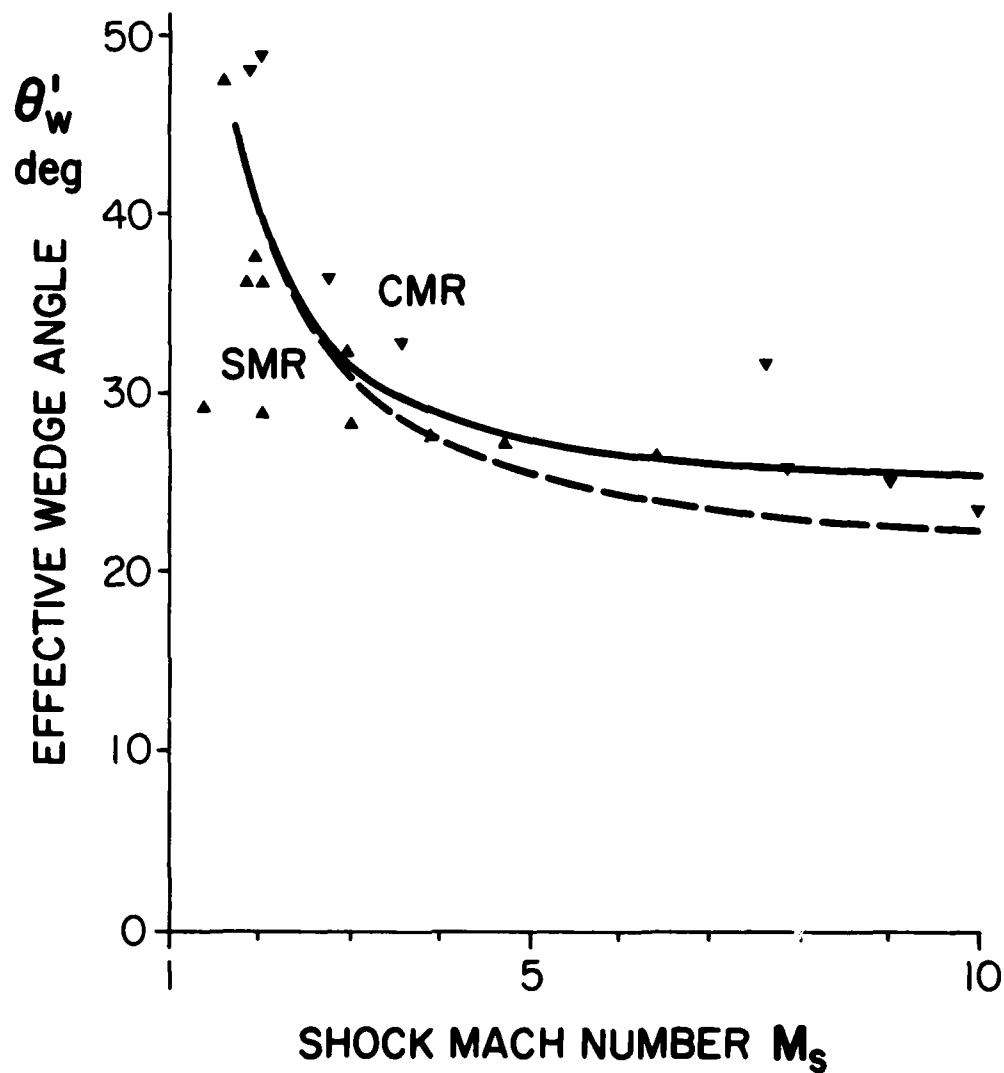


FIG. 23 COMPARISON BETWEEN FROZEN AND EQUILIBRIUM AIR OF SMR \leftrightarrow CMR TRANSITION BOUNDARIES OF NEW CRITERION.
 — FROZEN AIR, - - - EQUILIBRIUM AIR. EXPERIMENTS:
 ▲ - SMR, ▼ - CMR (REF. 21).

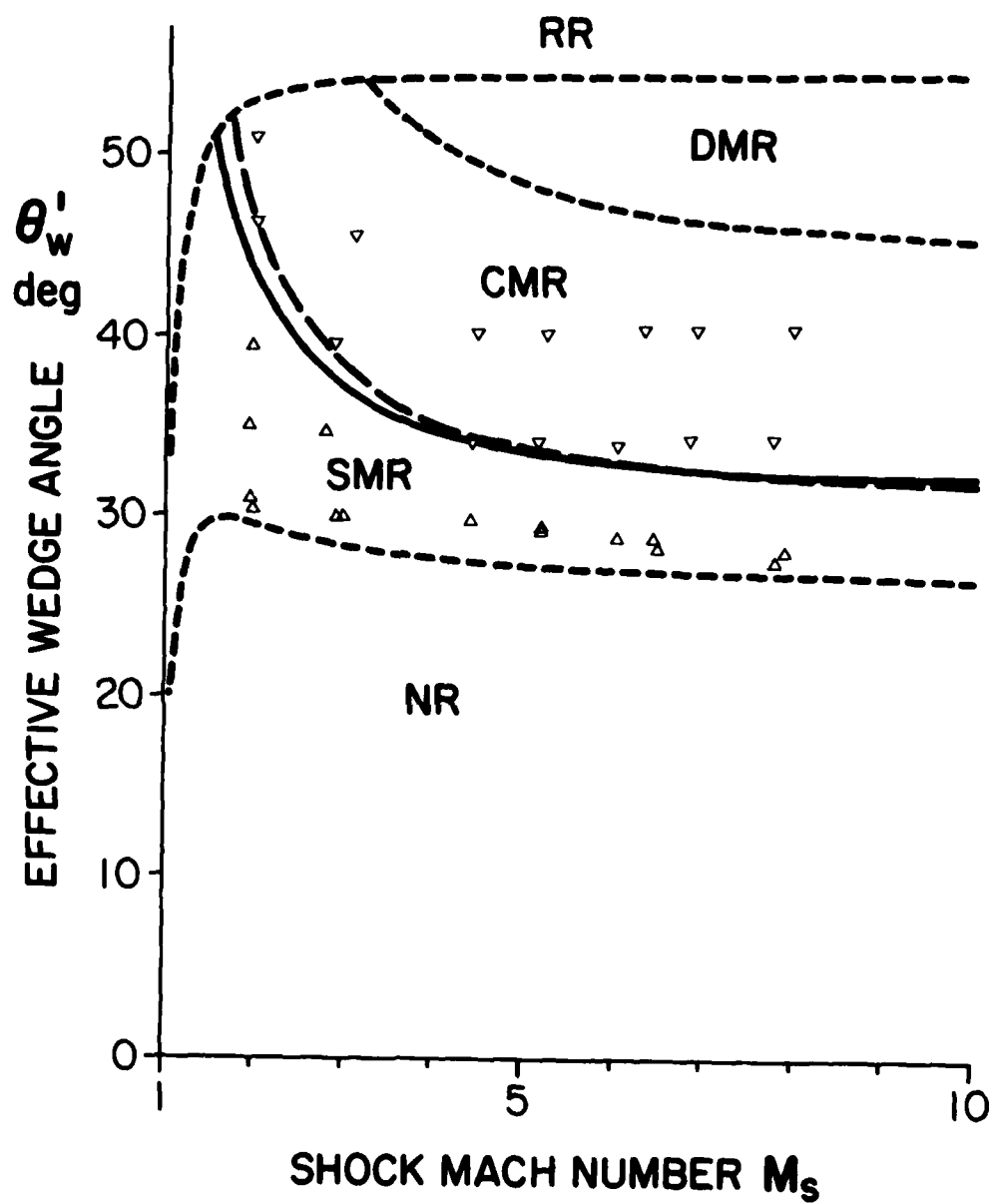


FIG. 24 $M_{2T} = 1$ LINE AND $\delta = 90^\circ$ LINE OF FROZEN ARGON.
 ——— $M_{2T} = 1$, — $\delta = 90^\circ$. EXPERIMENTS: Δ - SMR,
 ∇ - CMR (REF. 4).

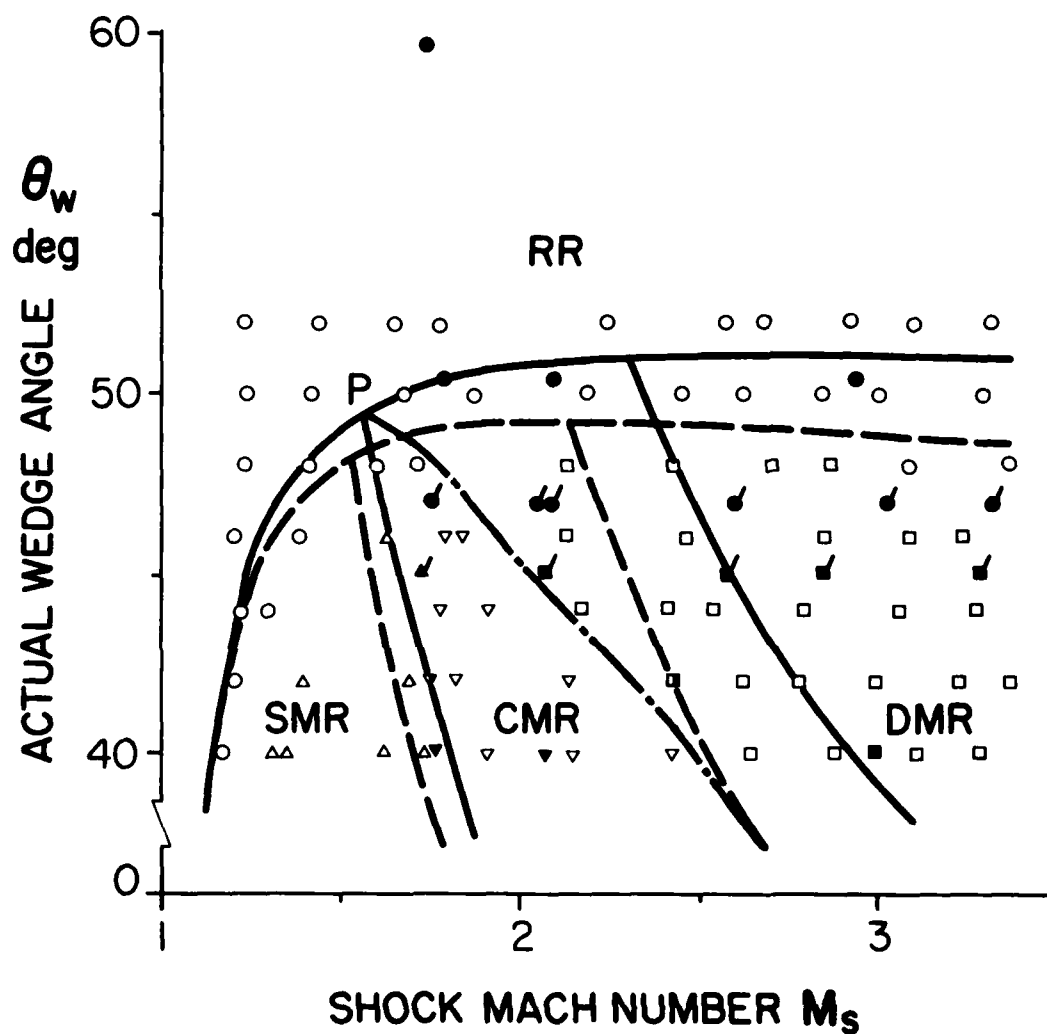
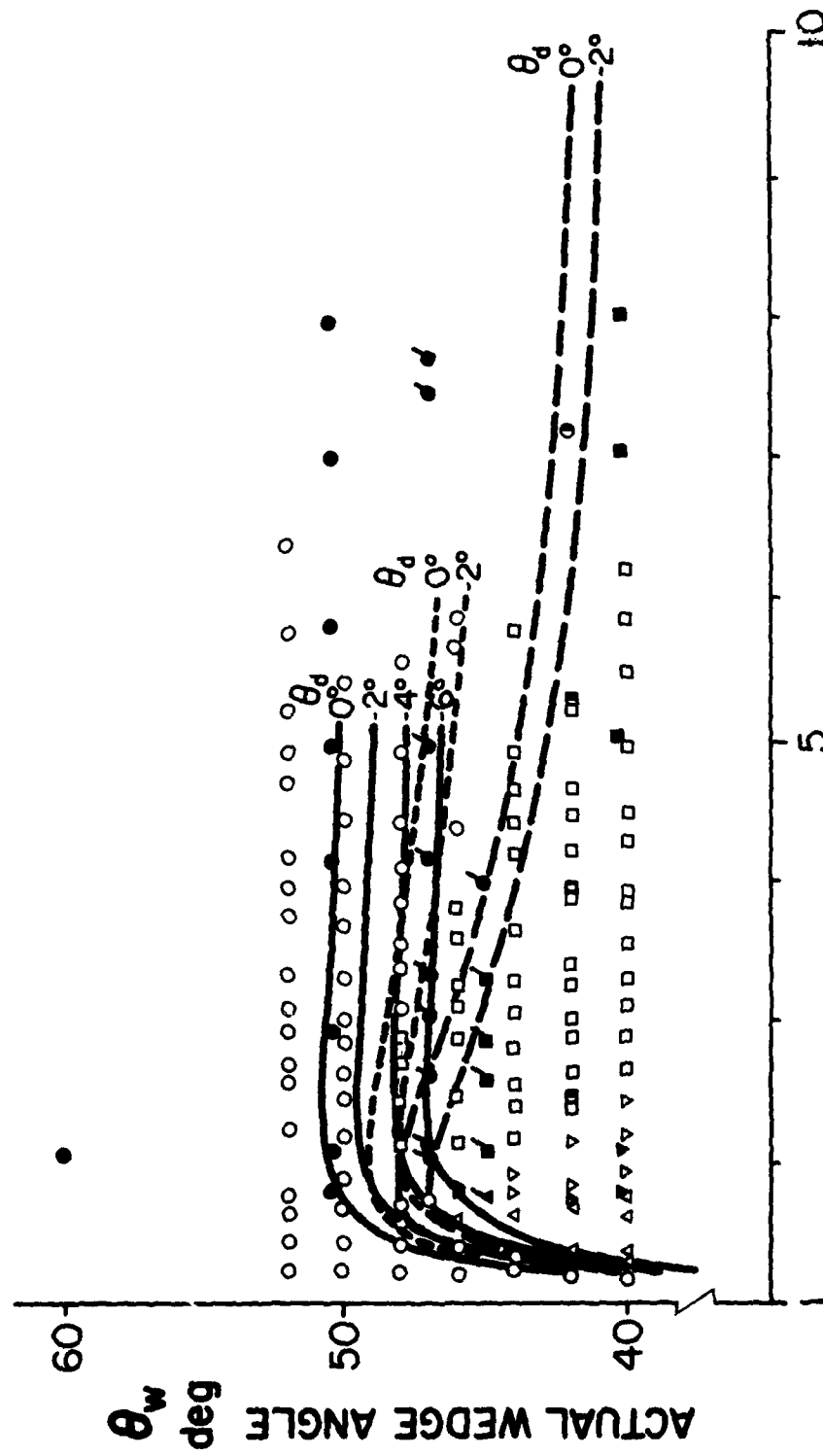


FIG. 25 EXPERIMENTAL CONVERGENCE OF CMR ∇ DMR BOUNDARY WITH SMR ∇ CMR BOUNDARY AT RR ∇ MR BOUNDARY FOR CO_2 .
 CALCULATED BOUNDARY: — FROZEN CO_2 , - - - EQUILIBRIUM CO_2 .
 EXPERIMENTAL POINTS: \circ - RR, Δ - SMR, ∇ - CMR, \square - DMR (REF. 26)
 \bullet - RR, \blacktriangledown - CMR, \blacksquare - DMR (REF. 14)
 \circ - RR, \blacktriangle - SMR, \blacksquare - DMR (REF. 22)
 ∇ - CMR, \square - DMR (REF. 25)
 - · - · - EXPERIMENTAL BOUNDARY BETWEEN CMR AND DMR.



SHOCK MACH NUMBER M_s

FIG. 26 COMPARISON OF EXPERIMENTAL RESULTS WITH CALCULATED $RR \pm MR$ BOUNDARIES FOR SEVERAL VALUES OF BOUNDARY-LAYER-DISPLACEMENT ANGLE θ_d FOR CO_2 .

— FROZEN CO_2 ($\gamma = 1.40$), --- PERFECT CO_2 ($\gamma = 1.29$),
 — EQUILIBRIUM CO_2 .
 EXPERIMENTAL POINTS: \circ - RR, Δ - SMR, ∇ - CMR, \square - DMR (REF. 26)
 \circ - RR, Δ - SMR, ∇ - CMR, \square - DMR (REF. 14)
 \circ - RR, Δ - SMR, ∇ - CMR, \square - DMR (REF. 22)
 \circ - RR, Δ - SMR, ∇ - CMR, \square - DMR (REF. 25)

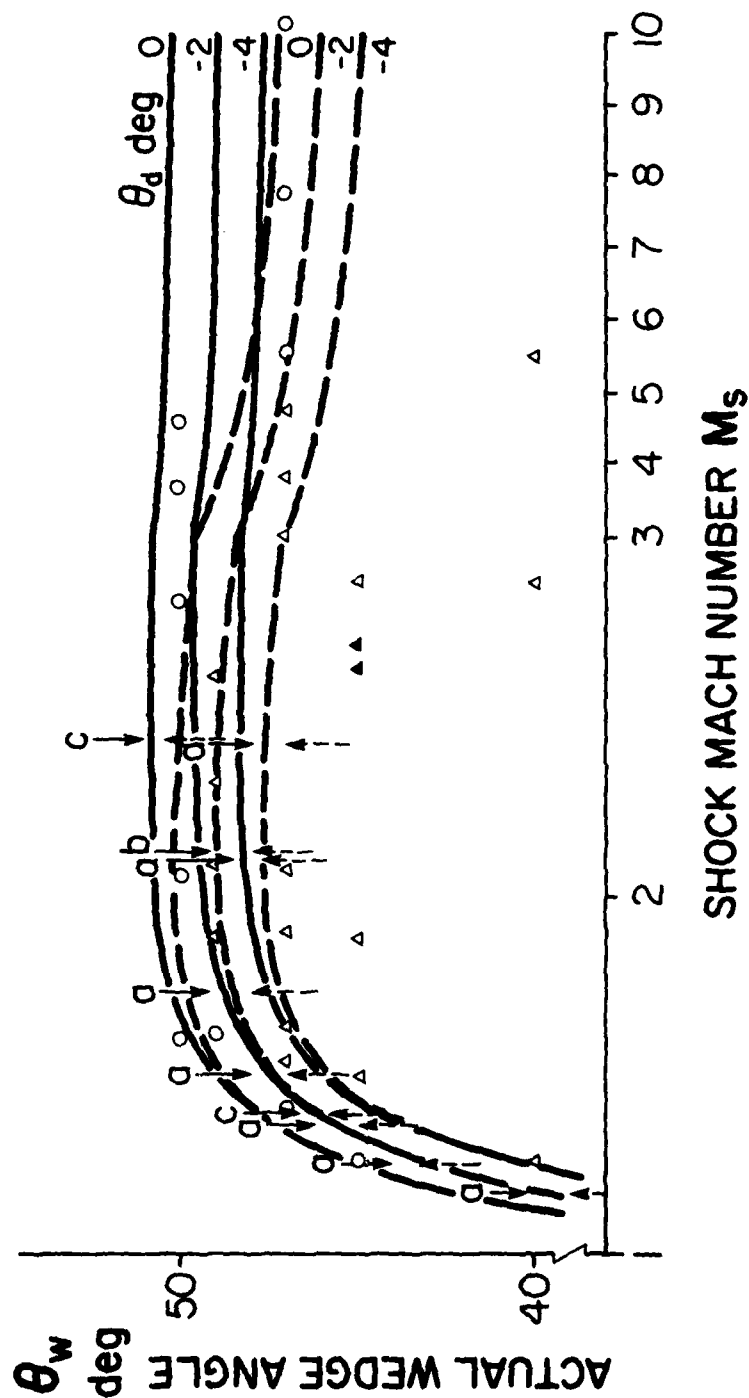


FIG. 27 COMPARISON OF EXPERIMENTAL RESULTS WITH CALCULATED $RR \neq MR$ BOUNDARIES WITH M_s FOR SEVERAL VALUES OF THE BOUNDARY-LAYER-DISPLACEMENT ANGLE θ_d FOR AIR.

— FROZEN AIR, - - - EQUILIBRIUM AIR.

EXPERIMENTS: \rightarrow REGION WHERE RR OBTAINED, $----->$ REGION WHERE MR OBTAINED (ARROWS ARE USED INSTEAD OF NUMEROUS POINTS FOR CLARITY).

a - REF. 6, b - REF. 27, c - REF. 28.

o - RR , Δ - MR (REF. 21), \blacktriangle - MR (REF. 15).

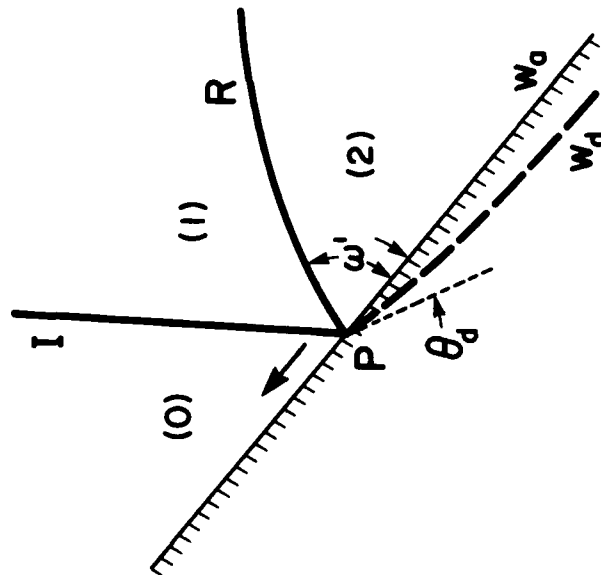


FIG. 28

BOUNDARY-LAYER DISPLACEMENT EFFECT BEHIND REFLECTION POINT P.

I - INCIDENT SHOCK WAVE; R - REFLECTED SHOCK WAVE, θ_d - DISPLACEMENT ANGLE; w_a - ACTUAL WEDGE SURFACE; w_d - DISPLACED WEDGE SURFACE; ω' - REFLECTED WAVE ANGLE.

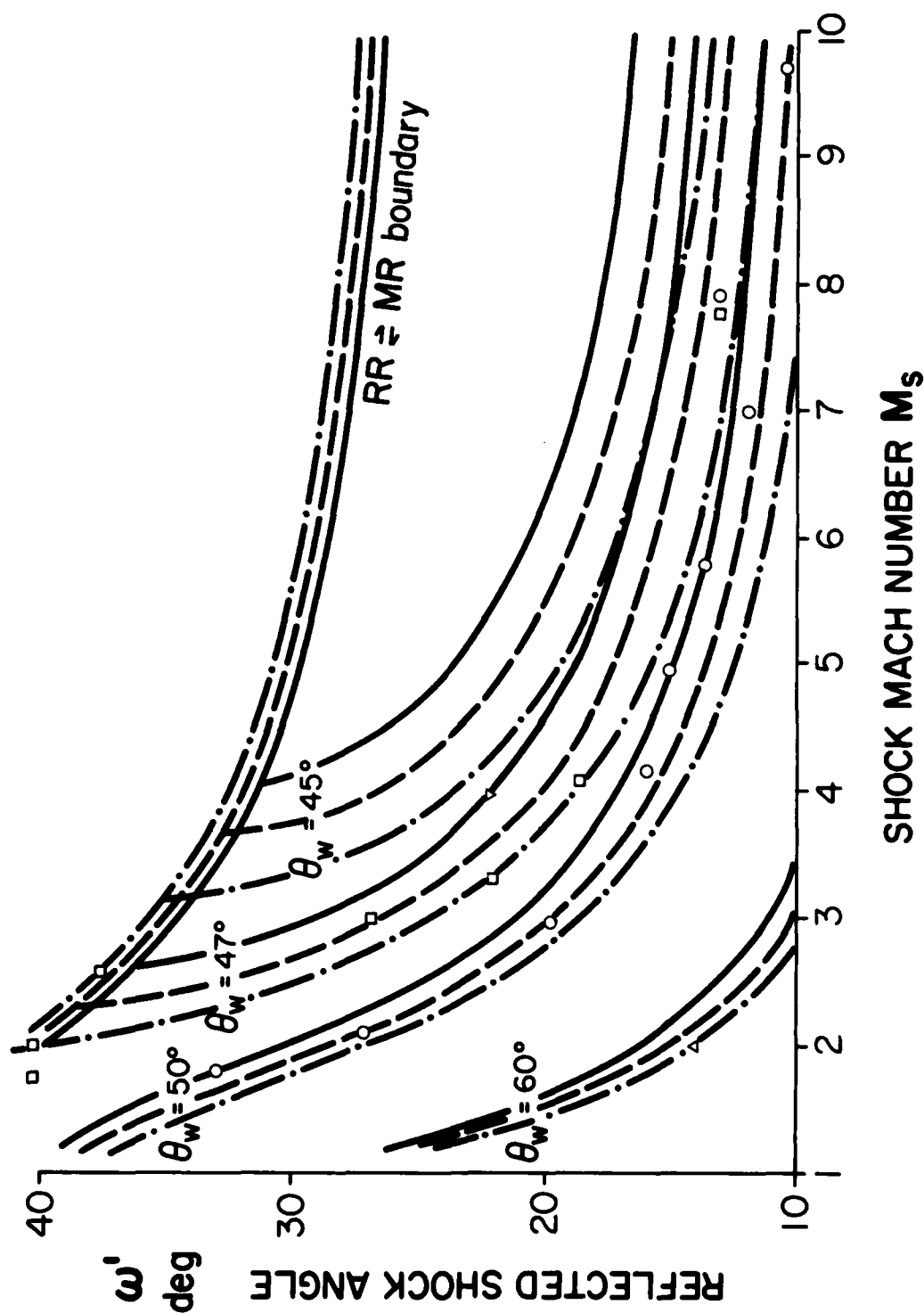


FIG. 29 COMPARISON OF EXPERIMENTAL REFLECTED-WAVE ANGLE ω' WITH CALCULATIONS OF SEVERAL BOUNDARY-LAYER-DISPLACEMENT ANGLES θ_d FOR EQUILIBRIUM CO_2 .
 $\theta_d = 0^\circ$, $---$ $\theta_d = -1^\circ$, $-\cdot-\cdot-$ $\theta_d = -2^\circ$, $T_0 = 300$ K,
 $p_0 = 15$ TORR. EXPERIMENTAL DATA: ∇ - $\theta_w = 45^\circ$, \square - $\theta_w = 47^\circ$,
 \circ - $\theta_w = 50.5^\circ$, Δ - $\theta_w = 60.1^\circ$ (REFS. 14, 22).

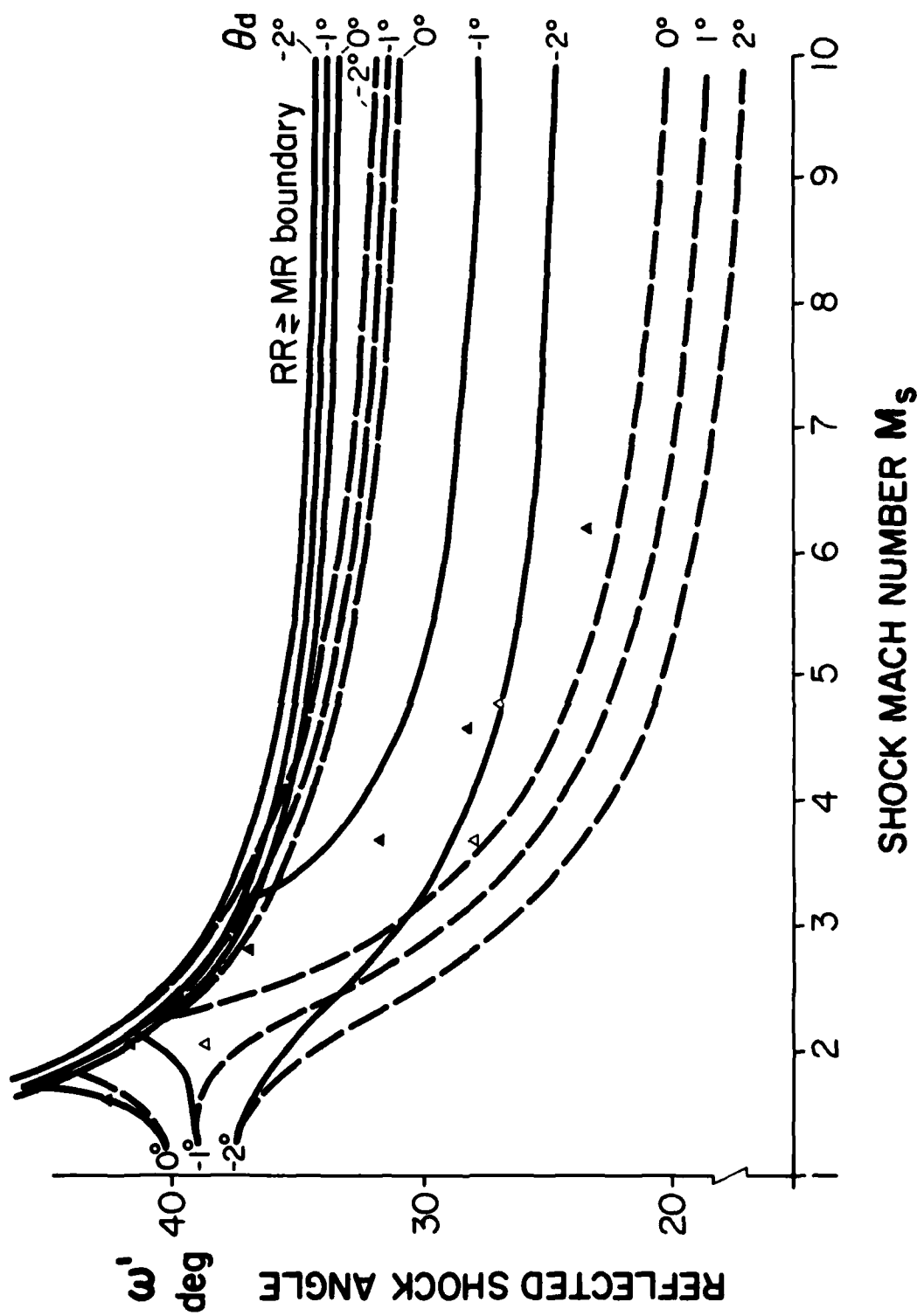


FIG. 30 COMPARISON OF REFLECTED-WAVE ANGLE ω' WITH CALCULATIONS FOR SEVERAL BOUNDARY-LAYER-DISPLACEMENT ANGLES θ_d FOR AIR AND N_2 AT $\theta_w = 50^\circ$.
 — FROZEN AIR ($\gamma = 1.4$), - - - EQUILIBRIUM AIR, $T_o = 300$ K, $p_o = 15$ TORR,
 EXPERIMENTAL DATA: \blacktriangle - AIR (REF. 21), Δ - N_2 (REF. 4).

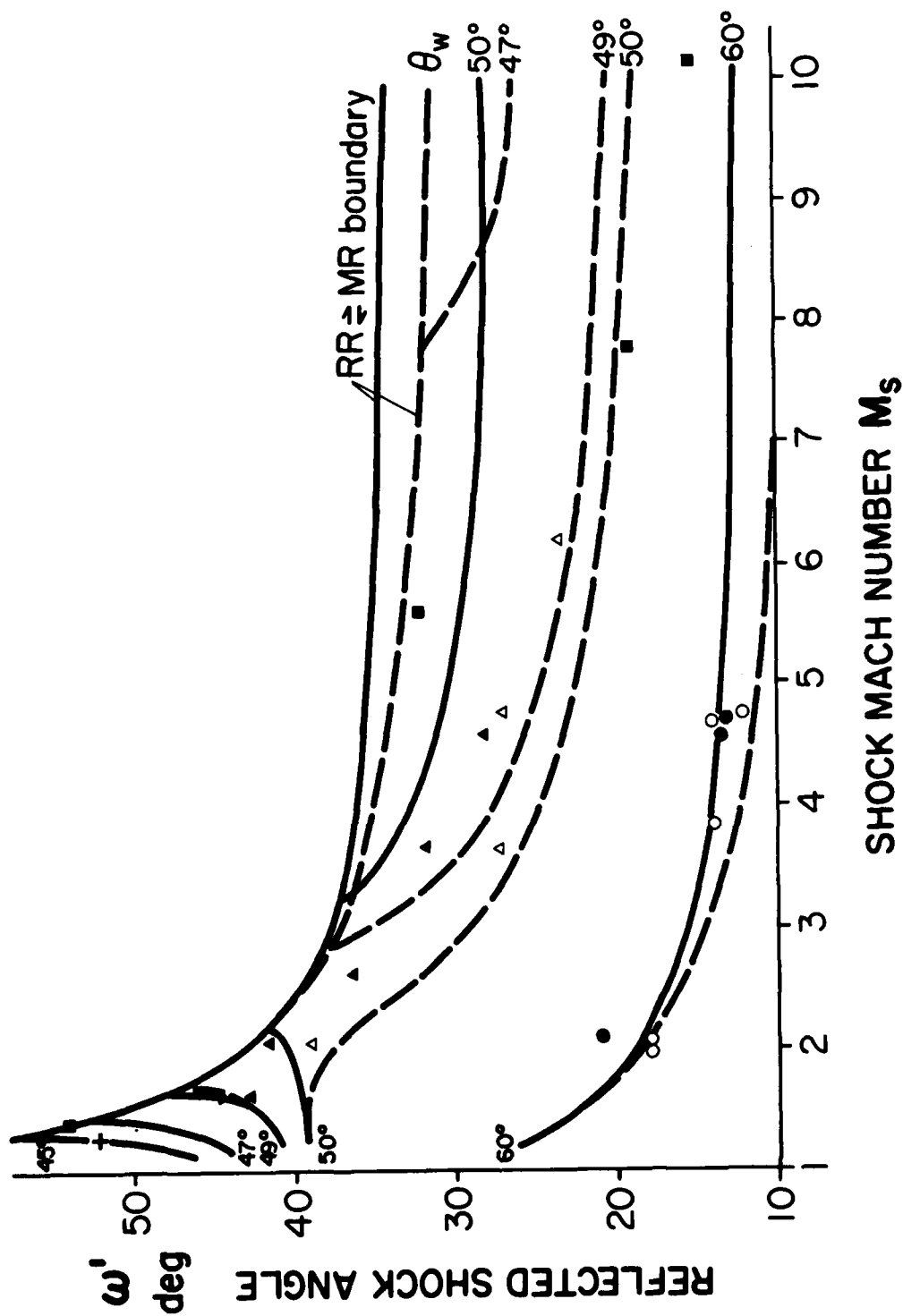


FIG. 31 COMPARISON OF EXPERIMENTAL REFLECTED ANGLE ω' WITH CALCULATIONS OF BOUNDARY-LAYER-DISPLACEMENT ANGLE $\theta_d = -1^\circ$ FOR AIR AND N_2 .
 — FROZEN AIR, - - - EQUILIBRIUM AIR, $T_0 = 300$ K, $p_0 = 15$ TORR.
 EXPERIMENTAL DATA: AIR: + - $\theta_w = 45^\circ$, ■ - $\theta_w = 47^\circ$, ▼ - $\theta_w = 49^\circ$,
 ▲ - $\theta_w = 50^\circ$, ● - $\theta_w = 60^\circ$ (REF. 21),
 N_2 : Δ - $\theta_w = 50^\circ$, ○ - $\theta_w = 60^\circ$ (REF. 4), □ - $\theta_w = 60^\circ$.

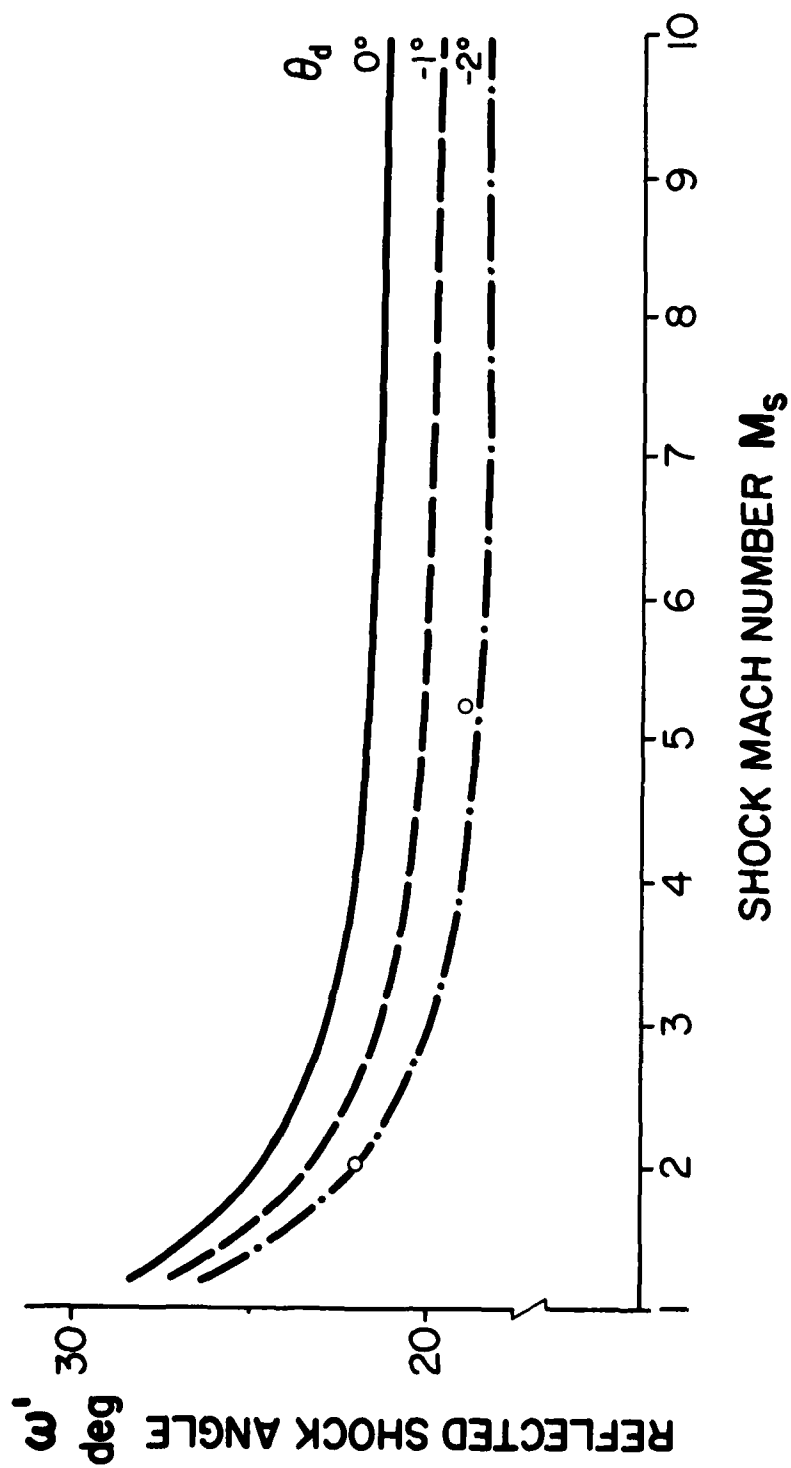


FIG. 32 COMPARISON OF EXPERIMENTAL REFLECTED WAVE ANGLE ω' WITH CALCULATIONS WITH SEVERAL BOUNDARY-LAYER-DISPLACEMENT ANGLES θ_d AT $\theta_w = 60^\circ$ FOR AR.
 o - EXPERIMENTAL DATA (REF. 4).

APPENDIX A

COMMENT ON PERFECT CO₂

The term perfect CO₂ was used previously in Refs. 13 and 14 to indicate a gas with a constant value of $\gamma = 1.29$ independent of temperature. However, from the following discussion, CO₂ with a constant $\gamma = 1.29$ has no physical validity. At room temperature, the vibrational modes of CO₂ are partly excited. The doubly-degenerate bending modes, which have a characteristic temperature of 960.2 K, are excited to 14% of their full excitation and have a contribution of 0.9R to C_V . The other two stretching modes contribute 0.7R to C_V . Consequently, along with contributions from the translational modes and rotational modes $C_V = 3.47R$ at room temperature, or $\gamma = C_P/C_V = 1.29$ at room temperature. However, behind a shock wave the translational and

rotational temperatures immediately jump to the Rankine-Hugoniot temperature T_{1f} . Since the vibrational energy is too slow to participate, it remains frozen on either side of the shock front and the temperature T_{1f} can be computed using $\gamma = 1.4$ (Ref. 31). After a period (relaxation time) the vibrational modes are activated and share in the energy through equipartition. The final equilibrium temperature $T_{1e} = T_{1f}$. For perfect CO₂ with $\gamma = 1.29$ has no physical basis. However, it is sometimes used in engineering applications to give an approximate answer for shock waves in CO₂ with vibrational excitation. The error becomes increasingly worse with rising shock Mach number (Ref. 31).

APPENDIX B

THREE-SHOCK THEORY

The three-shock theory provides a simple and effective analysis of oblique-shock-wave reflections. Even so, it includes some aspects which are physically unreasonable or inconsistent with experimental results. They are described below.

B.1 Behaviour of χ as $M_S \rightarrow 1$

The values of χ at fixed θ_w are approximately constant at high shock Mach numbers M_S , both experimentally and analytically. As M_S decreases, the values of χ increase except for large θ_w . Experimentally, χ has maximum values near $M_S = 2$ and decreases for other M_S . The calculated results of χ from the three-shock theory, however, do not have maxima for different θ_w but continue to increase as $M_S \rightarrow 1$, as shown in Fig. A-1.

Ben-Dor (Ref. 3) proposed an alternative method to obtain χ at small wedge angles ($\theta_w < 4^\circ$) which does give maxima and may agree with experiment despite his failure to obtain solutions of the three-shock theory for small θ_w and low M_S . His method is to assume that θ_w' at small θ_w coincides with the value at the no reflection (NR) boundary θ_{wNR} and $\chi = \theta_{wNR} - \theta_w$ at small wedge angles. Despite that his method gives a reasonable approximation to experiment results and is useful from an engineering point of view, he gave no physical explanation that θ_w' at small θ_w coincides with the NR boundary. His method does not give the necessary dependency of θ_w' ($= \theta_{wNR}$) for different θ_w . Since his suggestion is outside the three-shock theory realm, being only an assumption, it does not provide any clue for improving the three-shock theory or an alternative theory for the calculation of χ . The tendency to increase χ as $M_S \rightarrow 1$ is not considered realistic, not only because it does not agree with experimental results, but it also yields a no-solution region in the $(M_S - \theta_w)$ plane, as described in Appendix B.2.

The reason why the three-shock theory fails to give reasonable solutions at low Mach numbers may be as follows. The reflected shock wave is composed of two parts, one is a reflected shock wave emanating from the triple point and the other is a bow shock wave caused by the interaction of the incident flow with the flow deflected by the wedge. The two shock waves intersect at the kink or the second triple point in CMR or DMR, respectively. In SNR, the two shock waves blend smoothly so that an intersection point cannot be seen. The three-shock theory gives the position of only one of the two shock waves, which is the one emanating from the triple point. The actual shape of the entire reflected shock wave is considered to be determined by the two shock waves mentioned above and their interaction. At low Mach numbers, both the reflected shock wave from the triple point and the bow shock wave are weak. The former, however, is considered to become weaker more rapidly than the latter. Therefore, the position of the whole reflected shock wave is controlled by the bow shock wave rather than the reflected shock wave from the triple point. In the limit as the shock Mach number of the bow shock wave approaches 1 (Mach wave), or $\theta_w \rightarrow 0^\circ$, the bow shock will intersect the incident shock wave at a point $\theta_w' = \theta_{wNR}$, which is at a lower θ_w' than the limit of solution of the three-shock theory.

The reason is illustrated in Fig. A-2. Point O in Fig. A-2 was at the wedge corner when the incident shock wave collided with the wedge corner and it moves with the flow in region 1. Therefore, the flow in region 1 has a direction TO relative to T and the bow shock wave in the vicinity of T is normal to the flow. Since the bow wave is a Mach wave, the flow velocity in region 1 relative to the bow wave, or T, is sonic. If T is at θ_{wNR} , the flow Mach number in region 1 is also 1.0 according to the criterion of the NR boundary. It means that

T, which is the intersection point of the bow shock wave and incident shock wave in the limit of bow-shock Mach number $\rightarrow 1$, is at θ_{WNR} . Therefore, it is reasonable to assume that, at low incident Mach numbers and small wedge angles, the intersection point of the extension of the bow shock wave and the incident shock wave is nearer a point for which it has θ_{WNR} . Consequently, if the shape of the reflected shock wave is dominated by the bow shock wave, the bow shock wave will pull down the position of the reflected shock wave emanating from the triple point and eventually the position of the triple point itself is also pulled down from the position given by the solution of the three-shock theory. This results in a smaller λ than given by the solution of the three-shock theory.

It can be concluded that the three-shock theory is inadequate when the shock wave emanating from the triple point does not have a dominant effect on the whole shape of the reflected shock wave. In the region near the $RR \neq MR$ boundary, experimental results show that the position of the kink λ/L is no longer equal to the ratio between the flow velocity behind the incident shock wave and the velocity of the incident shock wave U_1/U_{s1} . This is also considered to be caused by the bow shock wave. Therefore, calculations which take into account the effects of the bow shock wave are necessary as $M_s \rightarrow 1$.

B.2 No-Solution Region in the $(M_s - \theta_w)$ Plane

The regions in the $(M_s - \theta_w)$ plane have an additional region, compared with those in the $(M_s - \theta_w)$ plane, namely a no-solution (NR) region. The flow Mach number behind the incident shock wave relative to the triple point must be $M_1 \geq 1$ for the existence of a reflected shock wave at the triple point. At a fixed M_s , M_1 decreases with decreasing θ_w and at a certain θ_w , $M_1 = 1$. No reflected shock wave can exist beyond this point. The line $M_1 = 1$ is the boundary of the NR region.

It was thought that there are no solutions of the three-shock theory in the region just above the boundary of the NR region. In other words, it was assumed that the NR boundary line corresponds to the line $\theta_w = 0^\circ$. At higher Mach numbers $M_s \rightarrow 4$, the line $\theta_w = 0^\circ$ (strictly, the line which is the limit of $\theta_w \rightarrow 0^\circ$) coincides with the NR boundary line within the error of calculations. At lower Mach numbers, however, the line $\theta_w = 0^\circ$ separates from the boundary of the NR region. Consequently, there arises a region between the $\theta_w = 0^\circ$ line and the boundary of the NR region in which no three-shock-theory solution exists (that is, no physical-

ly-realistic solution can exist even if solutions with negative θ_w are possible). The non-solution region for a gas with constant $\gamma = 1.4$ is shown in Fig. A-3.

Experimentally, many points exist in this no-solution region. Consequently, the theory is inadequate in this region. The existence of the no-solution region corresponds to the fact that λ continues to increase as $M_s \rightarrow 1$, as described in Appendix B.1.

Since the existence of this no-solution region is associated with the problem in Appendix B.1, the resolution of this unrealistic region might be possible in an analysis which takes into account the effect of the bow shock, as described in Appendix B.1.

B.3 Existence of Another CMR Region

Another strange result due to the three-shock theory is that it indicates the existence of another CMR region near the NR boundary. In this section, the usual transition criterion between SMR and CMR, $M_{2T} \geq 1$, is adopted. When viewing the variation of M_{2T} with θ_w at a fixed $M_s = 1.8$ (Fig. A-4) for a gas with constant $\gamma = 1.4$, for example, M_{2T} is 1.081 at $\theta_w = 45^\circ$. It means that the point P at $M_s = 1.8$ and $\theta_w = 45^\circ$ lies in a CMR region. The value of M_{2T} decreases as θ_w decreases. M_{2T} is sonic at $\theta_w = 39.32^\circ$ and then enters the SMR region. The decreasing value of M_{2T} is due to two causes. One is that M_{1T} decreases with decreasing θ_w and the other is that ϕ_1 approaches 90° with decreasing θ_w . The angle ϕ_1 becomes 90° at about $\theta_w = 13^\circ$ and keeps increasing with decreasing θ_w to values greater than 90° . An increase in $\phi_1 > 90^\circ$ has an effect to increase M_{2T} contrary to $\phi_1 < 90^\circ$. At a certain θ_w , this effect overrides the decreasing effect due to the decrease of M_{1T} , and M_{2T} begins to increase. Eventually, M_{2T} becomes sonic again at about $\theta_w = 3^\circ$. At wedge angles below this value of θ_w , M_{2T} is greater than 1, which means that it is in another CMR region according to the usual criterion.

This CMR region in the case of a gas with constant $\gamma = 1.4$ is shown in Fig. A-5. This CMR region is not realistic because the validity of the solutions of the three-shock theory is in doubt in the region of small θ_w and low M_s , as described in Appendices B.1 and B.2. This additional CMR region does not appear when the new condition $\phi_1 > 90^\circ$ (see Section 3.3) is added to the criterion because ϕ_1 in this region is well below 90° .

APPENDIX C

EFFECT OF SLIPSTREAM THICKNESS

Only the flow direction and pressure are identical in regions 2 and 3 separated by the slipstream but not the other physical quantities. Consequently, a thermal and velocity layer results, not unlike a

shear or boundary layer. It can be seen from Figs. 5 and A-10 (and other photographs in Refs. 1, 3, 4, 13 and 14) that this is an ideal way of generating a shear layer through wave interactions. The layer is

APPENDIX A

COMMENT ON PERFECT CO₂

The term *perfect* CO₂ was used previously in Refs. 13 and 14 to indicate a gas with a constant value of $\gamma = 1.29$ independent of temperature. However, from the following discussion, CO₂ with a constant $\gamma = 1.29$ has no physical validity. At room temperature, the vibrational modes of CO₂ are partly excited. The doubly-degenerate bending modes, which have a characteristic temperature of 960.2 K, are excited to 14% of their full excitation and have a contribution of 0.9R to C_V . The other two stretching modes contribute 0.7R to C_V . Consequently, along with contributions from the translational modes and rotational modes $C_V = 3.47R$ at room temperature, or $\gamma = C_P/C_V = 1.29$ at room temperature. However, behind a shock wave the translational and

rotational temperatures immediately jump to the Rankine-Hugoniot temperature T_{1f} . Since the vibrational energy is too slow to participate, it remains frozen on either side of the shock front and the temperature T_{1f} can be computed using $\gamma = 1.4$ (Ref. 31). After a period (relaxation time) the vibrational modes are activated and share in the energy through equipartition. The final equilibrium temperature $T_{1e} < T_{1f}$. *Perfect* CO₂ with $\gamma = 1.29$ has no physical basis. However, it is sometimes used in engineering applications to give an approximate answer for shock waves in CO₂ with vibrational excitation. The error becomes increasingly worse with rising shock Mach number (Ref. 31).

APPENDIX B

THREE-SHOCK THEORY

The three-shock theory provides a simple and effective analysis of oblique-shock-wave reflections. Even so, it includes some aspects which are physically unreasonable or inconsistent with experimental results. They are described below.

B.1 Behaviour of λ as $M_S \rightarrow 1$

The values of λ at fixed θ_w are approximately constant at high shock Mach numbers M_S , both experimentally and analytically. As M_S decreases, the values of λ increase except for large θ_w . Experimentally, λ has maximum values near $M_S = 2$ and decreases for other M_S . The calculated results of λ from the three-shock theory, however, do not have maxima for different θ_w but continue to increase as $M_S \rightarrow 1$, as shown in Fig. A-1.

Ben-Dor (Ref. 3) proposed an alternative method to obtain λ at small wedge angles ($\theta_w < 4^\circ$) which does give maxima and may agree with experiment despite his failure to obtain solutions of the three-shock theory for small θ_w and low M_S . His method is to assume that θ_w' at small θ_w coincides with the value at the no reflection (NR) boundary θ_{wNR} and $\lambda = \lambda_{wNR}$ at small wedge angles. Despite that his method gives a reasonable approximation to experiment results and is useful from an engineering point of view, he gave no physical explanation that θ_w' at small θ_w coincides with the NR boundary. His method does not give the necessary dependency of θ_w' ($= \theta_{wNR}$) for different θ_w . Since his suggestion is outside the three-shock theory realm, being only an assumption, it does not provide any clue for improving the three-shock theory or an alternative theory for the calculation of λ . The tendency to increase λ as $M_S \rightarrow 1$ is not considered realistic, not only because it does not agree with experimental results, but it also yields a no-solution region in the (M_S - θ_w) plane, as described in Appendix B.2.

The reason why the three-shock theory fails to give reasonable solutions at low Mach numbers may be as follows. The reflected shock wave is composed of two parts, one is a reflected shock wave emanating from the triple point and the other is a bow shock wave caused by the interaction of the incident flow with the flow deflected by the wedge. The two shock waves intersect at the kink or the second triple point in CMR or DMR, respectively. In SMR, the two shock waves blend smoothly so that an intersection point cannot be seen. The three-shock theory gives the position of only one of the two shock waves, which is the one emanating from the triple point. The actual shape of the entire reflected shock wave is considered to be determined by the two shock waves mentioned above and their interaction. At low Mach numbers, both the reflected shock wave from the triple point and the bow shock wave are weak. The former, however, is considered to become weaker more rapidly than the latter. Therefore, the position of the whole reflected shock wave is controlled by the bow shock wave rather than the reflected shock wave from the triple point. In the limit as the shock Mach number of the bow shock wave approaches 1 (Mach wave), or $\theta_w \rightarrow 0^\circ$, the bow shock will intersect the incident shock wave at a point $\theta_w' = \theta_{wNR}$, which is at a lower θ_w' than the limit of solution of the three-shock theory.

The reason is illustrated in Fig. A-2. Point O in Fig. A-2 was at the wedge corner when the incident shock wave collided with the wedge corner and it moves with the flow in region 1. Therefore, the flow in region 1 has a direction TO relative to T and the bow shock wave in the vicinity of T is normal to the flow. Since the bow wave is a Mach wave, the flow velocity in region 1 relative to the bow wave, or T, is sonic. If T is at θ_{wNR} , the flow Mach number in region 1 is also 1.0 according to the criterion of the NR boundary. It means that

laminar near its point of generation, the triple point, and further on it becomes turbulent and thicker. The thickness of the slipstream between the two flows violates one of the boundary conditions of the three-shock theory that the two flows are parallel. In this appendix, the actual displacement thickness of the slipstream between regions 2 and 3 is not estimated. Only the effect of an assumed displacement angle, which is the slope of the displacement thickness at the triple point on χ is estimated in order to evaluate whether or not this effect can explain the remaining discrepancies of χ between the experiments and the analytical predictions.

Figure A-6 shows a comparison of calculated results with and without displacement angles of 1° and 2° . The gas is equilibrium CO_2 at $M_5 = 5$.

Since the figure shows the relation between θ_w and θ_w' , the difference between the value along the longitudinal and transverse axis is the value of χ . A displacement angle of 2° can change the value of χ less than 1° , except at small wedge angles ($\theta_w < 10^\circ$). This is insufficient to explain the discrepancy in χ (which is about 2° in a typical case at $M_5 = 6$ and $\theta_w = 20^\circ$) because a displacement angle of 6° is necessary to explain the discrepancy and it is not likely to happen. It should be pointed out here, however, that the effect of the displacement angle is not negligibly small at small wedge angles. The displacement angle should be taken into account in calculations at small wedge angles regardless whether use is made of the three-shock theory which takes into account the effect of the bow shock wave, as suggested in Appendix B.1.

APPENDIX D

COMMENT ON TRANSITION CRITERION FOR CMR TO DMR

The discrepancy between the calculated $\text{CMR} \neq \text{DMR}$ boundary and experiment is not as simple as for the $\text{SMR} \neq \text{CMR}$ boundary. In the case of CO_2 shown in Fig. 18, the calculated boundary fails to account for many CMR points which lie in the DMR region. That is, the $\text{CMR} \neq \text{DMR}$ boundary line must be shifted upward to account for the experimental results, whereas in the case of Ar shown in Fig. A-7, the reverse occurs and the $\text{CMR} \neq \text{DMR}$ line has to be shifted downward. However, for N_2 and air, which are shown in Figs. A-8 and A-9, respectively, the experimental distributions agree well with the calculated boundaries (except at lower M_5 and large θ_w when the two triple points approach and coincide on the RR boundary line). All calculations were done in accordance with the discussion on relaxation lengths, that is, CO_2 as an equilibrium gas and Ar, N_2 and air as a frozen gas. These discrepancies are considered due to at least two causes. One is related to the classification of the experimental results and the other is due to the inappropriate transition criterion.

Experimentally, the distinction between CMR and DMR is made by whether or not there is another shock wave at the second triple point. It is difficult, however, to see a weak and short shock wave in an interferogram. Consequently, the classification sometimes depends on the observers. For example, the interferogram of Ar shown in Fig. A-10 was classified as a DMR by Ben-Dor (Ref. 4) and the one of CO_2 shown in Fig. A-11 was classified as a CMR by Ando (Ref. 14). There seems, however, no essential difference between these two interferograms, or one can, with greater assurance, classify them just in reverse, that is, Fig. A-10 as a CMR and Fig. A-11 as a DMR. If so, the experimental boundary of Ar may move towards the DMR region and

that of CO_2 towards the CMR region.

From the point of the criterion, a criticism described below can be offered. At a flow Mach number just over unity, a shock wave, if it is formed, must be normal to the flow direction, otherwise the Mach number of the normal component of the flow is less than 1 and no shock wave could be formed. As mentioned in Section 3.3, the flow comes right above (parallel to the incident shock-wave front), looked at from the reference frame attached to the second triple point. In the region where the transition from CMR to DMR takes place, the angle δ is larger than 90° (see Fig. 20). Therefore, the flow will be deflected toward the second triple point T' while passing through the reflected shock wave. As a result, the second Mach stem M' must slant below the horizontal line toward the Mach stem M (see Fig. A-12). The shadowgraph shown in Fig. 17 is just inside the DMR region. The direction of the flow after the deflection through the reflected shock wave, looked at from the second triple point, is calculated at an angle of about 5° toward the second triple point from the vertical line. Therefore, the second Mach stem should lie 5° below the horizontal line toward the Mach stem. Experimentally, however, the second Mach stem lies along the horizontal line, or it seems to have an opposite inclination in the vicinity of the second triple point. The second Mach stem seems to be formed as an extension of the bow shock wave rather than as a shock wave normal to the flow in region 2 at the very beginning of its formation. This difference is, however, too small to explain the whole discrepancy between the experiments and the calculated boundary, especially in the case of CO_2 . It gives only a clue to other necessary conditions for the transition lines which may exist.

APPENDIX E

SOME FUTURE STUDIES

There are still many aspects to be studied experimentally and analytically in the area of oblique-shock-wave reflections. Some of these are summarized in this appendix in order to assist in the continuation of the study of oblique-shock-wave reflections.

- (a) Experimental persistence of RR beyond the transition boundary.

More experiments are required prior to further analyses. Although the persistence of RR beyond the transition boundary of the detachment criterion itself is an apparent experimental fact, some experimental results seem inconsistent with each other. That is, both RR and MR are obtained in the same region of the $(M_s - \theta_w)$ plane from the results of different experiments (see Section 3.4). This might be due to unknown factors such as a difference in initial pressure and its effects on the boundary-layer-displacement angle θ_d . A knowledge of the exact position of the experimental transition boundary and its dependence on controlled initial conditions are required for further analyses of this problem. The experimental data are required not only at the boundary but also above and below the boundary to obtain information on the behaviour of quantities such as u' (in RR) and χ (in MR) when approaching the RR \neq MR boundary line.

- (b) Convergence of the SMR \neq CMR and CMR \neq DMR boundaries at the RR \neq MR boundary.

Experimental results show that the CMR \neq DMR boundary approaches the SMR \neq CMR boundary near the RR boundary and they eventually converge at the RR \neq MR boundary (see Fig. 25). This corresponds to the experimental fact that u/L approaches 0 and θ_w comes near to the RR \neq MR boundary. There is no analytical prediction of the position of the second triple point except for an empirical assumption that u/L is equal to the ratio between the velocity of the flow behind the incident shock wave and the incident shock wave velocity u_{l_0}/u_{s_0} . An analytical method to predict the position of the second triple point, especially near the RR boundary, is required. Experiments are also required since few data are available aside from the existing values of u/L in this region.

- (c) Prediction of the direction of the Mach-stem curvature.

As described in Section 3.3, the Mach stem at the triple point is not perpendicular to the wedge surface experimentally. This is because the Mach stem has curvature. This discrepancy affects the analytical solutions, especially the value of χ . For accurate analyses, the direction of the Mach stem at the triple point must be predicted. A semi-empirical formulation will be helpful until a better solution is obtained, which requires solving the two-dimensional flow field itself without numerically smearing the shock fronts.

- (d) Effect of the bow shock wave on the position of the triple point.

As described in Appendix B.1, the three-shock theory fails to predict χ at low M_s and small θ_w . This is believed to be due to the effect of the bow shock wave (see Appendix B.1). An analytical method to predict the strength of the bow shock wave and its effect on the position of the triple point is required.

- (e) Transition boundaries in the MR region.

There is experimental impreciseness in the transition boundaries for the types of MR. The imprecision in the classification between SMR and CMR arises from the definition of CMR itself. In the case between CMR and DMR, however, an interferogram (which responds to changes in ρ unlike schlieren to $d\rho/dx$ and shadowgraph to $d^2\rho/dx^2$) contributes to the uncertainty of the experimental transition line. A shock wave is easier to distinguish in a shadow or schlieren photograph rather than in an interferogram (as noted above). It is true that an interferogram includes more quantitative information than a shadowgraph. Even so, experiments using shadowgraphs are often required to give precise configurations which determine the positions of the experimental transition boundaries, especially between CMR and DMR. Consequently, more than one optical method of flow visualization should be used.

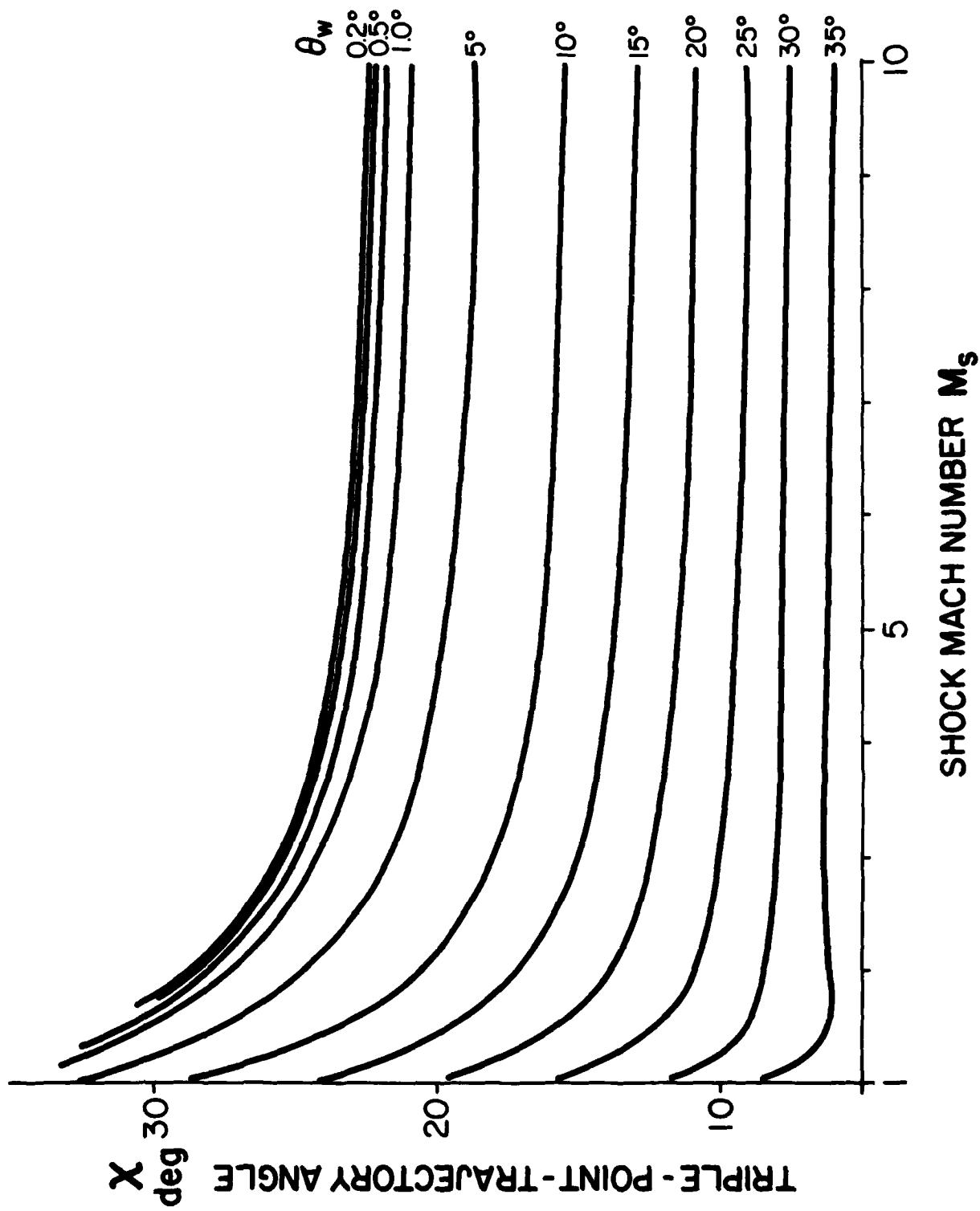


FIG. A-1 TRIPLE-POINT-TRAJECTORY ANGLE X VS INCIDENT SHOCK MACH NUMBER M_s .
FROZEN GAS, $\gamma = 1.40$.

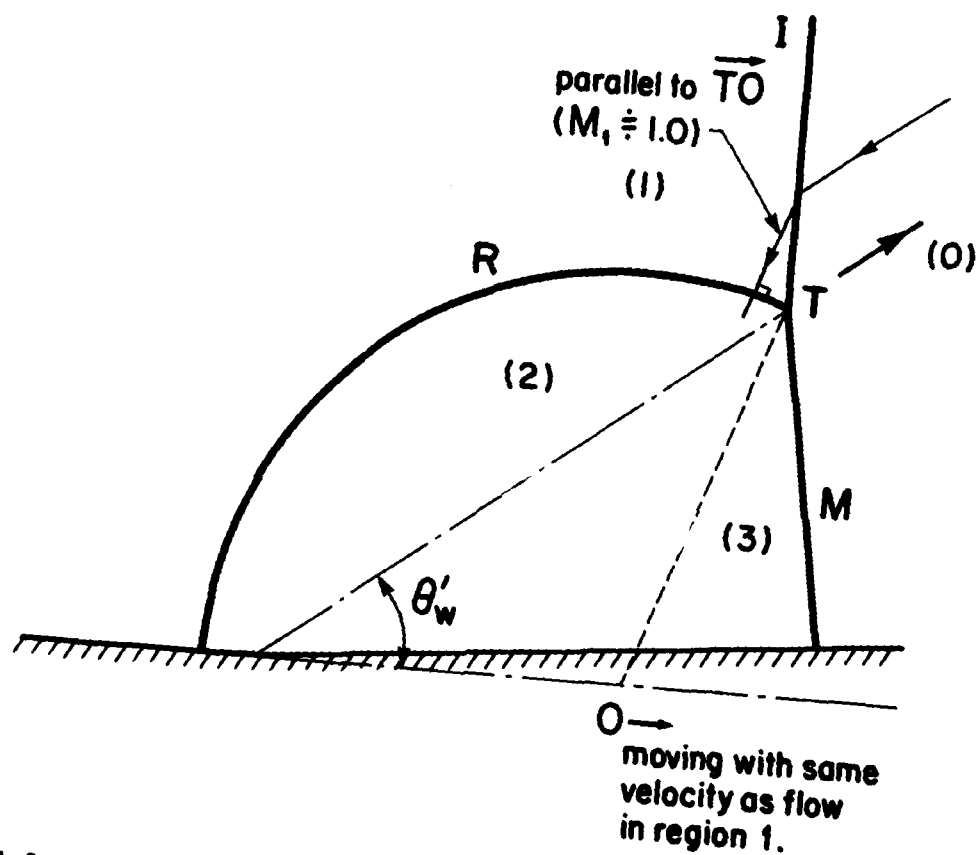


FIG. A-2 SCHEMATIC DIAGRAM SHOWING THAT TRIPLE POINT T SHOULD BE AT θ'_{wNR} WHEN $\theta_w \rightarrow 0^\circ$.

I - INCIDENT SHOCK WAVE, R - REFLECTED SHOCK WAVE, M - MACH STEM,
T - TRIPLE POINT, O - CENTRE OF REFLECTED SHOCK WAVE.

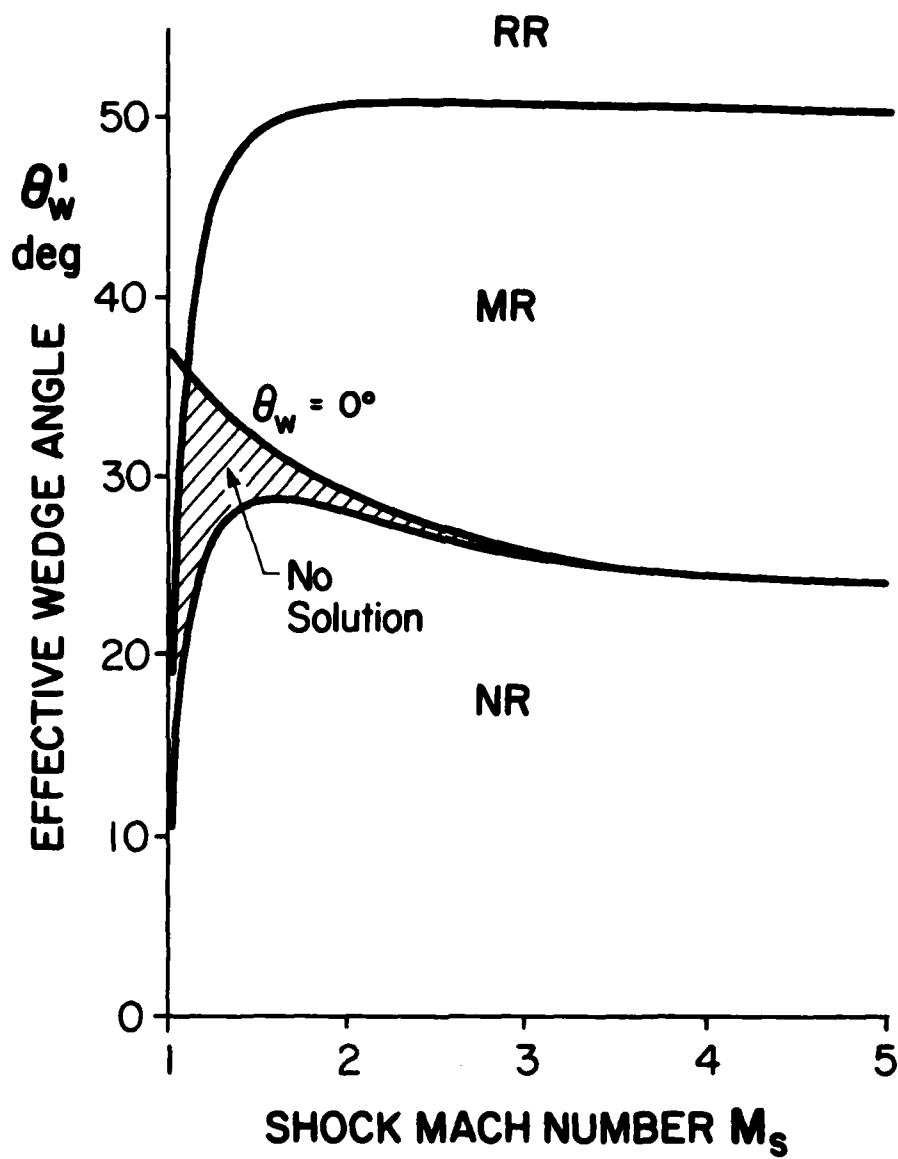


FIG. A-3 NO-SOLUTION REGION IN $(M_s - \theta'_w)$ PLANE FOR A FROZEN GAS $\gamma = 1.40$.

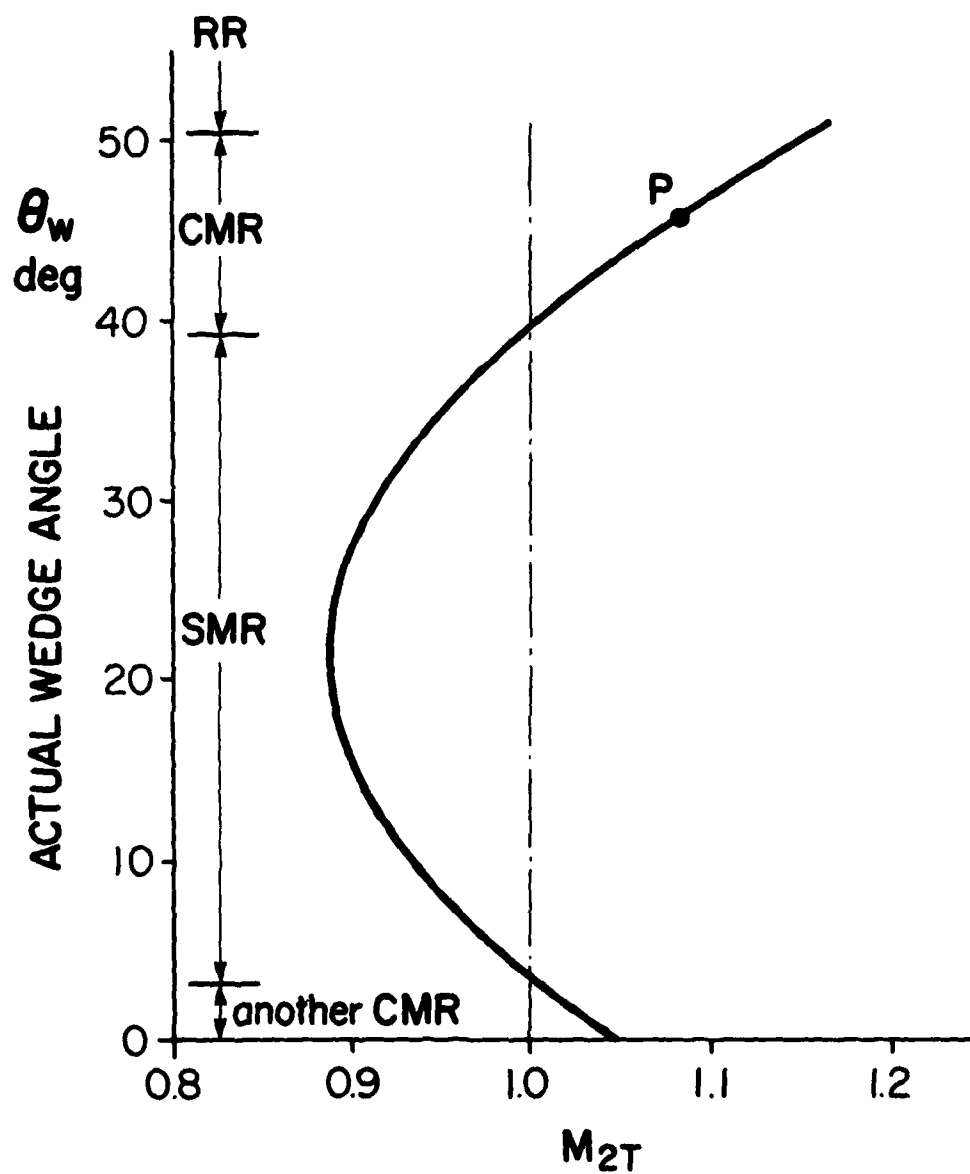


FIG. A-4 VARIATION OF M_{2T} WITH θ_w AT FIXED $M_s = 1.80$ FOR FROZEN GAS
 $\gamma = 1.4$.

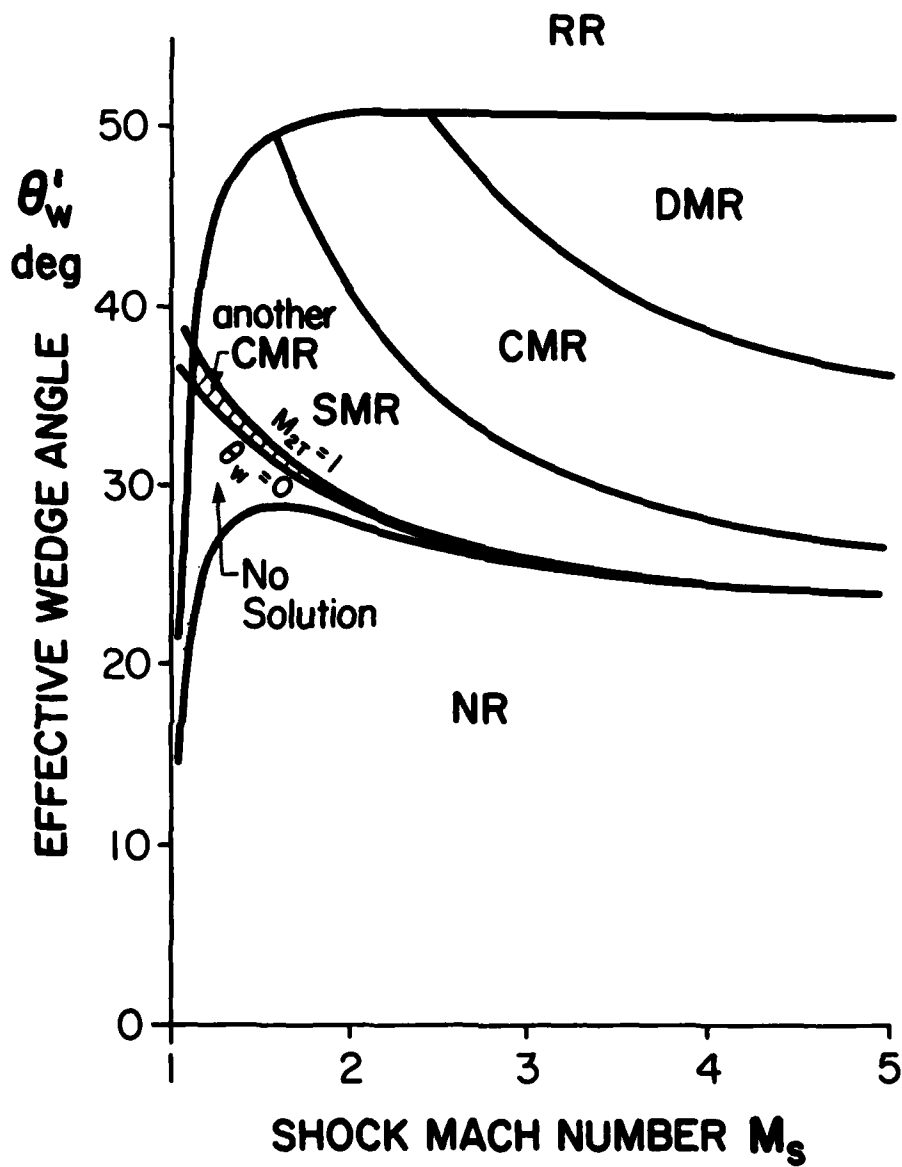


FIG. A-5 EXISTENCE OF ANOTHER CMR REGION FOR A FROZEN GAS $\gamma = 1.40$.

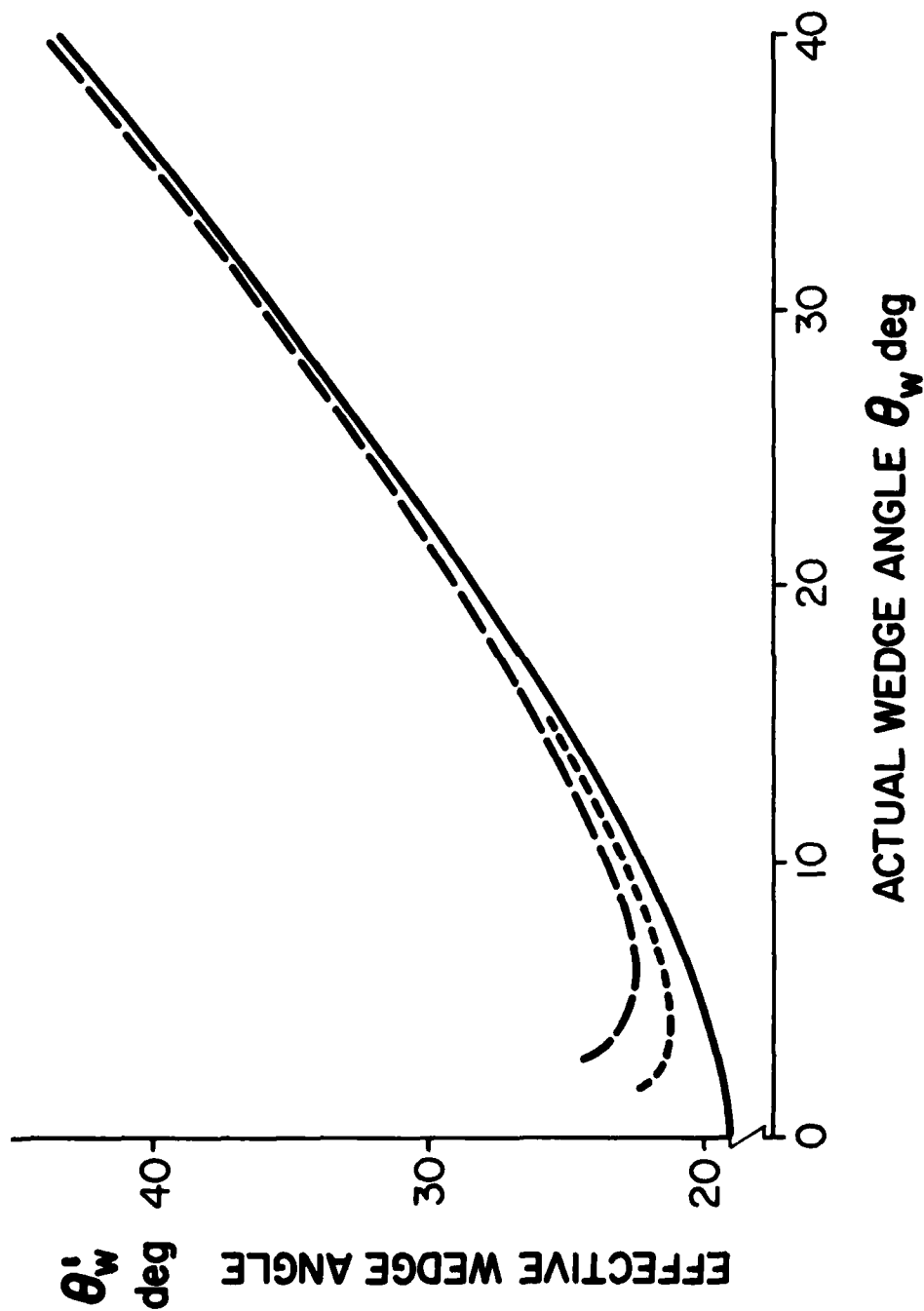


FIG. A-6 EFFECT OF SLIPSTREAM DISPLACEMENT ANGLE FOR EQUILIBRIUM CO_2
 AT $M_s = 5.0$.
 — DISPLACEMENT ANGLE 0° , - - - - - DISPLACEMENT ANGLE 1° ,
 - · - · - DISPLACEMENT ANGLE 2° .

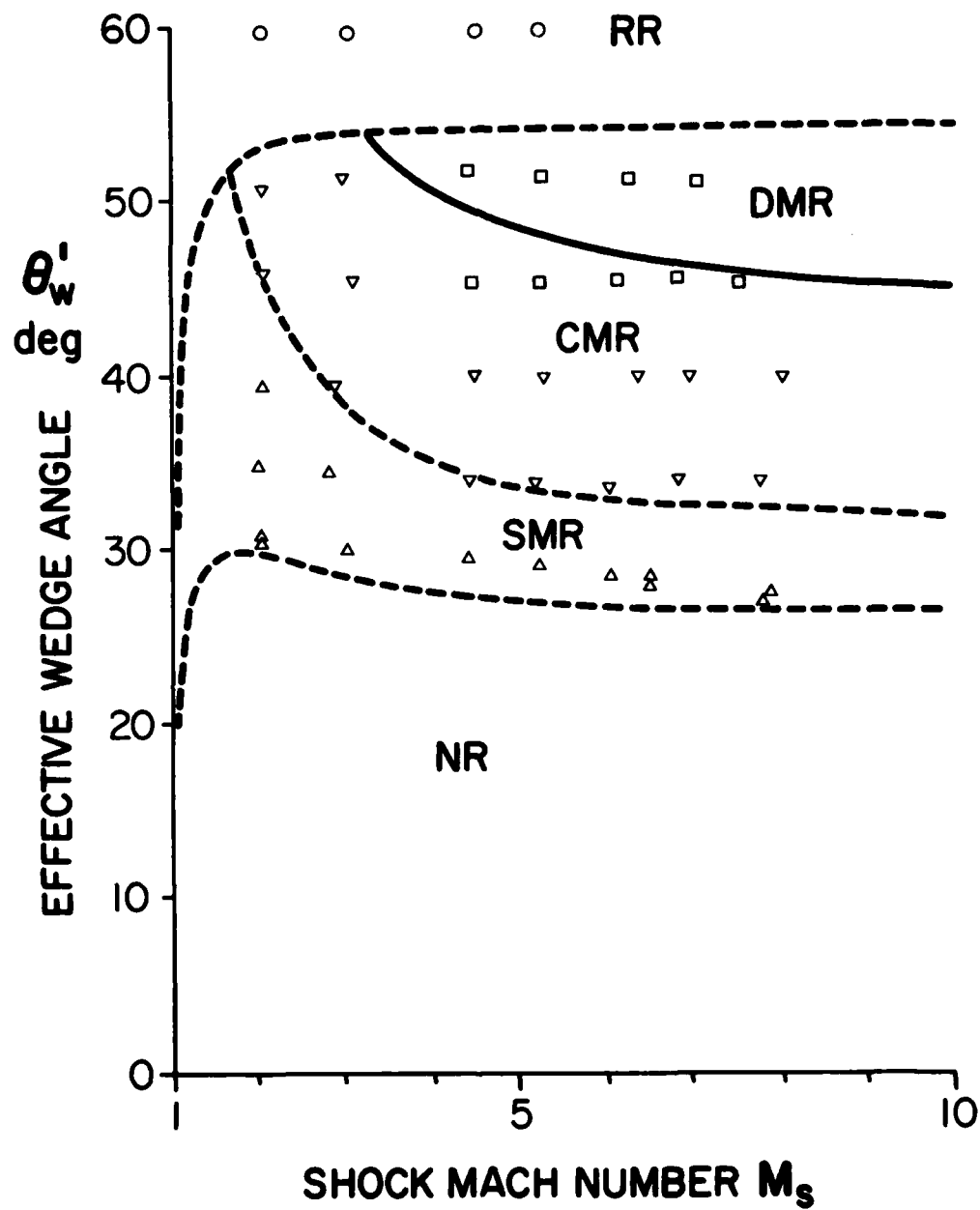


FIG. A-7 COMPARISON OF CALCULATED CMR ∇ DMR TRANSITION BOUNDARY WITH EXPERIMENTAL RESULTS FOR Ar.
EXPERIMENTS: o - RR, Δ - SMR, ∇ - CMR, \square - DMR (REF. 4).

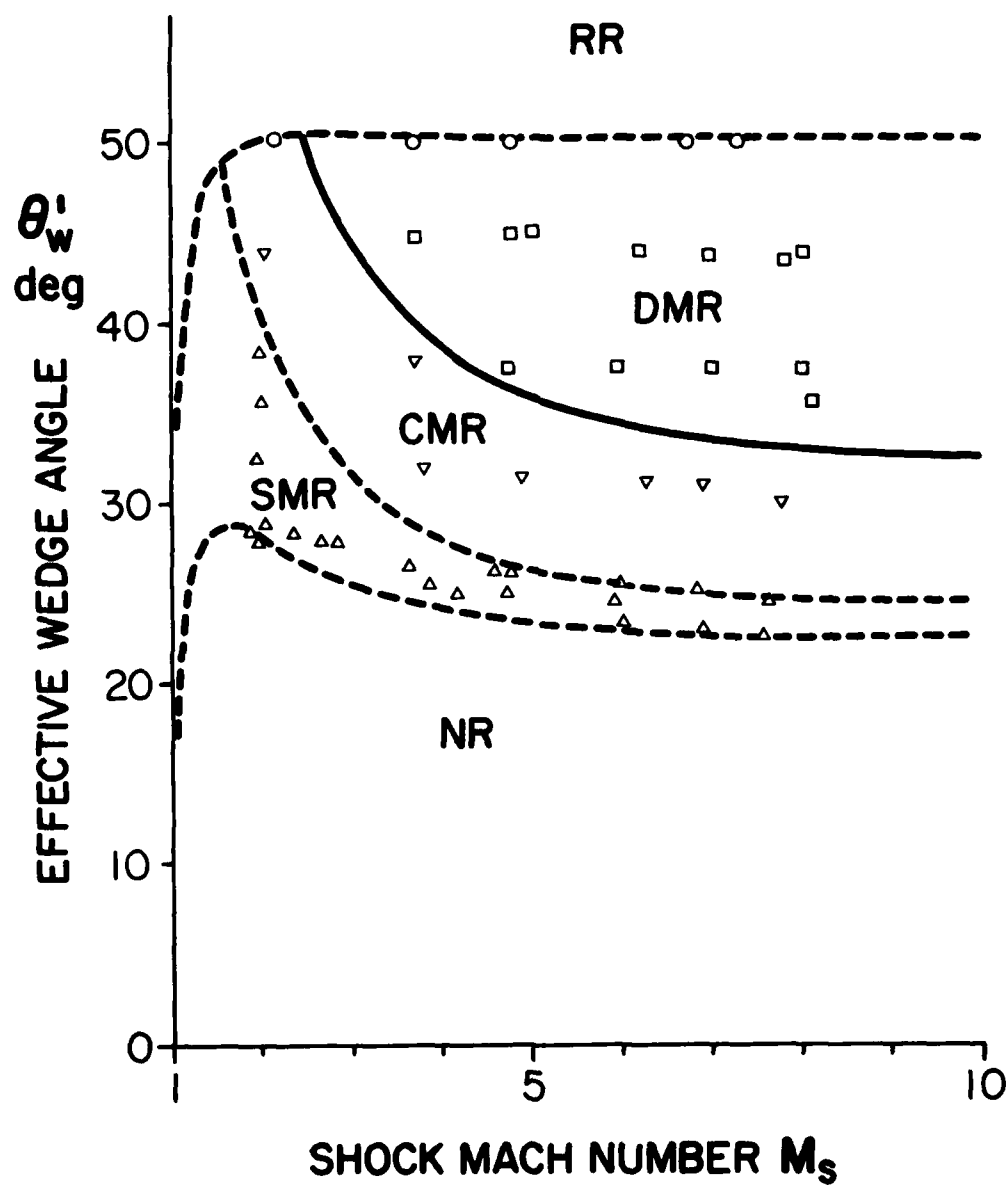


FIG. A-8 COMPARISON OF CALCULATED CMR ∇ DMR TRANSITION BOUNDARY WITH EXPERIMENTAL RESULTS FOR N_2 .
EXPERIMENTS: o - RR, Δ - SMR, ▽ - CMR, □ - DMR (REF. 4).

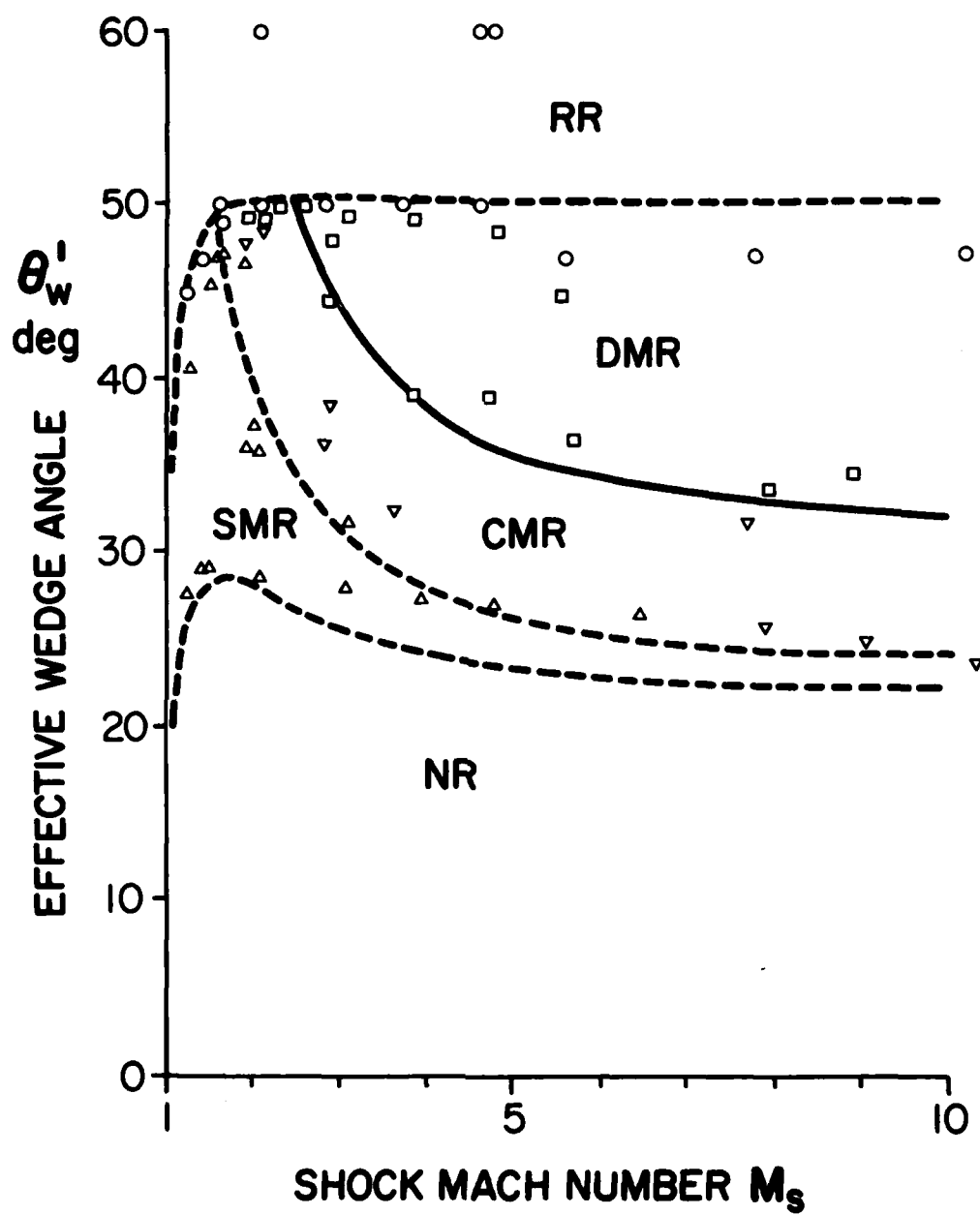


FIG. A-9 COMPARISON OF CALCULATED CMR ∇ DMR TRANSITION BOUNDARY WITH EXPERIMENTAL RESULTS FOR AIR.
EXPERIMENTS: \circ - RR, Δ - SMR, ∇ - CMR, \square - DMR (REF. 21).

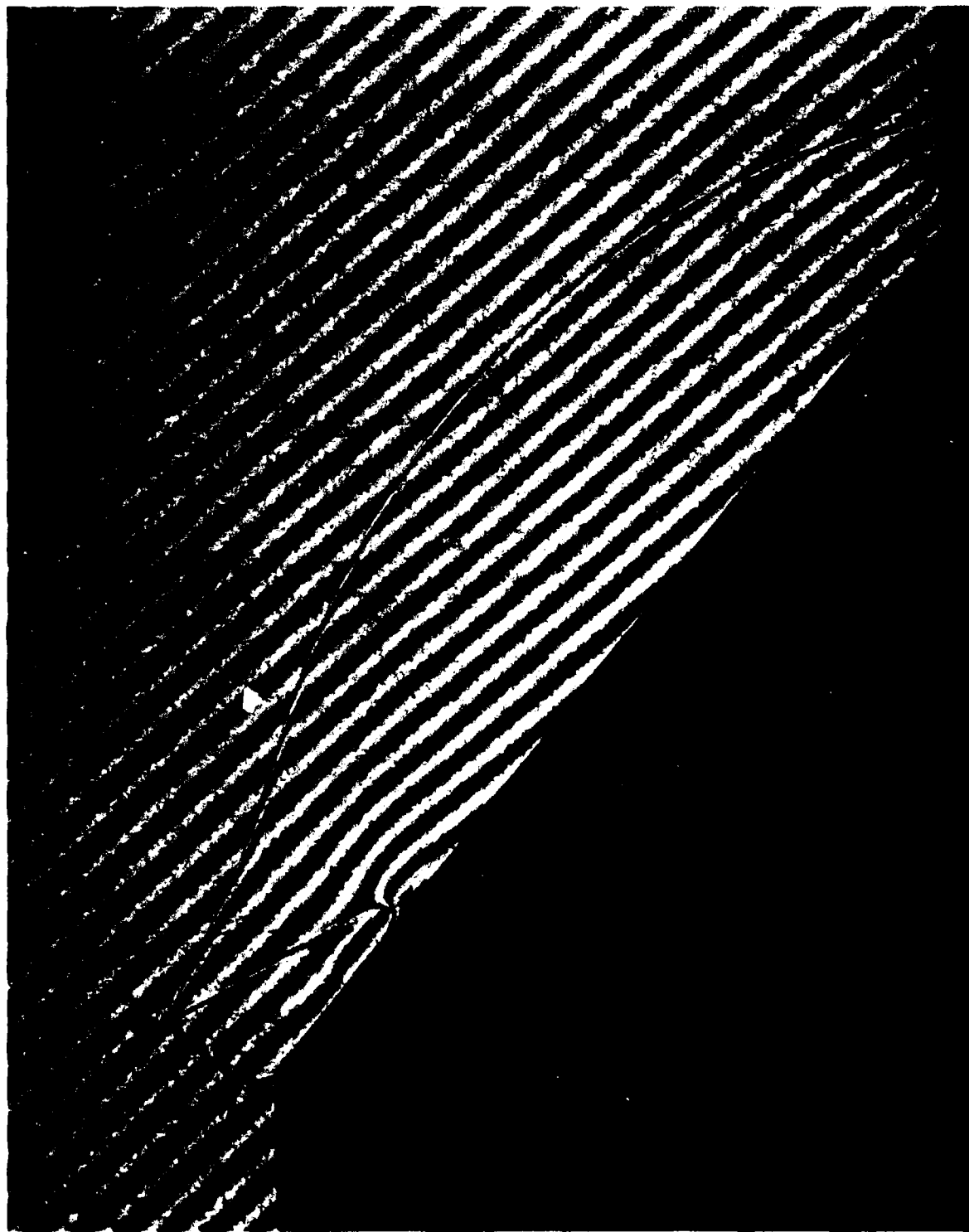


FIG. A-10 AN EXAMPLE CLASSIFIED AS A DMR BY BEN-DOR (REF. 4).
 $\theta_w \approx 40^\circ$, $M_s = 4.44$, $P_0 = 15$ TORR, $T_0 = 299.1$ K.

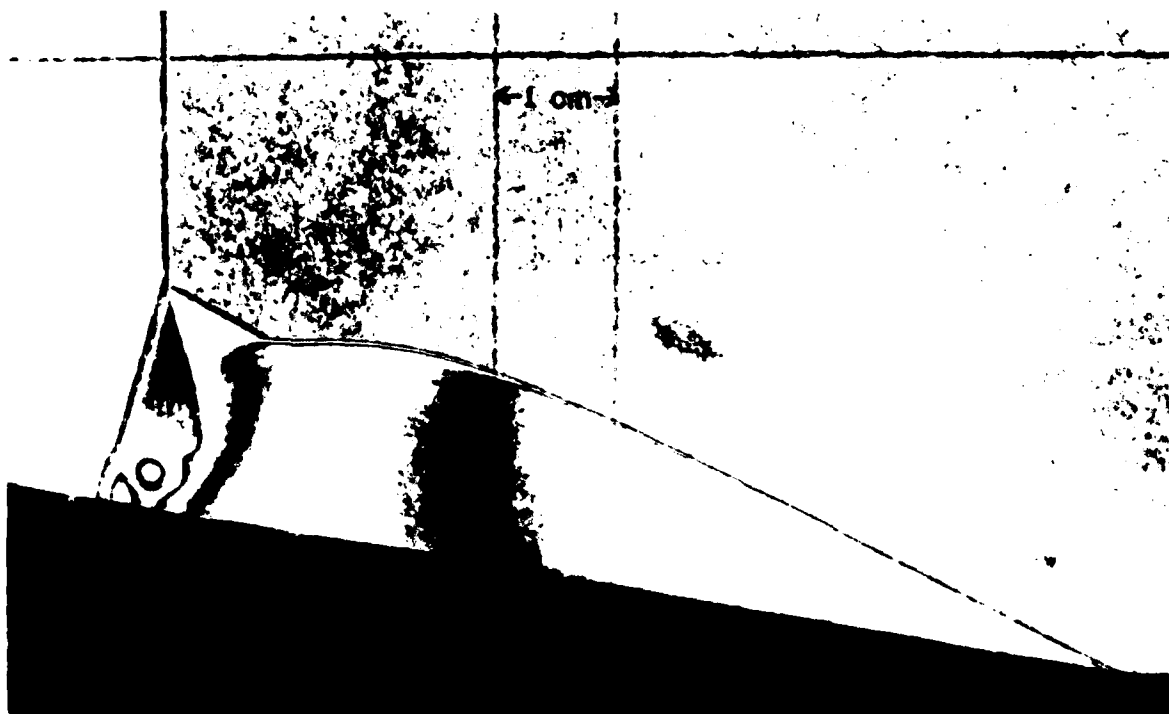


FIG. A-11 AN EXAMPLE CLASSIFIED AS A CMR BY ANDO (REF. 14).
 $\theta_w = 10^\circ$, $M_s = 9.21$, $p_o = 5.1$ TORR, $T_o = 296.9$ K.

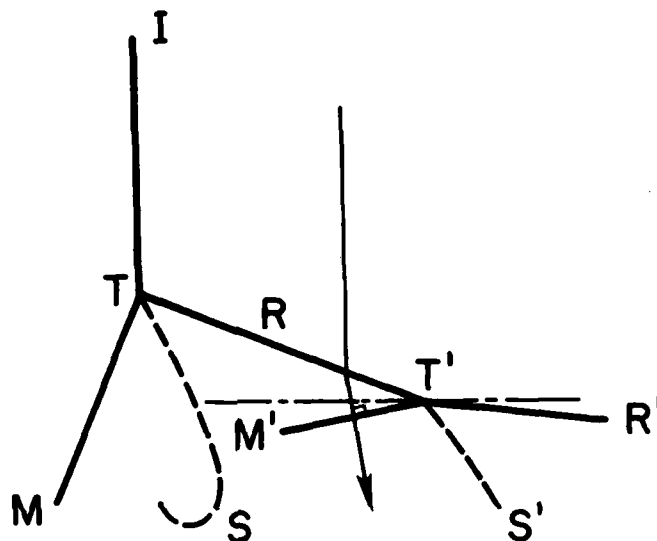


FIG. A-12 SCHEMATIC DIAGRAM ILLUSTRATING THE DIRECTION OF SECOND MACH STEM AT ITS VERY FIRST APPEARANCE.

—— SHOCK WAVE, - - - SLIPSTREAM, \rightarrow FLOW DIRECTION (RELATIVE TO T'), - · - · - HORIZONTAL LINE, I - INCIDENT SHOCK WAVE, R, R' - REFLECTED SHOCK WAVE, M - MACH STEM, M' - SECOND MACH STEM, T - TRIPLE POINT, T' - SECOND TRIPLE POINT, S - SLIPSTREAM, S' - SECOND SLIPSTREAM.

Institute for Aerospace Studies, University of Toronto (UTIAS)
4925 Dufferin Street, Downsview, Ontario, Canada, M3H 5T6

AN ASSESSMENT OF RECENT RESULTS ON PSEUDO-STATIONARY OBLIQUE-SHOCK-WAVE REFLECTIONS

Shirouzu, M., Glass, I. I.

1. Oblique-shock-wave reflections
2. Shock-tube flows
3. Optical methods
4. Numerical analysis

The assumptions and criteria used in existing analyses in determining the regions and transition lines of pseudo-stationary oblique-shock-wave reflections have been re-examined in order to improve the agreement between experiments and computed data for regular (RR), single-Mach (SMR), complex-Mach (CMR) and double-Mach reflection (DMR). It is shown that the relaxation lengths for vibration and dissociation determine whether frozen or equilibrium gas transition lines are applicable. For example, at an initial temperature of 300 K and a pressure of 15 torr (where much previous work was done) an equilibrium gas analysis would not be required for shock Mach numbers $M_2 < 9$ in N_2 , $M_2 < 6$ in O_2 , $M_2 < 8$ in air and $M_2 < 3$ in CO_2 . Yet, the available experimental data in N_2 , CO_2 and very recent results for air, which are based on the criterion (consistent with relaxation lengths) of the angle δ , between the incident and reflected shock wave, do not conclusively support the frozen or equilibrium gas calculations for N_2 and air. It does support CO_2 as an equilibrium gas contrary to a previous conclusion of agreement with $\gamma = 1.29$. A new additional and necessary criterion for the transition from single to complex Mach reflection improves the agreement between analysis and experiment and is consistent with the requirements of the relaxation length and the angle δ . However, it now appears that a more accurate criterion is required for the boundary line between CMR and DMR. A more detailed examination of the boundary-layer-displacement slope at the point of regular reflection appears to eliminate the so-called von Neumann paradox, and explains the persistence of regular reflection below the transition line for the occurrence of Mach reflection. It is also shown that at the triple point the Mach stem can vary from being perpendicular to the wedge surface in actual experiments by as much as -3.10° to 7.5° . Consequently, calculations of the triple-point-trajectory angle χ on the basis that the stem is perpendicular is not always well founded. It is verified that at lower shock Mach numbers M_2 and large wedge angles θ , the experimental evidence shows that the transition lines for SMR \neq CMR and CMR \neq DMR converge at a point on the RR \neq MR line, contrary to a previous simplified analysis.

Available copies of this report are limited. Return this card to UTIAS, if you require a copy.

Institute for Aerospace Studies, University of Toronto (UTIAS)
4925 Dufferin Street, Downsview, Ontario, Canada, M3H 5T6

AN ASSESSMENT OF RECENT RESULTS ON PSEUDO-STATIONARY OBLIQUE-SHOCK-WAVE REFLECTIONS

Shirouzu, M., Glass, I. I.

1. Oblique-shock-wave reflections
2. Shock-tube flows
3. Optical methods
4. Numerical analysis

The assumptions and criteria used in existing analyses in determining the regions and transition lines of pseudo-stationary oblique-shock-wave reflections have been re-examined in order to improve the agreement between experiments and computed data for regular (RR), single-Mach (SMR), complex-Mach (CMR) and double-Mach reflection (DMR). It is shown that the relaxation lengths for vibration and dissociation determine whether frozen or equilibrium gas transition lines are applicable. For example, at an initial temperature of 300 K and a pressure of 15 torr (where much previous work was done) an equilibrium gas analysis would not be required for shock Mach numbers $M_2 < 9$ in N_2 , $M_2 < 6$ in O_2 , $M_2 < 8$ in air and $M_2 < 3$ in CO_2 . Yet, the available experimental data in N_2 , CO_2 and very recent results for air, which are based on the criterion (consistent with relaxation lengths) of the angle δ , between the incident and reflected shock wave, do not conclusively support the frozen or equilibrium gas calculations for N_2 and air. It does support CO_2 as an equilibrium gas contrary to a previous conclusion of agreement with $\gamma = 1.29$. A new additional and necessary criterion for the transition from single to complex Mach reflection improves the agreement between analysis and experiment and is consistent with the requirements of the relaxation length and the angle δ . However, it now appears that a more accurate criterion is required for the boundary line between CMR and DMR. A more detailed examination of the boundary-layer-displacement slope at the point of regular reflection appears to eliminate the so-called von Neumann paradox, and explains the persistence of regular reflection below the transition line for the occurrence of Mach reflection. It is also shown that at the triple point the Mach stem can vary from being perpendicular to the wedge surface in actual experiments by as much as -3.10° to 7.5° . Consequently, calculations of the triple-point-trajectory angle χ on the basis that the stem is perpendicular is not always well founded. It is verified that at lower shock Mach numbers M_2 and large wedge angles θ , the experimental evidence shows that the transition lines for SMR \neq CMR and CMR \neq DMR converge at a point on the RR \neq MR line, contrary to a previous simplified analysis.

Available copies of this report are limited. Return this card to UTIAS, if you require a copy.

Institute for Aerospace Studies, University of Toronto (UTIAS)
4925 Dufferin Street, Downsview, Ontario, Canada, M3H 5T6

AN ASSESSMENT OF RECENT RESULTS ON PSEUDO-STATIONARY OBLIQUE-SHOCK-WAVE REFLECTIONS

Shirouzu, M., Glass, I. I.

1. Oblique-shock-wave reflections
2. Shock-tube flows
3. Optical methods
4. Numerical analysis

The assumptions and criteria used in existing analyses in determining the regions and transition lines of pseudo-stationary oblique-shock-wave reflections have been re-examined in order to improve the agreement between experiments and computed data for regular (RR), single-Mach (SMR), complex-Mach (CMR) and double-Mach reflection (DMR). It is shown that the relaxation lengths for vibration and dissociation determine whether frozen or equilibrium gas transition lines are applicable. For example, at an initial temperature of 300 K and a pressure of 15 torr (where much previous work was done) an equilibrium gas analysis would not be required for shock Mach numbers $M_2 < 9$ in N_2 , $M_2 < 6$ in O_2 , $M_2 < 8$ in air and $M_2 < 3$ in CO_2 . Yet, the available experimental data in N_2 , CO_2 and very recent results for air, which are based on the criterion (consistent with relaxation lengths) of the angle δ , between the incident and reflected shock wave, do not conclusively support the frozen or equilibrium gas calculations for N_2 and air. It does support CO_2 as an equilibrium gas contrary to a previous conclusion of agreement with $\gamma = 1.29$. A new additional and necessary criterion for the transition from single to complex Mach reflection improves the agreement between analysis and experiment and is consistent with the requirements of the relaxation length and the angle δ . However, it now appears that a more accurate criterion is required for the boundary line between CMR and DMR. A more detailed examination of the boundary-layer-displacement slope at the point of regular reflection appears to eliminate the so-called von Neumann paradox, and explains the persistence of regular reflection below the transition line for the occurrence of Mach reflection. It is also shown that at the triple point the Mach stem can vary from being perpendicular to the wedge surface in actual experiments by as much as -3.10° to 7.5° . Consequently, calculations of the triple-point-trajectory angle χ on the basis that the stem is perpendicular is not always well founded. It is verified that at lower shock Mach numbers M_2 and large wedge angles θ , the experimental evidence shows that the transition lines for SMR \neq CMR and CMR \neq DMR converge at a point on the RR \neq MR line, contrary to a previous simplified analysis.

Available copies of this report are limited. Return this card to UTIAS, if you require a copy.

Institute for Aerospace Studies, University of Toronto (UTIAS)
4925 Dufferin Street, Downsview, Ontario, Canada, M3H 5T6

AN ASSESSMENT OF RECENT RESULTS ON PSEUDO-STATIONARY OBLIQUE-SHOCK-WAVE REFLECTIONS

Shirouzu, M., Glass, I. I.

1. Oblique-shock-wave reflections
2. Shock-tube flows
3. Optical methods
4. Numerical analysis

The assumptions and criteria used in existing analyses in determining the regions and transition lines of pseudo-stationary oblique-shock-wave reflections have been re-examined in order to improve the agreement between experiments and computed data for regular (RR), single-Mach (SMR), complex-Mach (CMR) and double-Mach reflection (DMR). It is shown that the relaxation lengths for vibration and dissociation determine whether frozen or equilibrium gas transition lines are applicable. For example, at an initial temperature of 300 K and a pressure of 15 torr (where much previous work was done) an equilibrium gas analysis would not be required for shock Mach numbers $M_2 < 9$ in N_2 , $M_2 < 6$ in O_2 , $M_2 < 8$ in air and $M_2 < 3$ in CO_2 . Yet, the available experimental data in N_2 , CO_2 and very recent results for air, which are based on the criterion (consistent with relaxation lengths) of the angle δ , between the incident and reflected shock wave, do not conclusively support the frozen or equilibrium gas calculations for N_2 and air. It does support CO_2 as an equilibrium gas contrary to a previous conclusion of agreement with $\gamma = 1.29$. A new additional and necessary criterion for the transition from single to complex Mach reflection improves the agreement between analysis and experiment and is consistent with the requirements of the relaxation length and the angle δ . However, it now appears that a more accurate criterion is required for the boundary line between CMR and DMR. A more detailed examination of the boundary-layer-displacement slope at the point of regular reflection appears to eliminate the so-called von Neumann paradox, and explains the persistence of regular reflection below the transition line for the occurrence of Mach reflection. It is also shown that at the triple point the Mach stem can vary from being perpendicular to the wedge surface in actual experiments by as much as -3.10° to 7.5° . Consequently, calculations of the triple-point-trajectory angle χ on the basis that the stem is perpendicular is not always well founded. It is verified that at lower shock Mach numbers M_2 and large wedge angles θ , the experimental evidence shows that the transition lines for SMR \neq CMR and CMR \neq DMR converge at a point on the RR \neq MR line, contrary to a previous simplified analysis.

Available copies of this report are limited. Return this card to UTIAS, if you require a copy.

Institute for Aerospace Studies, University of Toronto (UTIAS)
4925 Dufferin Street, Downsview, Ontario, Canada, M3H 5T6

AN ASSESSMENT OF RECENT RESULTS ON PSEUDO-STATIONARY OBLIQUE-SHOCK-WAVE REFLECTIONS

Shirouzu, M., Glass, I. I.

1. Oblique-shock-wave reflections
2. Shock-tube flows
3. Optical methods
4. Numerical analysis

The assumptions and criteria used in existing analyses in determining the regions and transition lines of pseudo-stationary oblique-shock-wave reflections have been re-examined in order to improve the agreement between experiments and computed data for regular (RR), single-Mach (SMR), complex-Mach (CMR) and double-Mach reflection (DMR). It is shown that the relaxation lengths for vibration and dissociation determine whether frozen or equilibrium gas transition lines are applicable. For example, at an initial temperature of 300 K and a pressure of 15 torr (where much previous work was done) an equilibrium gas analysis would not be required for shock Mach numbers $M_2 < 9$ in N_2 , $M_2 < 6$ in O_2 , $M_2 < 8$ in air and $M_2 < 3$ in CO_2 . Yet, the available experimental data in N_2 , CO_2 and very recent results for air, which are based on the criterion (consistent with relaxation lengths) of the angle δ , between the incident and reflected shock wave, do not conclusively support the frozen or equilibrium gas calculations for N_2 and air. It does support CO_2 as an equilibrium gas contrary to a previous conclusion of agreement with $\gamma = 1.29$. A new additional and necessary criterion for the transition from single to complex Mach reflection improves the agreement between analysis and experiment and is consistent with the requirements of the relaxation length and the angle δ . However, it now appears that a more accurate criterion is required for the boundary line between CMR and DMR. A more detailed examination of the boundary-layer-displacement slope at the point of regular reflection appears to eliminate the so-called von Neumann paradox, and explains the persistence of regular reflection below the transition line for the occurrence of Mach reflection. It is also shown that at the triple point the Mach stem can vary from being perpendicular to the wedge surface in actual experiments by as much as -3.10° to 7.5° . Consequently, calculations of the triple-point-trajectory angle χ on the basis that the stem is perpendicular is not always well founded. It is verified that at lower shock Mach numbers M_2 and large wedge angles θ , the experimental evidence shows that the transition lines for SMR \neq CMR and CMR \neq DMR converge at a point on the RR \neq MR line, contrary to a previous simplified analysis.

Available copies of this report are limited. Return this card to UTIAS, if you require a copy.

Institute for Aerospace Studies, University of Toronto (UTIAS)
4925 Dufferin Street, Downsview, Ontario, Canada, M3H 5T6

AN ASSESSMENT OF RECENT RESULTS ON PSEUDO-STATIONARY OBLIQUE-SHOCK-WAVE REFLECTIONS

Shirouzu, M., Glass, I. I.

1. Oblique-shock-wave reflections
2. Shock-tube flows
3. Optical methods
4. Numerical analysis

The assumptions and criteria used in existing analyses in determining the regions and transition lines of pseudo-stationary oblique-shock-wave reflections have been re-examined in order to improve the agreement between experiments and computed data for regular (RR), single-Mach (SMR), complex-Mach (CMR) and double-Mach reflection (DMR). It is shown that the relaxation lengths for vibration and dissociation determine whether frozen or equilibrium gas transition lines are applicable. For example, at an initial temperature of 300 K and a pressure of 15 torr (where much previous work was done) an equilibrium gas analysis would not be required for shock Mach numbers $M_2 < 9$ in N_2 , $M_2 < 6$ in O_2 , $M_2 < 8$ in air and $M_2 < 3$ in CO_2 . Yet, the available experimental data in N_2 , CO_2 and very recent results for air, which are based on the criterion (consistent with relaxation lengths) of the angle δ , between the incident and reflected shock wave, do not conclusively support the frozen or equilibrium gas calculations for N_2 and air. It does support CO_2 as an equilibrium gas contrary to a previous conclusion of agreement with $\gamma = 1.29$. A new additional and necessary criterion for the transition from single to complex Mach reflection improves the agreement between analysis and experiment and is consistent with the requirements of the relaxation length and the angle δ . However, it now appears that a more accurate criterion is required for the boundary line between CMR and DMR. A more detailed examination of the boundary-layer-displacement slope at the point of regular reflection appears to eliminate the so-called von Neumann paradox, and explains the persistence of regular reflection below the transition line for the occurrence of Mach reflection. It is also shown that at the triple point the Mach stem can vary from being perpendicular to the wedge surface in actual experiments by as much as -3.10° to 7.5° . Consequently, calculations of the triple-point-trajectory angle χ on the basis that the stem is perpendicular is not always well founded. It is verified that at lower shock Mach numbers M_2 and large wedge angles θ , the experimental evidence shows that the transition lines for SMR \neq CMR and CMR \neq DMR converge at a point on the RR \neq MR line, contrary to a previous simplified analysis.

Available copies of this report are limited. Return this card to UTIAS, if you require a copy.

Institute for Aerospace Studies, University of Toronto (UTIAS)
4925 Dufferin Street, Downsview, Ontario, Canada, M3H 5T6

AN ASSESSMENT OF RECENT RESULTS ON PSEUDO-STATIONARY OBLIQUE-SHOCK-WAVE REFLECTIONS

Shirouzu, M., Glass, I. I.

1. Oblique-shock-wave reflections
2. Shock-tube flows
3. Optical methods
4. Numerical analysis

The assumptions and criteria used in existing analyses in determining the regions and transition lines of pseudo-stationary oblique-shock-wave reflections have been re-examined in order to improve the agreement between experiments and computed data for regular (RR), single-Mach (SMR), complex-Mach (CMR) and double-Mach reflection (DMR). It is shown that the relaxation lengths for vibration and dissociation determine whether frozen or equilibrium gas transition lines are applicable. For example, at an initial temperature of 300 K and a pressure of 15 torr (where much previous work was done) an equilibrium gas analysis would not be required for shock Mach numbers $M_2 < 9$ in N_2 , $M_2 < 6$ in O_2 , $M_2 < 8$ in air and $M_2 < 3$ in CO_2 . Yet, the available experimental data in N_2 , CO_2 and very recent results for air, which are based on the criterion (consistent with relaxation lengths) of the angle δ , between the incident and reflected shock wave, do not conclusively support the frozen or equilibrium gas calculations for N_2 and air. It does support CO_2 as an equilibrium gas contrary to a previous conclusion of agreement with $\gamma = 1.29$. A new additional and necessary criterion for the transition from single to complex Mach reflection improves the agreement between analysis and experiment and is consistent with the requirements of the relaxation length and the angle δ . However, it now appears that a more accurate criterion is required for the boundary line between CMR and DMR. A more detailed examination of the boundary-layer-displacement slope at the point of regular reflection appears to eliminate the so-called von Neumann paradox, and explains the persistence of regular reflection below the transition line for the occurrence of Mach reflection. It is also shown that at the triple point the Mach stem can vary from being perpendicular to the wedge surface in actual experiments by as much as -3.10° to 7.5° . Consequently, calculations of the triple-point-trajectory angle χ on the basis that the stem is perpendicular is not always well founded. It is verified that at lower shock Mach numbers M_2 and large wedge angles θ , the experimental evidence shows that the transition lines for SMR \neq CMR and CMR \neq DMR converge at a point on the RR \neq MR line, contrary to a previous simplified analysis.

Available copies of this report are limited. Return this card to UTIAS, if you require a copy.

Institute for Aerospace Studies, University of Toronto (UTIAS)
4925 Dufferin Street, Downsview, Ontario, Canada, M3H 5T6

AN ASSESSMENT OF RECENT RESULTS ON PSEUDO-STATIONARY OBLIQUE-SHOCK-WAVE REFLECTIONS

Shirouzu, M., Glass, I. I.

1. Oblique-shock-wave reflections
2. Shock-tube flows
3. Optical methods
4. Numerical analysis

The assumptions and criteria used in existing analyses in determining the regions and transition lines of pseudo-stationary oblique-shock-wave reflections have been re-examined in order to improve the agreement between experiments and computed data for regular (RR), single-Mach (SMR), complex-Mach (CMR) and double-Mach reflection (DMR). It is shown that the relaxation lengths for vibration and dissociation determine whether frozen or equilibrium gas transition lines are applicable. For example, at an initial temperature of 300 K and a pressure of 15 torr (where much previous work was done) an equilibrium gas analysis would not be required for shock Mach numbers $M_2 < 9$ in N_2 , $M_2 < 6$ in O_2 , $M_2 < 8$ in air and $M_2 < 3$ in CO_2 . Yet, the available experimental data in N_2 , CO_2 and very recent results for air, which are based on the criterion (consistent with relaxation lengths) of the angle δ , between the incident and reflected shock wave, do not conclusively support the frozen or equilibrium gas calculations for N_2 and air. It does support CO_2 as an equilibrium gas contrary to a previous conclusion of agreement with $\gamma = 1.29$. A new additional and necessary criterion for the transition from single to complex Mach reflection improves the agreement between analysis and experiment and is consistent with the requirements of the relaxation length and the angle δ . However, it now appears that a more accurate criterion is required for the boundary line between CMR and DMR. A more detailed examination of the boundary-layer-displacement slope at the point of regular reflection appears to eliminate the so-called von Neumann paradox, and explains the persistence of regular reflection below the transition line for the occurrence of Mach reflection. It is also shown that at the triple point the Mach stem can vary from being perpendicular to the wedge surface in actual experiments by as much as -3.10° to 7.5° . Consequently, calculations of the triple-point-trajectory angle χ on the basis that the stem is perpendicular is not always well founded. It is verified that at lower shock Mach numbers M_2 and large wedge angles θ , the experimental evidence shows that the transition lines for SMR \neq CMR and CMR \neq DMR converge at a point on the RR \neq MR line, contrary to a previous simplified analysis.

Available copies of this report are limited. Return this card to UTIAS, if you require a copy.